CHALMERS
UNIVERSITY OF TECHNOLOGY

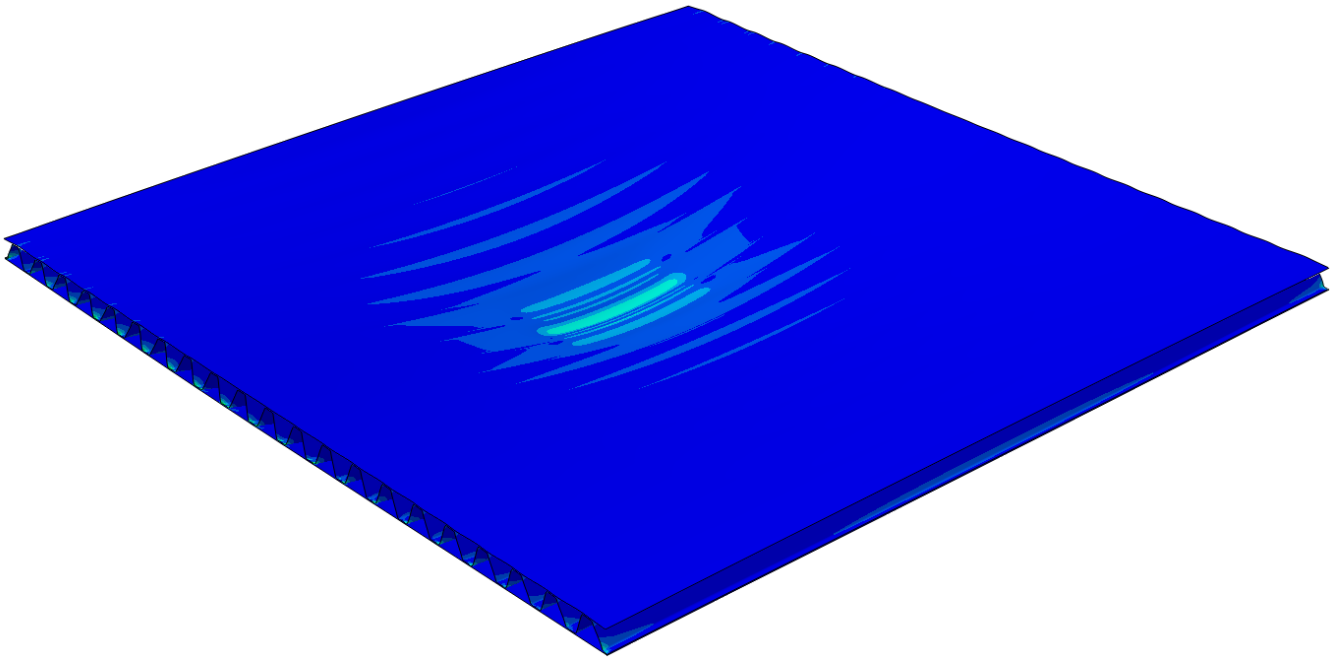

Multi-scale modelling of corrugated core steel sandwich panels subjected to out-of-plane loads

Master's Thesis in the Master's Programme Structural Engineering and Building Technology

JON DIFS
ALFRED RO

Department of Architecture and Civil Engineering
Division of Structural Engineering
Steel and Timber Structures
CHALMERS UNIVERSITY OF TECHNOLOGY
Master's Thesis BOMX02-17-99
Gothenburg, Sweden 2017

MASTER'S THESIS BOMX02-17-99

Multi-scale modelling of corrugated core steel sandwich panels subjected to out-of-plane loads

Master's Thesis in the Master's Programme Structural Engineering and Building Technology

JON DIFS
ALRFRED RO

Department of Architecture and Civil Engineering
Division of Structural Engineering
STEEL AND TIMBER STRUCTURES
CHALMERS UNIVERSITY OF TECHNOLOGY
Göteborg, Sweden 2017

Multi-scale modelling of corrugated core steel sandwich panels subjected to out-of-plane loads
Master's Thesis in the Master's Programme Structural Engineering and Building Technology
JON DIFS
ALFRED RO

Examensarbete BOMX02-17-99/Institutionen för Arkitektur och Samhällsbyggnadsteknik
Chalmers tekniska högskola 2017

Department of Architecture and Civil Engineering
Division of Structural Engineering
Steel and Timber Structures
Chalmers University of Technology
SE-412 96 Göteborg
Sweden
Telephone: + 46 (0)31-772 1000

Cover:
Corrugated core sandwich panel modelled with shell elements subjected to patch loading.
Department of Architecture and Civil Engineering, Göteborg, Sweden, 2017

Multi-scale modelling of corrugated core steel sandwich panels subjected to out-of-plane loads

Master's Thesis in the Master's Programme Structural Engineering and Building Technology

JON DIFS
ALFRED RO
Department of Architecture and Civil Engineering
Division of Structural Engineering
Steel and Timber Structures
Chalmers University of Technology

ABSTRACT

A promising alternative to the conventional orthotropic steel deck is the corrugated core sandwich panel. Due to the complicated core geometry, this type of sandwich panel is hard to evaluate with analytical methods and therefore often analyzed numerically, using the finite element method. It is desirable, from a design point of view, to simplify the structural analysis which at present relies mainly on 3D-modelling. These models require a lot of computer resources and the corresponding analysis usually take a considerable amount of time to run, i.e. they are not suitable for design or optimization purposes.

A study was conducted on how to approximate a full 3D finite element model, by combining contributions from a local 2D model and a homogenized ESL (Equivalent Single Layer)-model. This was performed for four different geometries of corrugated core sandwich panels. The models were investigated under the influence of a vertical local patch load.

First, the presented literature study focuses on corrugated-core sandwich panels, their structural behavior, how to effectively approximate the orthotropic structure as a homogenized single layer shell and a brief study on suggestions regarding FE-modelling. Thereafter, the conducted study is introduced, presented and discussed.

It was shown that the global moment in the direction orthogonal to the core gives rise to a local moment in the top face plate of the sandwich panel. It was shown that neglecting this local moment can lead to considerable errors. It was also found that the suggested approach gave accurate results when considering global load effects alone. However, when investigating global load effects together with the effect of the directly applied load, a considerable discrepancy compared to the 3D-model was shown. The study went on to investigate possible ways to capture this disagreement. Although none of the extended studies were deemed to be general enough to be used for design purposes, they give insight to the discrepancy between the full 3D-analysis and the simplified approach.

Keywords: Sandwich panel, FE-modeling, ESL, patch load, plate theory, homogenization

Flerskalig modellering av stålsandwichpaneler med korrugerad kärna utsatta för laster vinkelrätt planet

Examensarbete inom masterprogrammet Structural Engineering and Building Technology

JON DIFS
ALFRED RO

Institutionen för Arkitektur och Samhällsbyggnadsteknik
Avdelningen för Konstruktionsteknik
Stål- och träbyggnad
Chalmers tekniska högskola

SAMMANFATTNING

Den moderna korrugerade sandwichpanelen är ett mycket lovande alternativ till det konventionella ortotropa brodäcket av stål. På grund av den komplicerade geometrin är denna typ av sandwichpanel svår att utvärdera med analytiska modeller och utvärderas därför ofta numeriskt, med till exempel finita element metoden. Ur ett designperspektiv vore det önskvärt att förenkla modelleringsprocessen, som vid skrivande stund huvudsakligen förlitar sig på 3D-modellering. Dessa modeller kräver mycket datorkapacitet och är därav ej lämpliga för konstruktions- och optimerings-rutiner.

En studie genomfördes angående hur det strukturella beteendet hos en tredimensionell FE-modell kan förenklas med en lokal 2D-modell och en homogeniserad skalmodell. Studien utfördes för fyra olika geometrier av korrugerade sandwichpaneler. Modellerna analyserades under inverkan av ett vertikalt hjultryck.

Inledningsvis presenteras en litteraturstudie om stålsandwichpaneler med korrugerad kärna, deras strukturella beteende, hur en ortotrop struktur kan förenklas som ett homogeniserat skal och även kortfattat angående rekommendationer för FE-modellering av olika element. Därefter introduceras, presenteras samt diskuteras den genomförda studien.

Det visade sig att det föreslagna tillvägagångssättet gav exakta resultat då enbart globala lasteffekternas inverkan på spänningstillståndet i tvärsnittets olika delar utvärderades. När området direkt under lasten undersöktes så påvisades en skillnad mellan den fulla 3D-analysen och den förenklade 2D-analysen. Studien gick vidare till att undersöka möjliga förklaringar till den påvisade avvikelsen. Även om ingen av de justerade studierna ansågs vara generella nog för att användas till exempel vid dimensionering, så ger de insikt till avvikelsen mellan den fulla 3D-analysen och den förenklade 2D-analysen.

Nyckelord: sandwichpaneler, ESL, FE-modellering, homogenisering

Contents

Preface

This master thesis evaluates the possibility to simplify the modeling process of a corrugated core steel sandwich panel. The work was carried out during the spring of 2017 as a part of the ongoing research project concerning sandwich panels at the Division of Structural Engineering at Chalmers University of Technology.

First and foremost, we would like to extend a big thank you to our supervisor Peter Nilsson for his guidance, enthusiasm and continuous support throughout the entire project. Appreciation is given to our examiner, Associate Professor Mohammad Al-Emrani, for his insightful feedback on several occasions.

We would also like to thank everyone at WSP Bridge and Hydraulic Design in Gothenburg for the possibility to carry out our work at their office and for their welcoming and helpful attitude. Finally, we would like to thank Scanscot Technology for the sponsorship of two licenses for BRIGADE/Plus 6.1.

Gothenburg, July 2017

Jon Difs
Alfred Ro

Notations

Roman upper case letters

A_c	Area of the corrugation cross section perpendicular to the corrugations axis.
A_x, A_y	Cross sectional area of the sandwich panel.
$D_{x,}D_y$	Bending stiffness around the x- and y-axis of the sandwich panel.
D_{xy}	Twisting stiffness of the sandwich panel.
D_{Qx}, D_{Qy}	Out of plane transverse shear stiffness of the sandwich panel.
E	Elastic modulus of steel.
$E_{p.s}$	Elastic modulus for plain strain conditions.
E_x	Orthotropic material constant for bending the x-direction
E_y	Orthotropic material constant for bending in the y-direction
G	Shear modulus of steel.
G_c	Shear modulus of the corrugated core material.
G_{xy}	Orthotropic material constant for torsional moment in the xy-plane.
G_{xz}	Orthotropic material constant for transverse shear in the xz-plane.
G_{yz}	Orthotropic material constant for transverse shear in the yz-plane.
I_c^m	Second moment of area of the corrugated core.
M_{extra}	Additional global moment introduced in the last study.
M_m	Moment induced local moment factor.
M_s	Shear induced local moment factor.
M_x, M_y	Bending moment around the x and y-axis, respectively.
M_{xy}	Twisting moment in the xy-plane.
N_x, N_y	Normal force in the xy-plane in the x and y-direction respectively.
P	Applied point load in the 4-point bening model.
Q_x, Q_y	Transverse shear force in the yz- and xz-plane respectively.
R	Radius of the corrugation.

Roman lower case letters

d_w	Distance between welds.
f_1, f_2	Distance between the radials of each corrugated crest, bottom and top.
h	Distance between the center of mass of the face plates.
h_c	Total height of the corrugated core.

k	Shear correction factor 5/6.
p	Length of one half unit cell.
t_c	Thickness of the core material.
t_1	Thickness of the bottom face plate.
t_2	Thickness of the top face plate.
t_w	Weld thickness.
v_x, v_y	Poisson's ratio of the faceplate material.
w_l	Total local deflection.
w_Q	Local deflection caused by global shear
w_{tf}	Local deflection caused by the thick face plate effect.
w_q	Local deflection caused by the applied patch load.

Greek lower case letters

θ	Angel of the corrugation.
γ_x	Shear angle in the x-direction.
γ_z	Shear angle in the y-direction.
γ_{xz}	Shear strain in the xz-plane caused by Q_y.
γ_{yz}	Shear strain in the yz-plane caused by Q_x.

Abbreviations

DOF	Degree of freedom
BC	Boundary condition
ESL	Equivalent single layer
FEM	Finite element method
FE	Finite element
FEA	Finite element analysis
GMAW	Gas metal arc welding
HAZ	Heat Affected Zone
MIG	Metal Inert Gas
SSP	Steel sandwich panel
TIG	Tungsten Inert Gas
HLAW	Hybrid laser arc welding

1 Introduction

Orthotropic steel bridge-decks for bridge applications were first used after the 2nd World War, when the shortage of steel required the engineers to come up with new efficient structural solutions. However, as material prices dropped and salaries for engineers and welders increased, the usage of the orthotropic steel decks declined and research development came to a halt [1]. Today, steel decks are used almost exclusively in either moveable bridges or bridges with very long spans, where minimal self-weight is a requirement [2].

The conventional orthotropic plate deck consists of a top steel plate with welded longitudinal stiffeners, which can be either open or closed [2]. This deck has a very complex structural behavior which was not anticipated by the engineers in early design. Some effects were therefore overlooked, like the highly orthotropic behavior which creates high stress concentrations in certain areas and makes the deck very prone to fatigue damage [3].

To tackle the problems with conventional steel plate decks, a new design have been proposed by for example [2] and [4]. The proposed structure is the corrugated-core steel sandwich panel (SSP), where the largest difference compared to the conventional plate bridge deck is the use of two face plates, as opposed to one, see Figure 1. Compared to the conventional bridge deck, the SSP is less orthotropic and has a higher stiffness-to-mass ratio. Furthermore, the production process of the SSP is more industrialized compared to the conventional bridge deck [5].

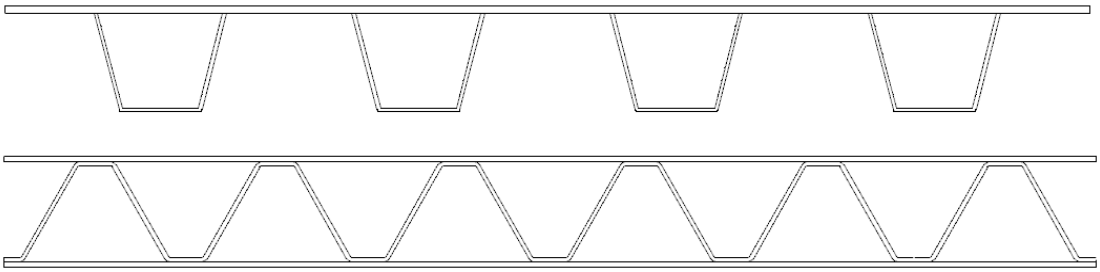

Figure 1 *Cross sectional sketch of a conventional orthotropic steel deck (top), steel sandwich panel (bottom).*

The corrugated core SSP is promising for several applications areas of bridge construction, both for repairs and construction of new bridges. An example of a replacement can be a shift of a degraded concrete deck to a steel deck. By doing this replacement a decrease in self-weight can be achieved, which can be beneficial due to increasing traffic loads. An application for corrugated core SSP's for new bridge structures could be as a hollow box section made completely out of SSP or as a deck above steel girders [6].

Despite being a promising alternative, research is still ongoing in many areas regarding the corrugated sandwich panel - in regions related to civil engineering applications as well as in other engineering disciplines. A historically problematic aspect of the conventional steel deck, has been the issue regarding fatigue cracking from stresses due to local patch loads. This area has seen a great amount of research for the conventional deck specifically. However, this is not the case for corrugated-core SSP's and therefore

little is known of the local structural response for this panel when subjected to a local patch load.

1.1 Purpose and aim

Previous studies on the application of SSP's have shown promising results – such as reductions for both weight and cost compared to a conventional orthotropic steel deck. But before the corrugated core SSP can be used for bridge construction, the structural behavior and fatigue performance must be further evaluated. This has previously been done for certain load cases, such as transverse shear force [7], but no studies have been performed for a case with a vertical locally applied patch load. Thus, this thesis aims to investigate the structural behavior of a corrugated core SSP, under the influence of a vertical local patch load applied on the upper face plate.

Specifically, the following results were sought to be achieved during the work:

- Establish a set of 2D Finite Element models to simplify a full 3D corrugated core steel sandwich panel in a commercial FE-software.
- Describe the local force distribution in the sandwich panel exposed to a patch load, considering global forces and moments.
- Describe the local force distribution in the sandwich panel exposed to a patch load, considering global moments and forces together with the effect of the directly applied load.

1.2 Method

To introduce the subject at hand, a literature study was conducted at the beginning of the project. The literature study focused on production and structural response of steel sandwich panels, elastic behavior of a homogenized corrugated core sandwich panel, finite element modelling of SSPs and the response under local patch loads for other core configurations.

In the performed study, three different FE-models of different scale were created in the commercial software BRIGADE/Plus 6.1-11. Four different geometric cases were used to make sure that the results will be valid for a wide variety of corrugated core SSP's. Because of the need to be able to create models with varying geometries and the large amount of computed analyses, the studied cases were modelled using scripts.

Calculations used for input data were handled in Mathcad 15.0 and output data was post-processed in Microsoft Excel.

1.3 Limitations

This thesis focuses exclusively on corrugated core steel sandwich panels. Other types of core geometry will be mentioned but not investigated to any extent. The sandwich panels were only investigated for four different geometry configurations. Dual weld lines at each core crest was the only joint configuration considered in the project.

Linear elastic material response was assumed throughout the entire project. Further, the material model was assumed to be isotropic. Additionally, non linarites such as the contact between face plates and core due to relative displacements and also buckling, will not be considered.

This project will focus mainly on local patch loading as the investigated load case. Other load cases were used at certain points, but only for comparison and verification purposes. Self-weight of the analyzed members is not included in the analyses.

2 Sandwich panels

Sandwich structures used in engineering generally consist of two face plates which are separated by a core. The face plates are designed to carry bending moments and in-plane loads, while the core is designed to carry shear loads. Usually, the face plates have a high density and stiffness, compared to the core. By splitting the face plates with a low density core, a high flexural resistance is achieved while still maintaining a low weight and thus obtain a high stiffness-to-mass ratio [8].

Sandwich structures are currently used in a number of engineering fields including naval, cardboards, aircraft and spacecraft [9]. This implies that sandwich structures can be made in many different configurations and shapes, see Figure 2. A number of different profiles and materials (both isotropic and orthotropic) are commonly utilized when constructing sandwich panels [10]. However, the most promising core structure for bridge application is the corrugated core [10] .

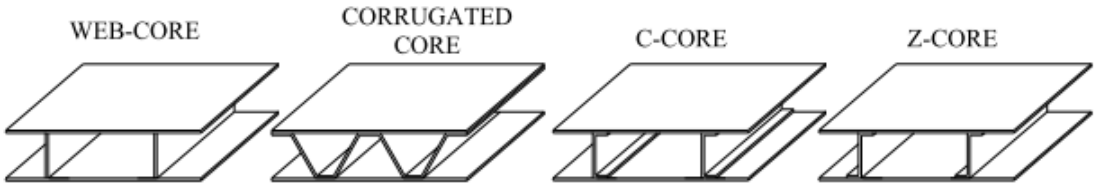

Figure 2 Examples of different web configurations [11].

The history of SSP dates back to the 1950s, when the properties of the SSP was already sought by the aircraft industry [12]. However, no cost-efficient way of joining the panel parts had yet been discovered and the development was stopped until new means of welding were invented. More recent research in the SSP-field has to some extent been conducted by the marine industry, though also for civil use and mainly in Europe [13].

2.1 Production

In production of SSP's, one difficulty is the joining of the face plates to the core. There are several ways of joining a steel sandwich panel, these include [8]:

- Welded joints
- Mechanically fastened joints
- Adhesively bonded joints
- Combined joints

The most commonly used joining technique being welding, the other with limited use or still under research [8]. A traditional welding technique such as gas metal arc welding is for example used in the production of conventional orthotropic steel bridge decks. However, it does not have a high enough energy density to perform a through thickness stake weld for the rather large thicknesses needed for bridge SSP's [6]. Instead, laser welding or hybrid laser-arc welding is proposed for joining of SSP's [6].

For the case when the sandwich panel is used as a bridge superstructure, or other similar applications where large areas have to be covered, joining between individual panels is needed. This joint will probably be done on site by manual work and might therefore be prone to fatigue damage [4]. However, this joint is out of scope for this thesis.

2.1.1 Laser welding

Laser welding utilizes the high energy density of the laser beam, which can be up to 50 kW [14]. The energy is very focused and amongst the highest of the welding techniques known today. As a result, the produced weld has a low width to depth ratio and low residual stresses as the surrounding material close to the weld path is not affected [14]. Moreover, it is possible to reach a high speed due to the fully automated process [8]. A simple draft on the effect of the laser beam on the surrounding area, can be seen in Figure 3.

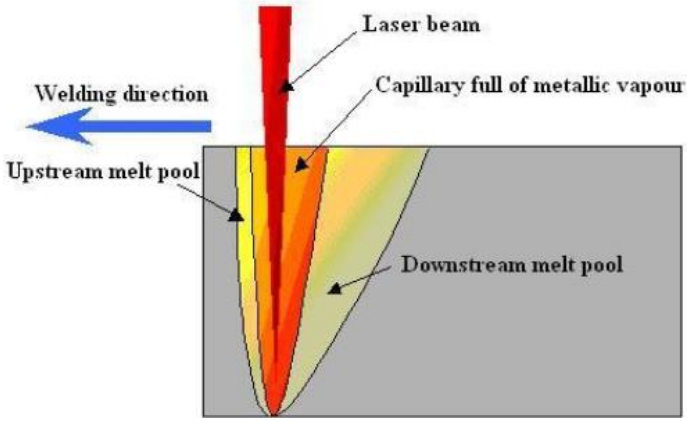

Figure 3 Basic draft of laser welding [[SOURCE]].

Although laser welding is very promising in certain regards, some of the drawbacks of the technique should be mentioned as well. These include, but are not limited to, a high initial and maintenance cost, poor efficiency (down to 2% for the highest performing) and a reduced ability to handle gap bridging [14].

2.1.2 Hybrid laser-arc welding

Hybrid Laser Arc Welding (HLAW) combines the use of laser welding with traditional Gas Metal Arc Welding (GMAW) to gain several advantages over conventional welding techniques [5].

While there are many positive aspects about GMAW, such as affordability and a high weld quality, the energy density capability is not sufficient to create a through thickness stake weld. Usually a semi-automatic production method is used when assembling conventional bridge decks, which may give rise to local irregularities and thus stress concentrations, which creates areas more prone to fatigue damage. To increase the energy density, which is the main drawback of GMAW, an additional laser beam can be used thus creating a hybrid solution.

HLAW is a highly automated welding process, while the operator still has precise control over the properties of the weld. This is beneficial with regards to distortion [5]. As stated earlier HLAW combines the main advantages of traditional welding and laser welding, which creates the following benefits:

- Highly automated which leads to low distortion and precise welding

- Small heat affected zone. The very high density of the laser heats the weld part and welds it before the neighboring material is affected by the heat leading to very low residual stresses which is good from a fatigue strength point of view.
- Speed is a major advantage of HLAW, since it is five to ten times faster compared to conventional methods.
- Due to the gas arc, the HLAW produces oxide free welds with guarantees good weld quality and safety conditions.

Nevertheless, there are obstacles related to HLAW in general and for usage in bridge construction in particular. Essentially, there are small amounts of published technical guidance for designers and welding engineers, with no standard being available in Europe yet [5]. According to [5], additional development is needed for codes, procedures and specifications, with extra focus on steel bridge components being crucial in this case. In 2014, the availability of HLAW was limited to 100 modules worldwide, with not a single one in Sweden [6].

3 Plate theory for SSP

Due to the geometry of SSP's, the structural stiffness will vary greatly in different directions of the sandwich member [6]. The core plates provide continuous support to the face plates in the longitudinal direction, but transversally the face plates are only periodically supported by the core. The connection method will also affect the structural behavior, where for example welds will rarely have the same thickness as the plates that are welded together [11]. It can thus be concluded that the SSP is a highly orthotropic structure.

To simplify the analysis of an SSP it can be homogenized, meaning that the periodic material behavior in every direction is simplified with an average stiffness constant. Homogenization of the member leads to a large reduction of the number of unknown variables. In the following sub-chapters where the stiffness constants and the governing equations will be presented, the sign convention and geometric definitions seen in Figure 4 will be used. The same kind of coordinate system will also be used for the finite element models introduced later. Additionally, the term "longitudinal" refers to the direction along the x-axis while "transversal" refers to the direction along the y-axis.

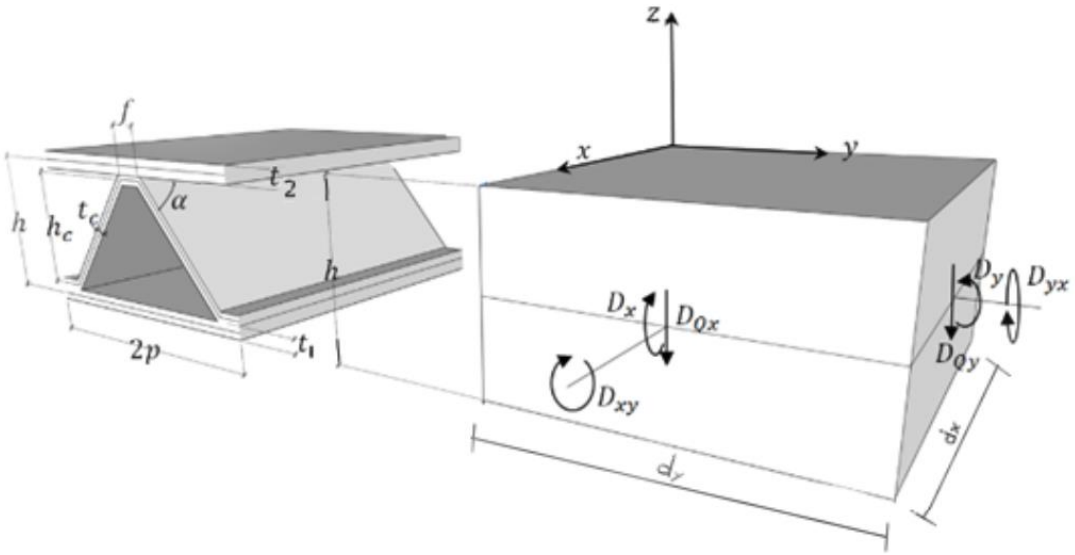

Figure 4 Definitions used in the homogenization of a corrugated steel panel [15].

3.1 Physical constants

The physical properties of the sandwich plate can be described by seven constants. The bending stiffnesses, D_x and D_y, the shear stiffness in the yz-plane (perpendicular to the corrugation axis) D_{Q_x} and the shear stiffness in the xz-plane (parallel to the corrugation axis) D_{Q_y}. The remaining three are the twisting stiffness D_{xy} and poisson ratio's ν_x and ν_y. The presented physical constants in this chapter were first derived by Libove and Hubka in 1951 [16].

If the only force acting on the small element in Figure 4 is a bending moment M_x, then D_x can be defined as the ratio between the moment and the primary curvature as:

$$D_x = -\frac{M_x}{\frac{\partial^2 w}{\partial^2 x^2}} \tag{1}$$

ν_x can then be defined as the ratio between the Poisson curvature and the primary curvature as:

$$\nu_x = -\frac{\frac{\partial^2 w}{\partial^2 y^2}}{\frac{\partial^2 w}{\partial^2 x^2}} \quad (2)$$

In a similar way, if only M_y is acting, D_y and ν_y is defined as:

$$D_y = -\frac{M_y}{\frac{\partial^2 w}{\partial^2 y^2}} \quad (3)$$

$$\nu_y = -\frac{\frac{\partial^2 w}{\partial^2 x^2}}{\frac{\partial^2 w}{\partial^2 y^2}} \quad (4)$$

For ν_f, being the Poisson's ratio in the flange, the ratios associated with bending can be expressed as follows:

$$\nu_x = \nu_f \quad (5)$$

$$\nu_y = \nu_x \frac{D_y}{D_x} \quad (6)$$

If only a twisting moment M_{xy} is acting on the small element dxdy, then a twisting distortion $\frac{\partial^2 w}{\partial x \partial y}$ is created. Consequently, D_{xy} is the ratio between the twisting moment and distortion as:

$$D_{xy} = -\frac{M_{xy}}{\frac{\partial^2 w}{\partial x \partial y}} \quad (7)$$

If only a vertical shear force, Q_x, is acting on the two opposite faces on a small element dxdy perpendicular to the corrugation, then the two faces will translate equally in opposite directions, see Figure 5, and create a shear angle γ_x.

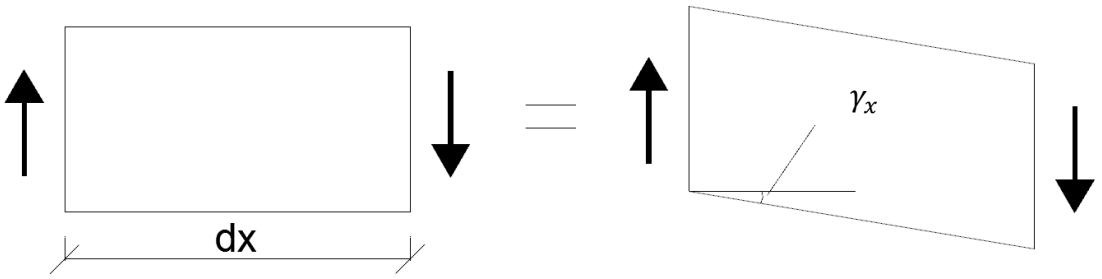

Figure 5 Shear force acting on a small element dx

The corresponding shear stiffness, D_{Qx} can then be defined as the ratio between the shear force and angle as:

$$D_{Qx} = \frac{Q_x}{\gamma_x} \quad (8)$$

By applying the same methodology, the shear stiffness in a plane orthogonal to the corrugation axis can be defined by:

$$D_{Qy} = \frac{Q_y}{\gamma_y} \quad (9)$$

3.2 Elastic stiffness constants

Elastic constants for homogenized corrugated core SSP's were derived by Libove & Hubka [16]. The constants derived by [16] were used in the project, except for D_y, which was taken from [17]. The elastic modulus in z-direction (direction of plate thickness) was assumed to be infinite, i.e. assuming the thickness to stay constant. Additionally, in the derivation they assumed only one connection between the core and face plates (i.e. one weld).

3.2.1 Elastic bending stiffness

The bending stiffness around the axis perpendicular to the corrugation D_x and the axis parallel to the corrugation D_y can be calculated as follows:

$$D_x = EI_x \tag{10}$$

$$D_y = \frac{EI_y}{1-\nu_1^2\left(1-\frac{EI_y}{EI_x}\right)} \tag{11}$$

where:

$$EI_x = E_c I_c^m + \frac{E_1 t_1 h^2}{2} \tag{12}$$

$$EI_y = \frac{E_1 t_1 h^2}{2} \tag{13}$$

and:

ν_1 Poisson's ratio of face-sheet material

E_1 Modulus of elasticity of face-sheet material

E_c Modulus of elasticity of core material

I_c^m 2nd moment of area, per unit width, of corrugation cross-sectional area about middle plane

t_1 Thickness of each face-sheet

h Distance between middle surfaces of face plates

If the faceplates are of different thickness (or any other reason that the center of gravity is not in the middle of the cross section), the parallel axis theorem should be applied to calculate the second moment of area of the cross section.

3.2.2 Torsional stiffness

The torsional stiffness of the sandwich panel can be calculated according to:

$$D_{xy} = 2GJ \tag{14}$$

$$GJ = \frac{G_1 t_1 h^2}{2} \tag{15}$$

where:

G_1 Shear modulus of elasticity of face sheet material

3.2.3 Transverse shear stiffness in the x-direction

The shear stiffness in the plane parallel to the corrugation axis can be calculated according to Equation 16.

$$D_{Q_x} = \frac{G_c I t_c h}{P \int_0^l Q \, ds} \tag{16}$$

where:

I Moment of inertia of width 2p of cross-section parallel to yz-plane, taken about the centroidal axis parallel to y-axis

$2p$ Corrugation pitch

l Length of one corrugation leg measured along the center line

s Coordinate measured along center line of corrugation leg

However, if the moment is assumed to be taken solely by the face plates which gives a constant shear flow in the corrugation, then the expression in Equation 16 can be simplified to the expression presented in Equation 17.

$$D_{Q_x} \sim \frac{G_c t_c h^2}{pl} = \frac{G_c t_c^2}{(A_c)^p} \left(\frac{h}{p}\right)^2 \tag{17}$$

The horizontal shear stiffness is defined by:

$$G_{xy} = GA = \frac{G_c t_c^2}{A_c} + Gt_1 + Gt_2 \tag{18}$$

Since several of the stiffness constants depend heavily on the assumptions that the corrugated core sandwich has a constant height, h, and the cross-section remain undistorted, tests were conducted to test the viability of these assumptions. As can be seen in last pages of [16], practical tests match the calculated values closely.

3.3 Transverse shear stiffness in the y-direction

The transverse shear stiffness for a dual-welded corrugated core plate, as opposed to the single welded plate considered in [16], was determined by Nilsson et al. in [17]. The derivation by Nilsson et al. included effects from rotational flexibility of welds as well as effects of shear deformations in the constituent elements of the sandwich plate.

An analytical solution was derived by solving Equation 19 for a stiffness matrix ***K***, force vector ***F*** and translation vector ***a***:

$$\boldsymbol{F} = \boldsymbol{K}\boldsymbol{a} \leftrightarrow \mathbf{a} = \mathbf{K}^{-1}\mathbf{F} \tag{19}$$

Where

$$\boldsymbol{F} = \begin{bmatrix} F_1 \\ F_2 \\ F_3 \\ F_4 \\ F_5 \\ F_6 \\ F_7 \end{bmatrix}$$

$$\boldsymbol{a} = \begin{bmatrix} a_1 \\ \vdots \\ a_7 \end{bmatrix}$$

$$\boldsymbol{K} = \begin{pmatrix} k_{11} & \cdots & k_{17} \\ \vdots & \ddots & \vdots \\ k_{71} & \cdots & k_{77} \end{pmatrix}$$

The system of equations in Equation 19 were defined for a half corrugation unit, as can be seen in Figure 6 (left). Figure 6 (right) shows the idealized response of the half corrugation unit when subjected to a unit shear load.

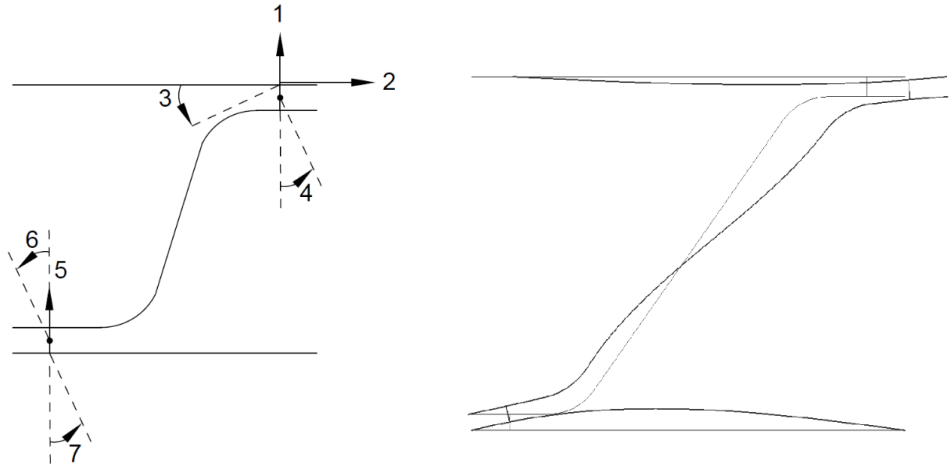

Figure 6 Deformation after the suggested load, from Nilsson et. al [17].

Defining an externally applied unit shear force as Q_y and the shear strain as γ_{yz}, the transverse shear stiffness could be expressed as Equation 20:

$$D_{Qy} = \frac{Q_y}{\gamma_{yz}} \tag{20}$$

where the shear strain was defined as

$$\gamma_{yz} = \frac{a_2}{h} + \frac{w}{p} \tag{21}$$

Here, a_2 is the translation in the second degree of freedom, h is the center distance between top and bottom face plates, p is the total width of a half corrugation unit and

w is the vertical deformation at the coordinate (y,z) = (p,h). The derivation presented in [17] assumed the vertical deformation to be equal to zero, because the cross-sectional height was also assumed to remain constant, which leads to the following expression for the shear stiffness:

$$D_{Qy} = \frac{h}{\mathrm{a}_2} \tag{22}$$

The calculation of the transverse shear stiffness is based on the direct stiffness method. By implementing a unit translation separately for each DOF, with all other DOF set to zero, the entries of the stiffness matrix ***K*** was determined. Since the translations are either one or zero, each set of reaction forces will constitute one column of the stiffness matrix ***K***, corresponding to the DOF with a unit translation. After determining ***K***, the DOF's of ***a*** can be solved by inserting a known force vector ***F*** into Equation 19. Once ***a*** is solved, the transversal shear stiffness is easily calculated with Equation 22.

4 FE-modelling of steel sandwich panels

Due to the complex geometry of the sandwich panel, using analytical methods to solve for displacement or stress in the individual members of the panel can be very difficult. Since the beginning of the 1960s, numerical methods such as the finite element method (FEM), have been used to analyze complicated structures. Although the digital computer had to be developed before FEM matured enough to be used commercially [18].

Currently, there are several commercial software available to carry out FEAs. These software, of varying complexity and resolution, contain several element types and interaction techniques that can be used in modelling and analysis of sandwich panels. However, although a wide range of element types exist in these software, it is important to use the right type of element and an adequate mesh size to gain sufficiently accurate results. It is also possible that a different type of element can model the same type of problem, but a certain element might have a higher computational cost or give less accuracy [19]. Consequently, time and reliability can be assessed by exploring the different available elements.

As a result of the complex nature of FEM and the wide range of modelling choices, this chapter aims to create knowledge of how FE modelling of sandwich panels has been carried out in previous research projects. A large focus is placed on different available element types and which aspects should be considered when choosing a certain FE-element. Additionally, the interaction technique used for weld modelling is reviewed. The oldest sources are from the beginning of the 90s and the latest are newly published. This is good to keep in mind as the computational resources have seen a tremendous increase over this time frame.

4.1 Structural element types for FE-modelling

The three most commonly used element types in FE-modelling are the beam-, shell- and solid-elements [20]. These also have different sub-categories depending on application and properties sought.

4.1.1 Solid elements

Solid, or “continuum”, elements are referred to as the standard element in the commercial FE-software Abaqus/CAE [21]. This element category does not include elements such as beams or shells, or any type of special-purpose- or connector-element. Examples of a standard 6-node and 8-node solid element can be seen in Figure 7. Solid elements can be used for both linear and non-linear analysis, including plasticity and contact modelling, and are suitable for a large variety of applications, such as stress, heat transfer and acoustics. Because of the versatility and many fields of application of solid elements, it is important that the particular application is matched by the choice of element type.

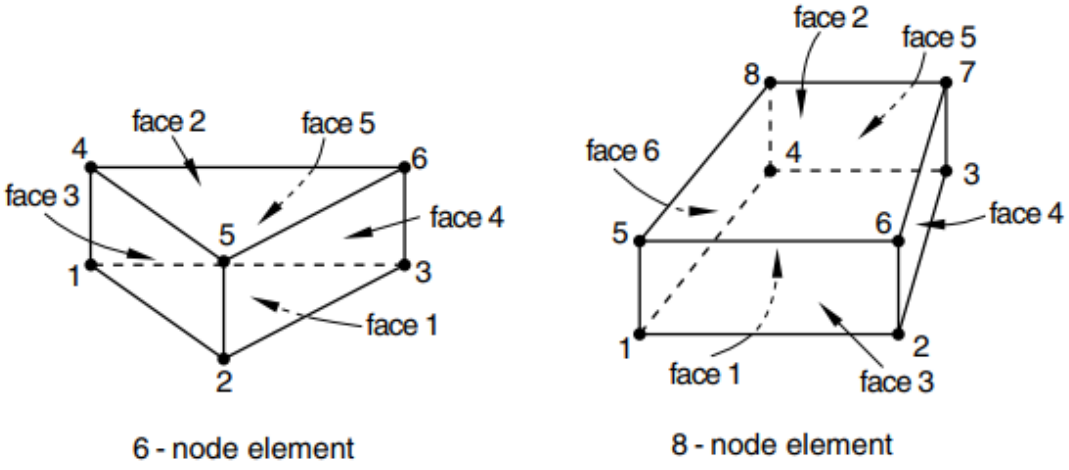

Figure 7 Examples of available solid elements in Abaqus [21].

Abaqus/CAE offers solid elements in one, two or three dimensions. The geometries can be specified as triangular or quadrilateral shapes, triangular or brick prisms, and can have parabolic or cylindrically curved edges. All of the geometric options can be modelled with linear or quadratic interpolation elements, as well as specifying whether full or reduced integration should be utilized when running an analysis.

The choice between first- or second-order elements depends on the nature of the studied problem [22]. Second-order elements are better at evaluating cases with severe element distortion and they are generally more versatile than first-order elements. The increased versatility comes mainly from being able to capture accurate results while using fewer elements compared to first-order elements [21]. Thus, second-order elements capture stress concentrations more effectively and are superior for certain geometric features, such as curved surfaces, since they can be modelled with fewer elements along the curvature. The trade-off between first- and second-order elements can often be described as a higher number of first-order elements with a lower computational requirement versus a lower amount of second-order elements with more heavy computation [22].

4.1.2 Beam elements

A beam element is a one dimensional element either in three-dimensional space or in a two-dimensional plane [21]. Beam elements are related to the assumptions related to beam theory, which formulate the one-dimensional approximation of a higher order dimension continuum. Beam elements have a stiffness related to deformation of the beam's main axis – the possible deformations being axial stretch and bending, as well as torsion for the case of three dimensional space. The main advantage of beam elements is that they can be modelled with very simple geometries and that they are easy to evaluate, due to having relatively few degrees of freedom compared to other structural elements [21]. The critical issue for beam elements is often to evaluate whether the approximations related to these elements are appropriate for the problem at hand.

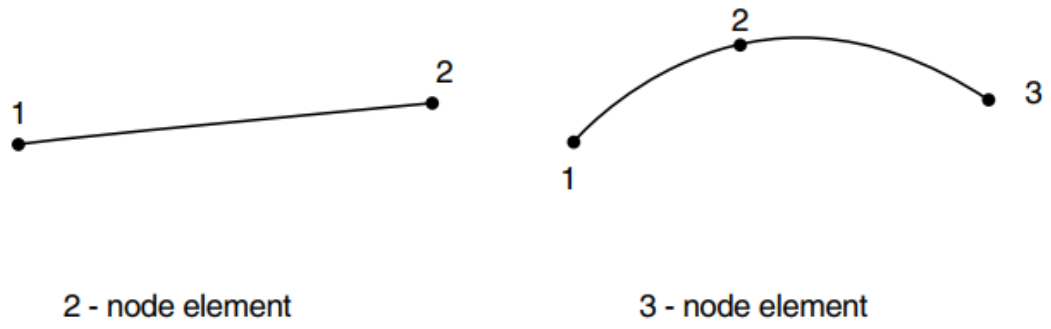

Figure 8 Simple examples of a structural beam element in Abaqus [21].

FE-software offer a variety of available beam elements. The choice of beam element type is defined on several different levels which can be combined interchangeably according to what properties are desired, including; beam or pipe element type, defined in either plane or space, with linear, quadratic, cubic or initially straight cubic interpolation formulations, having an open or closed section and with the additional choice of a hybrid formulation [21].

One important distinction for beam elements is made between the Euler-Bernoulli and Timoshenko beam-theories. The Euler-Bernoulli beam is preferably used when the beam can be classified as "slender" – cross-sectional dimensions being less than approximately 1/15 of the axial length [21]. Since Euler-Bernoulli-beams are assumed to have a small cross-section, transverse shear deformations are neglected.

The Timoshenko beam, on the other hand, is defined for more prominent cross-section dimensions – up to approximately 1/8 of the axial length [21] - which allows for transverse shear deformations to be included in the analysis. This type of beam element is more suitable for "thick" beams, although it can also be used for slender beams. Timoshenko beam modelling can give useful results for cross-sectional dimensions up to 1/8 of the axial length of the element [21]. For even more stout geometries, it is recommended to not use beam elements.

4.1.3 Shell elements

Generally, it is recommended to use shell elements when the out of plane thickness is considerably smaller than the other dimensions. Additionally, according to the formulation of shell elements, the out of plane thickness is only considered as a structural property in the analysis. A state of plane stress is present in all shell elements, whereby the out of plane stress should not be important to the user [23]. If this is sought, solid elements should be used instead. In general, shells are more computationally efficient than solid elements but less than the beam element.

The shell element relates to what is known in mechanics [24] as the Kirchhoff and Mindlin-Reissner plate theories, where the latter considers shear deformations. Shell elements can therefore be divided into two different sub-classes, called thin (Kirchhoff) and thick (Mindlin-Reissner). Thick shells should be used when the transverse shear deformation have a considerable impact on the structure, analog to the Mindlin-Reissner plate theory.

In general, most FE-software such as ANSYS [25] and Abaqus/CAE [23] contain shell elements with formulation of both theories, in Abaqus/CAE this is for example the S4R

element and in ANSYS the SHELL181-element. However, special-purpose elements that are more efficient in either the thick or thin formulation also exist and can be used for enhanced performance.

Shell elements can be either rectangular or triangular and have at least one integration point in-plane. Higher order shell elements have an additional node in-between every corner node, see Figure 9 (right side), this also means that the shape function is of higher order i.e. quadratic or even cubic.

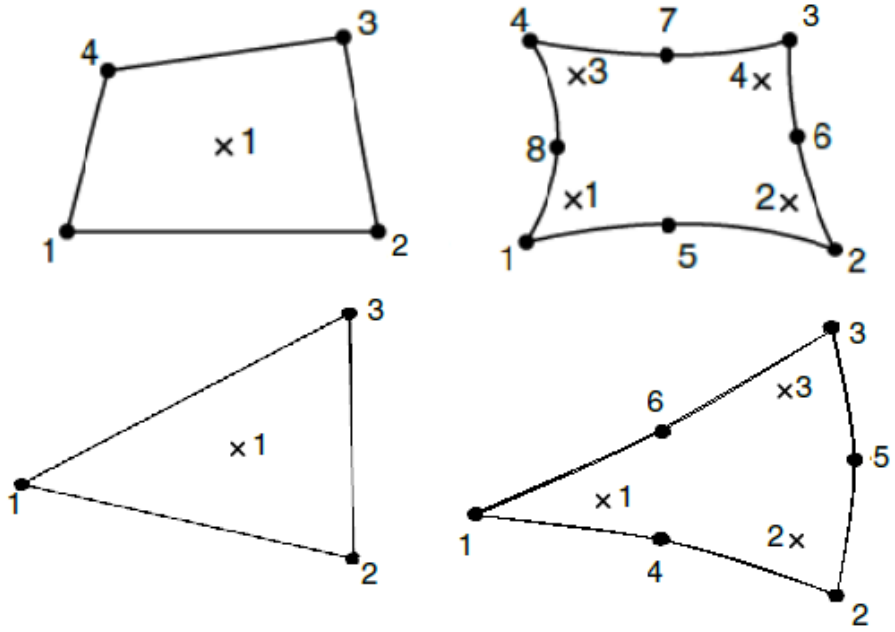

Figure 9 *Quadrilateral shell element with 4/8 nodes and 1/4 integration point(s) (top), triangular 3/6 node element with 1/3 integration point(s) (bottom) [21].*

Displacements are calculated in the nodes and stresses in the integration point(s). For linear analysis, three integration points over the thickness (also known as Gauss points) are enough while non-linear analysis with plastic deformations might require more [23].

4.2 Previous FE-modelling of SSP's

This chapter will look at some previously conducted studies of SSP's and specifically how FE-modelling was approached, in terms of assumptions, element choice and modelling of welds.

4.2.1 Previous 3D-modelling of SSP's / corrugated core SSP

One of the early attempts to model a 3D steel sandwich panel, utilizing FE-analysis, was conducted by Tan et al. [26] in 1989. This paper compared the results for a 3D corrugated core SSE FE-model (Figure 10) with a closed form solution as well as experimental results. Tan et al. built the entire 3D-model using S8R (standard shell, 8-node, reduced integration) shell elements, which they further claim to be an element meant mainly for modelling of thin plates [26]. This statement contradicts more recent sources, such as the Abaqus User's Manual [21], which refers to the S8R-element as a typical thick shell element. Whether there was a misunderstanding from the side of Tan

et al. or if the naming or structural formulation of elements in Abaqus have changed since 1989, remains unclear to the authors.

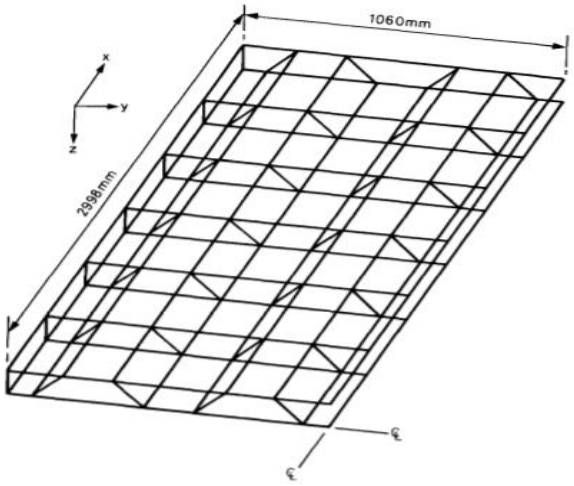

Figure 10 3D mesh model of the SSP considered by Tan et al. [26]

More recent studies show a variety of different element choices for 3D FE-modelling of corrugated core SSP's. A 4-node shear deformable shell element with reduced integration (S4R) is used for example by Kazemahvazi & Zenkert [27] and Valdevit et al. [28].

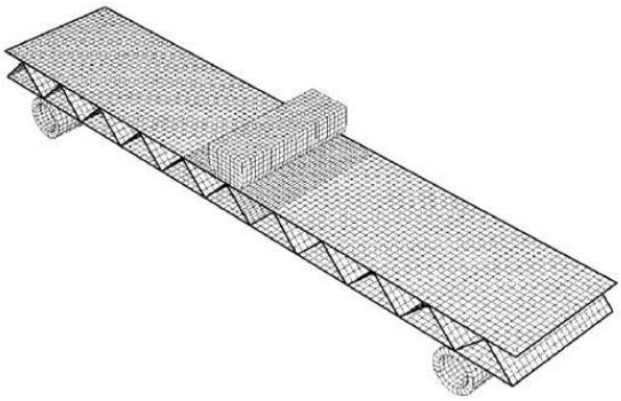

Figure 11 Studied geometry case by Valdevit et al, loading case with distribution transversally [28].

Leekitwattana et al. [29], who evaluate steel bi-directional corrugated-strip-core sandwich beams in the FE-software ANSYS (11.0), create their entire geometry with a linear elastic 8-node solid element (SOLID45), see Figure 12.

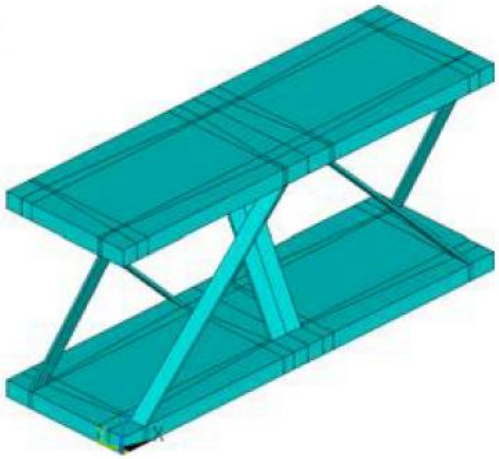

Figure 12 *FE-model of a bi-directional corrugated-strip-core sandwich panel, created with solid elements [29].*

Yet another approach was carried out by Romanoff et al. [30], when studying the response of laser-welded web-core sandwich panels subjected to patch loading. Here, a 3D web-core steel sandwich panel was modelled both with solid and shell elements, and then these were both compared to results from an approach based on only 2D-models. The geometry modelled with solid elements can be seen in Figure 13. The element types used for the FE-model were C3D20 (continuum stress/displacement element, 3-dimensional, 20 nodes) solid elements and parabolic, reduced integration S8R shell elements. Additionally, the computing times required to run the models were noted in [30] as 20 minutes for the shell model and 9 hours for the solid model.

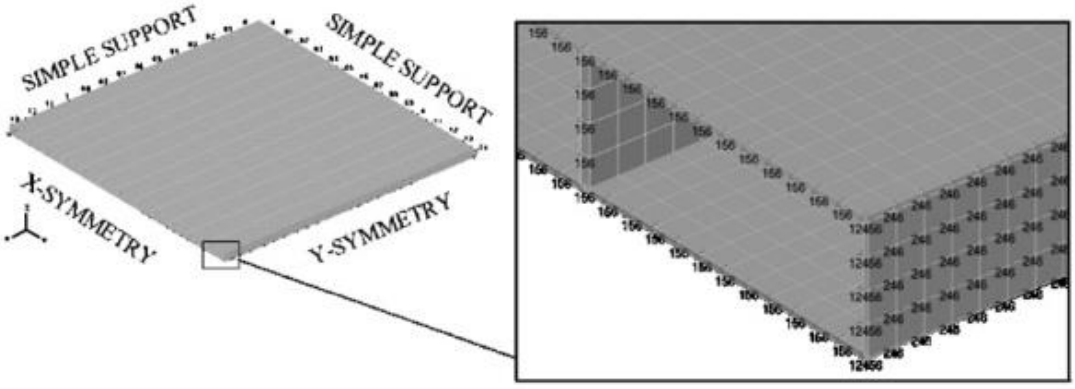

Figure 13 *Web-core steel sandwich panel 3D FE-model, as created and studied by Romanoff et al. [30].*

4.2.2 Previous FE-modelling of welds in a 3D environment

Since the welds are one of the most critical parts of the corrugated core SSP, they will naturally have a big importance in the FE-model as well. They are also quite complicated, in terms of modelling technique, as they must act as a connection between the face plates and corrugated core. Some previously used approaches to FE-modelling of welds will here be presented.

Starting again with [26], Tan et al. chose to model their web-core-connections as spot-welds. The welds were created as Timoshenko deep-beam elements (B31), where one

of the main concerns was to achieve compatibility between the beam element and the S8R shell elements used for the rest of the model.

Neither [27] nor [28] mention any considerations concerning modelling of welds. Leekitwattana et al. [29] model their welds as complete rigid connections between the face plates and core.

Romanoff et al. [30] used two different approaches to weld modelling, depending on the type of elements used for the rest of the model.

- When S8R shell elements were used for the model, all welds were assumed to provide a completely stiff response and they were simulated as rigid constraints between face plate and core, inserted at the position of the weld.
- When the sandwich panel was modelled with solid elements, the welds were instead simulated with spring elements. The stiffness's inserted into the spring elements were calculated based on theory that was also developed separately in [30].

4.3 Equivalent Single Layer approach

The ESL-approach and the so-called "layer-wise theory", are the most prominent methods used for analyzing layered materials [24]. These layered materials can, in a similar manner to the SSP, have a low stiffness core surrounded by higher stiffness face sheets. In the layer-wise theory the stresses in the different layers are considered depending on the stiffness of each corresponding layer, while in the ESL-approach the stiffnesses of the layers are smeared out over the thickness, essentially preventing the stress in the individual layers to be evaluated. In the sandwich theory described in Chapter 3 a similar assumption is made, where the periodicity of the corrugated SSP is transformed into a homogeneous stiffness. This leads to a decreasing number of unknowns which makes the structural response easier to solve (and thus faster FEAs).

The homogenization process results in an inability to capture local response, meaning that the equivalent single layer approach (ESL) cannot be used for analysis of individual members. Nevertheless, by using the ESL modelling technique, the elastic constants from Chapter 3 can be used in FE-modelling and the global behavior can be analyzed. As the initial problem is simplified, utilization of the ESL-approach can be beneficial in the early design phase and should preferably be combined with analytical solutions or hand calculations [8].

In research related to the sandwich panel, the ESL-approach has previously been successfully applied to check the global verification of 3D-models as well as sectional constants, for different core configurations [11, 31]. The approach has also been applied in a more practical way, by Dackman & Ek [15], where an ESL model was used to represent the deck of a steel girder bridge with a sandwich deck. This study showed promising results, however, the effect of a locally applied load was neglected. The same was carried out by [32] whom also modelled a bridge deck to investigate panel to panel joints. All FE-analyses were carried out with eight-node second-order elements using the Abaqus/CAE or the MSC Marc software.

4.4 Modelling of local behavior

The homogenization theory proposed by Libove and Batdorf [12] does not capture the local behavior of the sandwich panel under a patch load [30]. This is a direct consequence of the assumption that local bending of the face plates under direct load is omitted. However, from research conducted by Romanoff et al. [30] and Bright and Smith [33], it was concluded that the impact of local loads is important for the overall stress prediction of the sandwich panel. Since it is very plausible that local patch loads create local effects, such as a local bending moment in the top face plate, the global response calculated according to Libove and Batdorf should be complemented by a local analysis.

4.4.1 Multi-scale approach

In a study on the web-core sandwich, Romanoff et al. [30] argues that the local deflection caused by a directly applied load can be added to the global behavior through super positioning. An assumption is made for the global model, similarly to assumptions by Libove and Batdorf [12], where a unit cell is homogenized and only the average response in every direction is considered. This approximation leads to zero local deflection w_q directly under the load, which does not reflect reality. It was therefore concluded that the local patch load deflection must be solved separately from the global deflection if the homogenization approach is to be used.

Therefore, an additional FE-model was introduced to capture the local response. This model focuses on the geometry immediately surrounding the area of load application, see Figure 14.

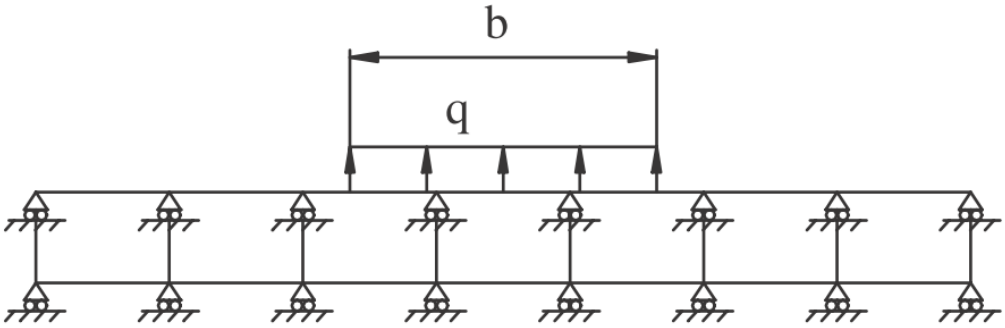

Figure 14 *2D local model used to capture the local response from patch loading [30].*

Further, the local deflection of the face plate was divided into one part caused by global shear, and one part related to "thick plate behavior". The thick face plate effect is further explained in [34]. The last factor contributing to the local deflection, is the local deformation caused directly by the patch load [30]. The described approach is illustrated in Figure 15.

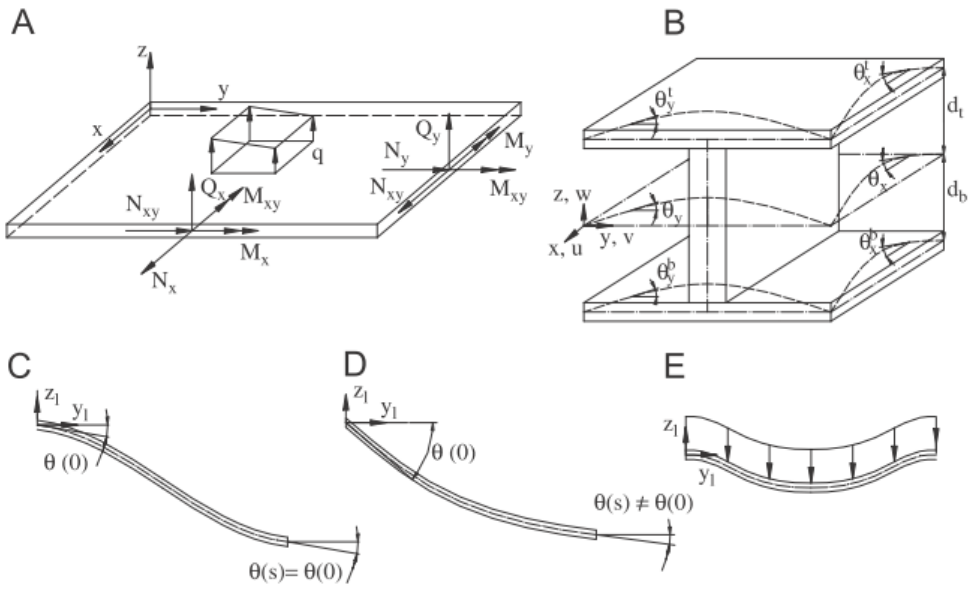

Figure 15 *Rotations in web core sandwich element under local patch loads, deflection due to global shear (C), deflection due to thick face plate (D) and deflection due to patch load (E) [30].*

The resulting total local deflection can thus be described by:

$$w_l = w_Q + w_{tf} + w_q \tag{23}$$

where w_Q is the deflection related to shear; assuming equal slopes at the cell edges, w_{tf} is the deflection caused by the thick face plate effect, assuming unequal slopes at the cell edges and w_q is the deflection from the local model caused by directly applied load.

To validate the suggested approach, it was proposed that an alternative 3D model of the sandwich plate, consisting of either plate or solid elements, should be created for the purpose of comparing the resulting deflections. If boundary conditions for the local model could be chosen so that the total deflection aligned with the result from the global model, then the simplified approach should in theory be valid for any chosen geometry for the sandwich element. In the end, results in [30] between the suggested approach from Equation 23 and 3D FE-analyses matched very closely.

Because the detailed 3D analysis must capture both the local and global behavior in the same model, it requires both accurate modelling of a large geometry as well as sufficient resolution of the small details around welds. This type of model will thus inherently have a large number of elements. The main advantage that the simplified approach offers is a drastic reduction for the time required to run the computational analysis of the models. It was reported in [30] that the models for the suggested approach took 15 seconds to run, while the 3D shell element rendering of the same geometry took 20 min and the solid element option took 9 hours.

5 Case studies

This chapter will preface the performed case study. First, the four investigated geometric configurations of SSP's are introduced and then the three different loading cases, as well as their intended purposes for the study, are presented.

5.1 Properties of the investigated sandwich panels

As the structural behavior of a corrugated core sandwich can vary greatly depending on the geometric properties, four different geometric cases were evaluated. The properties of the studied cases were given a lot of variance, in order to increase the width of the study, while still being somewhat reasonable design alternatives. A summary of the properties of the four studied geometry cases can be seen in Table 1.

Table 1 Geometric properties of the considered cases.

Notation	Unit	Case 1	Case 2	Case 3	Case 4
t_2	[mm]	8	9	6	15
t_c	[mm]	6	7	6	9
t_1	[mm]	5	9	10	10
$f_1=f_2$	[mm]	50	75	100	150
h	[mm]	132	300	100	450
t_w	[mm]	2	2	2	2
$R_1=R_2$	[mm]	12	14	14	20
d_w	[mm]	30	30	50	60
θ	[°]	65	80	40	55

The notations used in Table 1 and throughout the rest of the report, represent the following properties; $t_{1,2}$ is the thickness of the bottom and top face plate respectively, t_c is the thickness of the core plate, $f_{1,2}$ is the respective length of the bottom and top

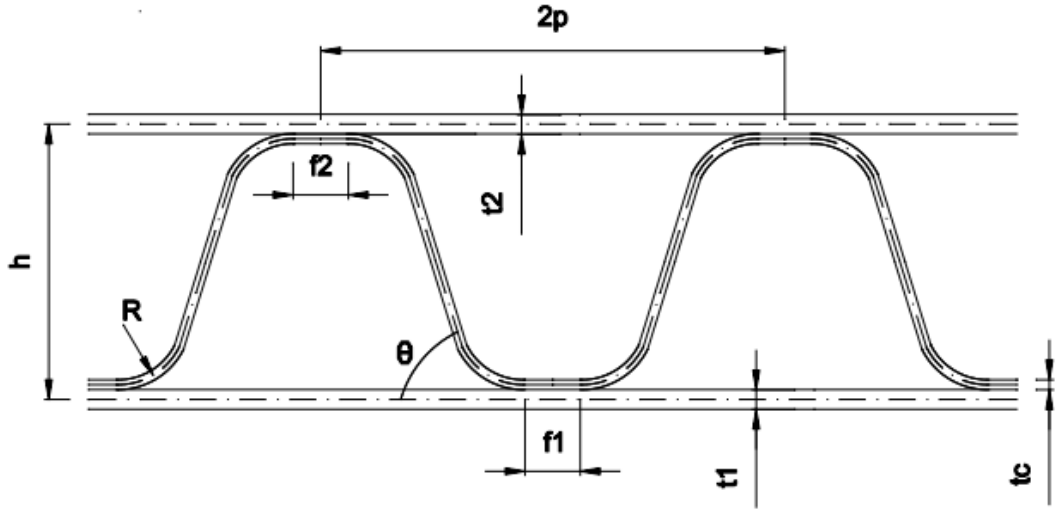

Figure 16 Geometric notations used in case study [6].

horizontal parts of the core, h is the center distance between the face plates, t_w is the thickness of the welds, $R_{1,2}$ is the radius of the lower and upper rounded parts of the corrugated core, d_w is the distance between the welds at each crest and θ is the angle from the face plates to the tilted parts of the core. This is visually described in Figure 16.

5.2 Load cases

A variation of load cases were considered and used to validate and investigate different aspects. Having several load cases allowed for a more flexible approach when addressing unexpected results and also providing more depth to the analysis.

5.2.1 Load case 1

Load case 1 was the main load case used throughout the study and was meant to simulate the behavior of a sandwich panel exposed to patch loading, see Figure 17a. The patch load was applied on the top face plate as a pressure load over 0.5x0.5 m^2 with a magnitude of 240 kPa, equivalent to a total load of 60 kN. In accordance with the theory presented, this patch load should be able to be placed anywhere on the model, however, to avoid influence from support boundaries the load was generally placed close to the center.

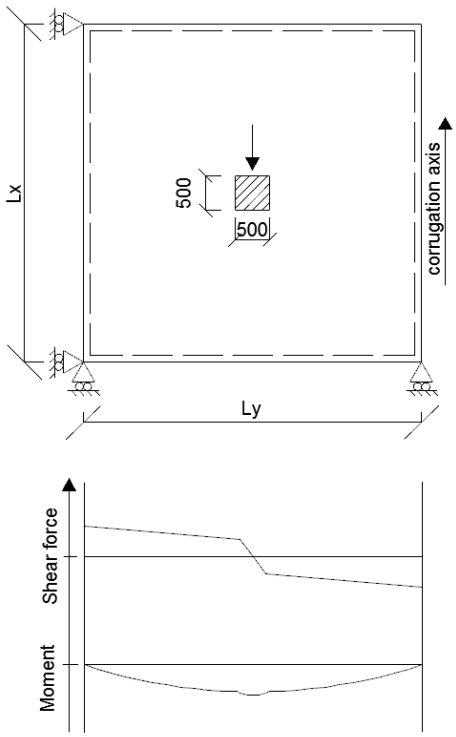

Figure 17 a) Drawing of load case 1. b) Principal plot of the global transversal shear and moment at Lx/2.

To allow for plate action in x- and y-directions, movement in z-direction (vertically) was restricted with simply supported boundary conditions along all four edges. Additionally, rigid-body-motion was prevented by restricting the plate in two corners each for both in-plane directions.

Transversal shear force and moment distribution created by load case 1 can be seen in Figure 17b. The shear force will vary over the model due to how the load is distributed to supports in the longitudinal direction.

5.2.2 Load case 2

The second load case was introduced mainly to provide a case that was more simple to analyze, compared to load case 1. Case 2 has a 120 kPa pressure load applied on an area of the top face plate corresponding to the entire model length and a width of 0.5 meters, see Figure 18a. Vertical boundary conditions were applied on the two outer edges in transversal direction and rigid body motion is prevented similarly as for load case 1.

The combination of the extended pressure load and decreased vertical boundary conditions, transforms the plate action from load case 1 to transversal beam action for this case. With the plate acting as a beam, the transversal shear force will be constant and the moment distribution will be linear between the applied forces and boundary conditions, see Figure 18b.

Results from load case 2 were easy to analyze mainly due to the state of constant shear forces, since this narrows down plausible erroneous contributing factors. Also, shear forces were assumed to be constant for some approaches used throughout the study, so then this load case could be used to validate those approaches.

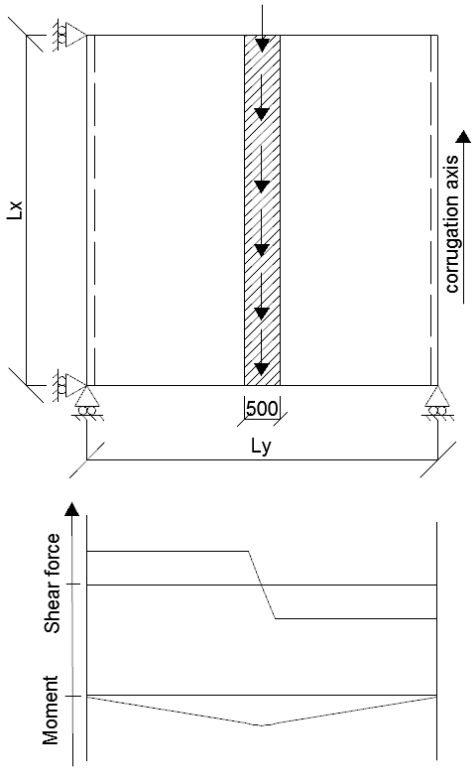

Figure 18 a) Drawing of load case 2. b) Principal plot of the global transversal shear and moment at Lx/2.

5.2.3 Load case 3

Load case 3, see Figure 19, utilizes the same boundary conditions as case 1; all four edges restricted vertically while rigid body motion is prevented with additional in-plane restrictions. A global pressure load was applied over the whole top faceplate with a magnitude of one unit pressure, 1 Pa.

This load case was used to verify the global response of the 2D homogenized shell model against the 3D model.

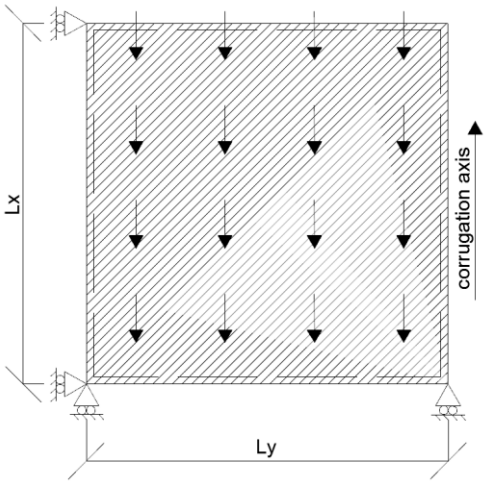

Figure 19 Drawing of load case 3.

6 FE-models used for the study

All FE-models were created and analyzed using the software BRIGADE/Plus 6.1-11 (which is based on Abaqus/CAE 6.14) developed specifically for FE-analysis of bridges. These software have a Python interpreter which allows the user to create scripts to aid modelling and analysis. This was utilized in the creation of all models built in this project.

To act as a reference point for the study, a 3D finite element model was established and analyzed. A 2D homogenized shell model was used to simulate the global behavior of the 3D model and later a 2D beam model was introduced to simulate the local behavior directly below the patch load. Where the results diverged, causes to the differences were identified and attempted to capture with alternative models and approaches.

6.1 3D shell FE-model

To act as a point of reference in the verification study, a fully detailed model of an approximately 5x5 m^2 sandwich deck was created. For geometry case 1 this corresponded to a width of 21 corrugation units. 21 unit cells were also used for the width of the other geometry cases, but the longitudinal lengths were adjusted to maintain an aspect ratio of about 1.

As can be seen in Figure 20, the 3D FE-model used shell elements for the face plates and the web. Eight-node quadrilateral elements with quadratic shape functions and reduced integration, S8R, were used for the mesh. The Young's modulus was chosen to 210 GPa and Poisson's ratio to 0.3.

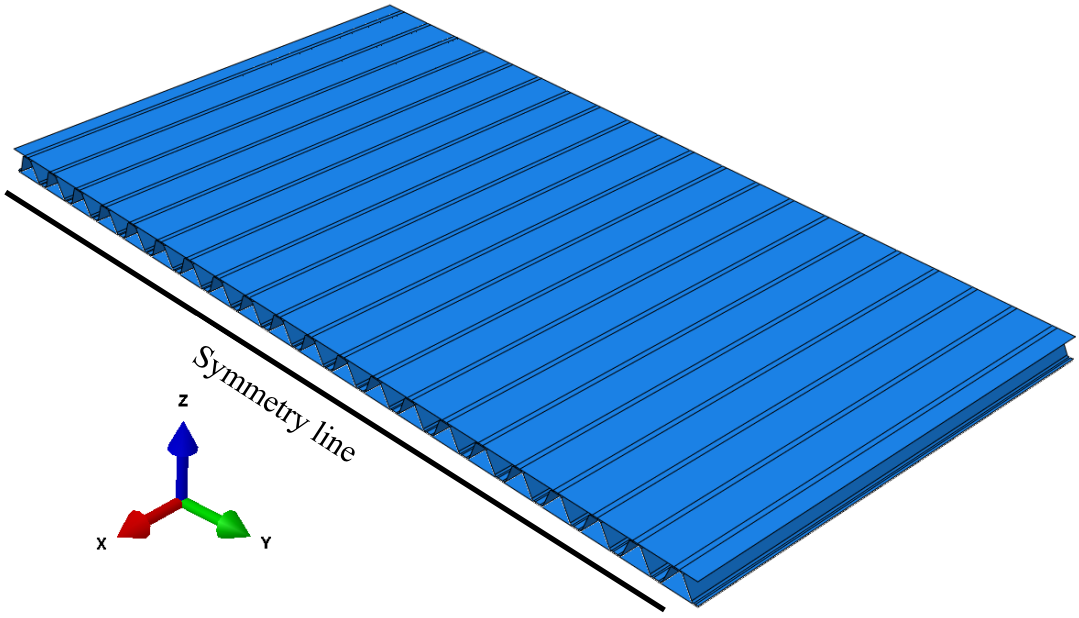

Figure 20 The final 3D model in BRIGADE/Plus, geometry case 1.

Rigid connections between the core and face plates was used to simulate the welds. As such, the welds were not physically modelled, but rather just implemented as rigid constraints. This is similar to the assumption made by Libove and Hubka [16] in their derivation of the sectional constants presented in Chapter 3, although they assume only a single welded connection per corrugation cell.

Since the final model turned out to be very large and computationally heavy, attempts were made to reduce the size of the model. The symmetric shape was utilized by introducing a symmetric boundary condition around the x-axis, at half the length in the direction parallel to the corrugation axis. This was done by preventing movement in x-direction and rotation around y- and z- axes for all nodes on the boundary.

6.1.1 Convergence study for mesh size

A convergence study was carried out to determine an appropriate size for the mesh of the 3D FE-model. The study included local moment in the top face plate and maximum vertical translation, both investigated by their dependence on the total number of elements used in the model. Results can be seen in Figure 21a (translation) and Figure 21a (local moment). The translation for each mesh size was extracted as the maximum deflection in the mid span, while the transversal local moment in the top faceplate was extracted from a certain chosen node with the exact same coordinates for all investigated cases.

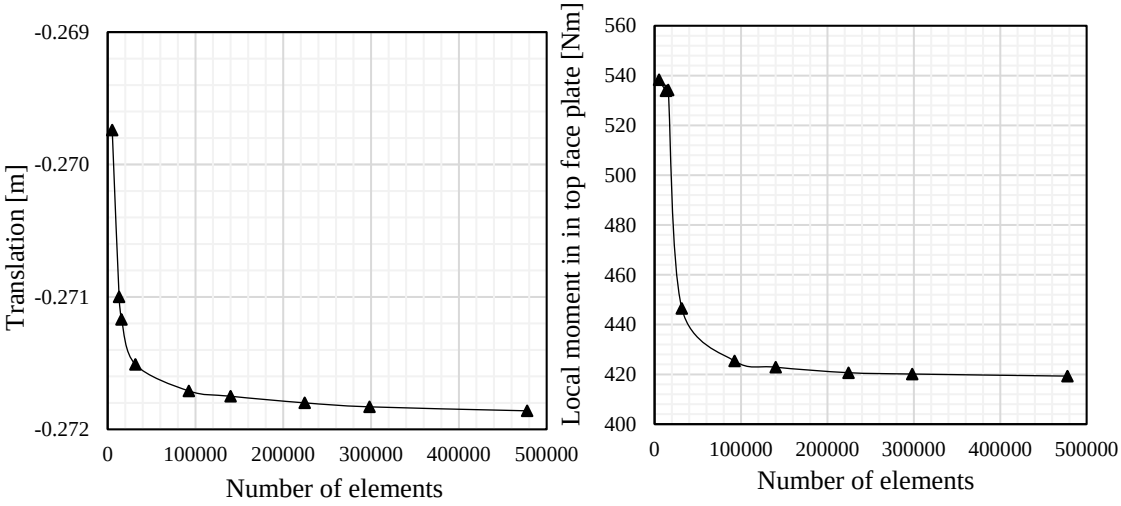

Figure 21 *a) Convergence with regards to translation. b) Convergence with regards to local moment in the top plate.*

As can be expected, the vertical translation converges faster than the local moment. This is realized by noting that very different scales were used for the graphs in Figure 21, where the changes for translation were small compared to changes in local moment.

Although convergence was reached for around 150 000-200 000 elements, another aspect had to be considered for the choice of a global mesh size. In order to correctly capture the behavior in between welds, it was noticed that at least three elements were required in transversal direction. Combining the restrictions set for the mesh between welds, with a global mesh corresponding to 150 000 elements, this led to a very bad element aspect ratio that the modelling software struggled to produce. To assure consistency a global mesh size of 0.0125 m, corresponding to about 300 000 elements, was chosen for the FE-model. Similar results could be seen for the other geometric cases, see Appendix A, and the same or slightly larger mesh was used in these cases.

6.2 2D homogenized equivalent single layer FE-model

The 2D Equivalent Single Layer (ESL) plate was modelled using a single shell plane, see Figure 22. The in-plane sizes longitudinally and transversally were set as the size of the 3D-model and the section shell thickness was defined as the height between the face plates, h. Eight-node quadrilateral elements (S8R) with quadratic shape functions were used and a set global mesh size of 0.01 m was used for the whole model.

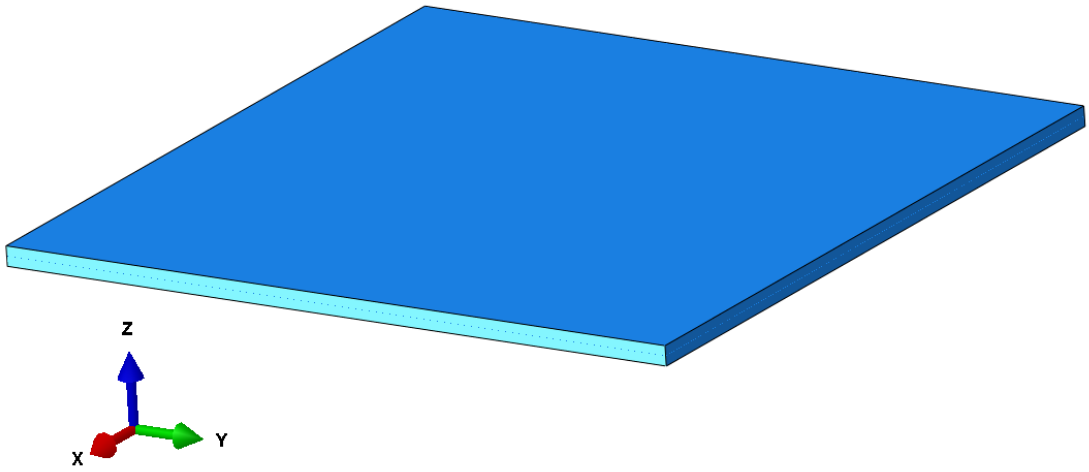

Figure 22 The ESL-shell modelled in BRIGADE/Plus, with shell thickness enabled.

The material property was defined as "lamina", which allows the user to define the bending stiffnesses E_x and E_y, possion's ratio ν_{12}, twisting stiffness G_{xy} and the shear stiffnesses G_{xz} and G_{yz}. The elastic constants presented in Chapter 3 were converted into engineering constants according to Equations 24a and 24b given by [31].

$$E_x = \frac{12D_x}{h^3} \qquad E_y = \frac{12D_y}{h^3} \qquad \nu_{xy} = \nu_x \tag{24a}$$

$$G_{xy} = \frac{6D_{xy}}{h^3} \qquad G_{xz} = \frac{D_{Qx}}{kh} \qquad G_{yz} = \frac{D_{Qy}}{kh} \tag{24b}$$

Where h corresponds to the vertical height between the face sheets and the shear correction factor k taken as 5/6.

The equivalent elastic constants D_x, D_y, D_{xy} and D_{Qx} were determined according to Chapter 3. Table 2 shows the engineering constants for each investigated geometry case.

Table 2 Stiffnesses of the different geometric cases.

Notation	Unit	Case 1	Case 2	Case 3	Case 4
E_x ($*10^{10}$)	[N/m]	7.991	5.39	11.50	4.235
E_y ($*10^{10}$)	[N/m]	6.083	3.886	9.697	3.441
ν_{xy}	-	0.3	0.3	0.3	0.3
G_{xy} ($*10^{10}$)	[N/m]	2.288	1.454	3.694	1.303
G_{xz} ($*10^{9}$)	[N/m]	3.273	3.615	1.126	1.207
G_{yz} ($*10^{7}$)	[N/m]	13.39	2.394	11.92	2.624

6.2.1 Global verification of ESL shell model.

The global response of the ESL shell model was verified against the 3D-model by comparing the maximum global deflection. One 3D-model and one ESL model was constructed with each case geometry and then studied under a uniform load distributed on the whole top face plate, load case 3, see section 5.2.3. The deflection in the 3D-model was extracted from the bottom plate, to avoid any interference from local deflections in the top plate and web, while the ESL deflection corresponds to an averaged value due to the homogenization of the cross-section. The deflections were extracted at the same in-plane coordinate. The results of the study can be seen in Table 3.

Table 3 Comparison in deflection under one unit pressure.

Case	3D	ESL-shell	Difference
1	2.72E-07	2.72E-07	0.00%
2	7.18E-07	7.10E-07	1.18%
3	7.12E-07	7.10E-07	0.30%
4	3.74E-06	3.61E-06	3.50%

Deflections were compared for the fully converged case of both models. A difference between 0.0% and maximum of 3.5% can be seen. The deflections for case 2 and 3 modelled with the ESL-approach have the same deflection, this is purely a coincidence – case 2 is much stiffer but has a greater span. Generally, the cases with a large distance between the face plates compared to the unit cell width 2p have a greater deviation from the deflection of the 3D-model. This is probably related to the boundary condition and how they are implemented in the different models, on the mid-section in the ESL-plate while on the edges of the bottom plate in the 3D-model. Consequently, the ESL-model was deemed verified.

6.3 2D beam model

A 2D cross section model made of beam elements was introduced to capture the local response directly under the patch load. The model was created using 21 unit cells, to make sure to represent an "infinitely" wide deck and thus avoid influence from edges, see Figure 23 (top). Second order 3-node beam elements, B22, were used to model the web and face plates. The depth in the out-of-plane direction was set to one meter to make the resulting load effects have the unit of [xx/m] similar to the the shell models.

A separate load area was introduced in this model, onto which the patch load was applied. The load area was modelled using a beam element with a very low stiffness that was rigidly connected to the top faceplate. The load was applied as a pressure load, 120 kN/m^2 over 0.5 meters in the y-direction making the total load equal to 60 kN.

As the local model is a cross sectional cut of a larger structure, assumed infinite also in the depth direction (x-direction), it is reasonable to assume plain strain condition for this case. Consequently, the material properties were calculated to match this assumption according to Equation 25:

$$E_{p.s} = \frac{E}{1-\nu^2} \tag{25}$$

Where E is the elastic modulus of steel, 210 GPa and ν the Poisson's ratio, 0.3, for the same material. Inserting E and ν into Equation 24 yields $E_{p.s} = 230$ GPa.

Modelling of welds was done in a similar manner as for the 3D-model - i.e. not modelling them with physical elements, but instead using kinematic couplings. The connection was set as fixed, essentially making the coupled nodes share all DOF:s. As an extension of this methodology, the weld connection simulated the behavior assumed by Libove and Hubka. Because of the computationally efficient beam elements, a fine mesh of 1 cm was used in this model.

A crucial part of the 2D beam-model was the choice of boundary conditions, specifically for the local supports. A set up whereby the cross section was prevented to translate in the z-direction under every bottom weld point was introduced. However, due to having dual weld lines in this case, a reference point was introduced in the middle of the welds. Then a set coupling connections were established between the reference point and the weld point nodes, which connected the vertical translation DOF. Consequently, the support boundary condition was actually modelled on the reference point instead of under the weld lines. The complete set up is shown in Figure 23 (bottom). By using this approach it was possible to avoid the rotational constraints in the plate between the welds, caused by modelling the boundary conditions directly on the weld nodes.

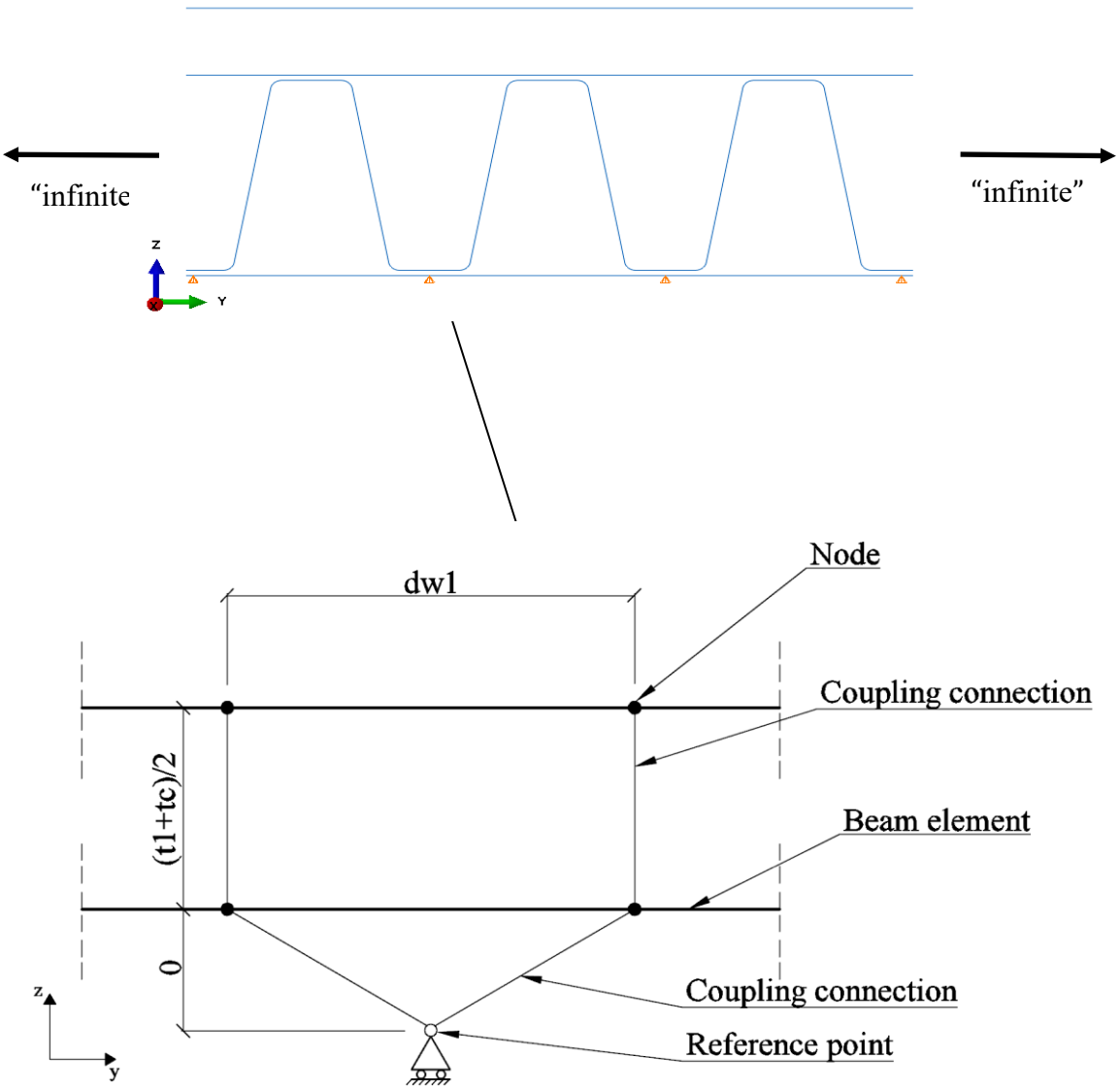

Figure 23 *Cut of three unit cells from the 2D beam model for geometry case 2 (top). Detailed description of the modelling choices done in the weld region (bottom).*

7 Local sectional forces due to global deflection

One of the most prominent drawbacks of the ESL approximation is that the single layer is not able to simulate local load effects, as explained earlier. The approach utilized in this thesis relies on the simulation the global response with an ESL shell model. In a second step, the local load effects in the constituent plates of the cross section are calculated. The implications of these effects will be further discussed and evaluated in this chapter, with respect to global shear forces and global moment.

7.1 Contribution from global shear

Shear forces in the corrugated sandwich panel are taken mainly by the corrugated core. The shear forces will be transferred through the welds and distributed to the core. Vertical deformation of the face plates, due to the global vertical shear force, induces a secondary moment in the face plate on both sides of the weld.

The secondary moment due to shear is included in the results from the 3D model, since this model accurately transfer forces through the welds to the flanges, making it able to capture local effects. The ESL model, on the other hand, is not able to include these local effects in the results. Thus, the additional local moment contribution must be calculated with a separate approach.

The method used in this section is based on combining the global shear forces extracted from the ESL model with a secondary shear factor, M_s, which expresses the resulting secondary local moment in the top face plate due to subjection to a unit global shear force.

7.1.1 Determining the local moments

Determination of the secondary shear factor M_s is based on the theory that was developed by Nilsson et al. in [17], previously used to determine the transverse shear stiffness for the corrugated core SSP. The theory is also able to describe all sectional forces in the constituent members of the sandwich panel under transverse shear force analytically.

By continuing from the final steps established in Chapter 3.4, the translation vector $\boldsymbol{a}$ was solved for in Equation 19. At this point, the secondary shear factor M_s can be determined by inserting a unit shear force in the direction of the first DOF (see Figure 6) and calculating the change in bending moment in the top flange on both sides of the weld. Note that two unique values for M_s are acquired at the weld - one on the left side and one on the right side – since the moment is partly transferred to the core. A summary of the calculated secondary shear factors can be seen in Table 4.

Table 4 Value of the secondary shear factor.

M_S:	Case 1	Case 2	Case 3	Case 4
In span	0.0107	0.0304	0.0156	0.0466
Between welds	0.0113	0.0136	0.0139	0.0291

The distribution of the shear induced local moment over one unit cell can be seen in Figure 24. Note that direction of the moment can vary depending on geometric

properties and that the moment in-between welds can also be lower than the moment directly outside depending on the stiffness distribution in the area.

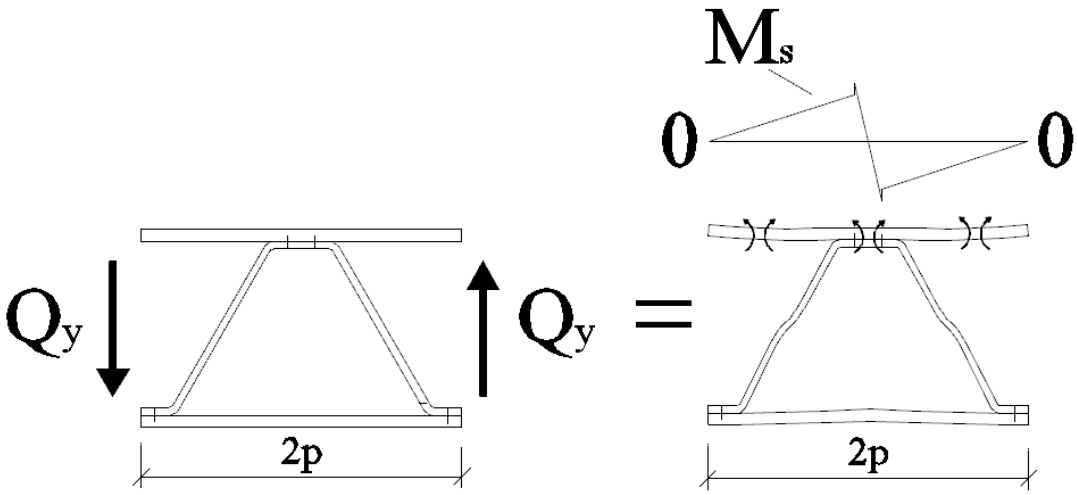

Figure 24 *Distribution of the local moment in the top face plate caused by one unit of transversal shear.*

In the derivation of the local moment, Nilsson et al. assumed a constant shear force Q_y acting on the unit cell. In cases where there is beam action involved this is a reasonable assumption. However, if plate action is present there are two directions for the load to distribute to the supports whereby the global shear distribution will be varying over the unit cell. How the local moment distribution looks if the shear is Q_y on one side and $Q_y + \Delta Q_y$ on the other side of the unit cell is unknown and probably dependent on the magnitude of ΔQ_y and the geometric properties of the unit cell. Nevertheless, for all load cases considered in this project the global shear is assumed to be constant over the unit cell in accordance with the theory presented in [17].

7.2 Local moment in top plate due to global acting moment

In the first iteration of the study, it was noticed that it was difficult to describe the behavior in between welds and between unit cells. There was a clear constant offset between the moment curve from the 3D model and the local moment from global shear force. After studying the problem more in depth, it could be seen that the local moment in the 3D model increases when the global moment increases. This can be seen both for load case 1 and 2 but is more prominent in load case 2 due to a larger transversal moment.

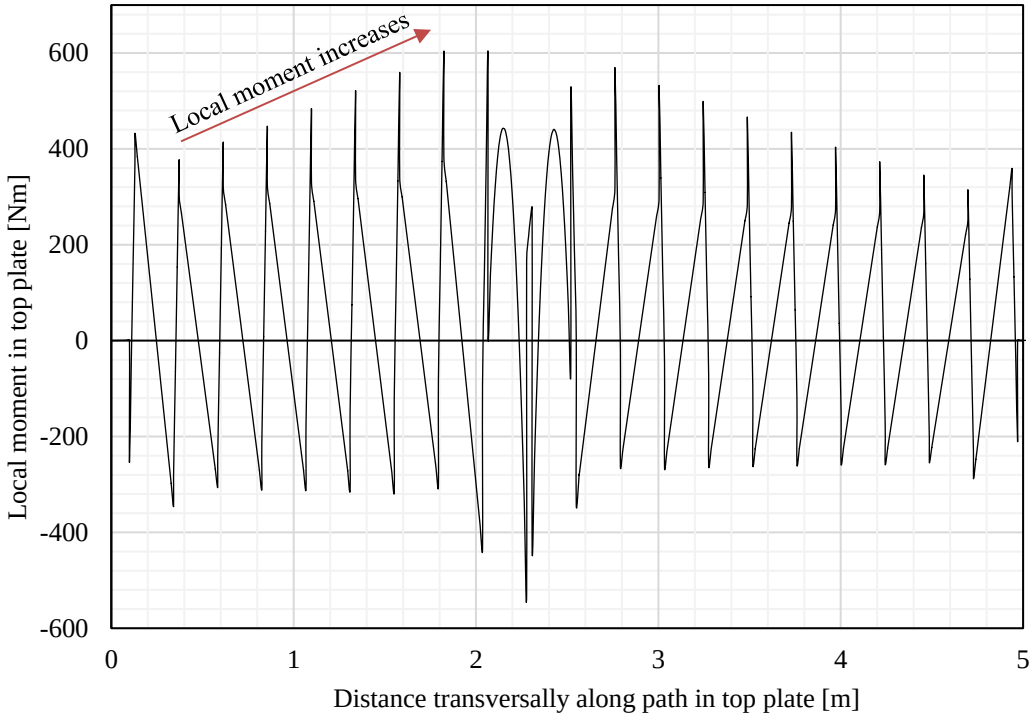

Figure 25 *Plot of local moment in the top plate of the 3D model taken from a path transversally over the whole width.*

It can therefore be concluded that the bending moment around the corrugation axis in the 3D model gives rise to a secondary local bending moment in the face plates of the sandwich structure as described in Figure 26.

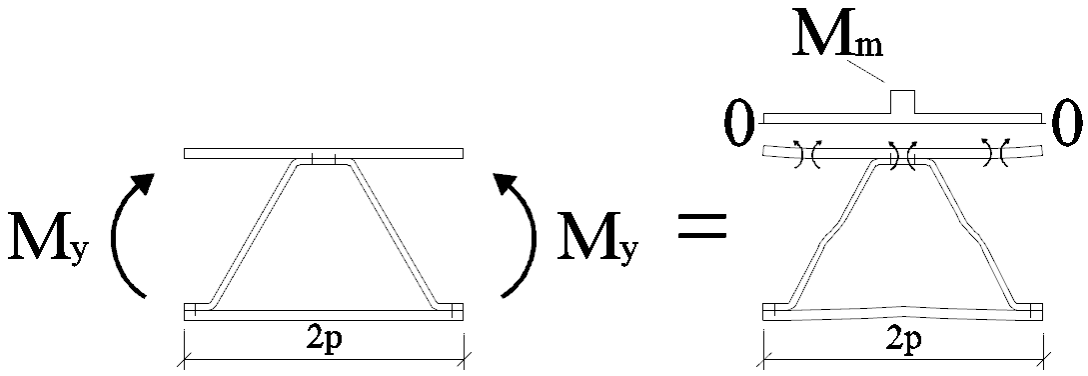

Figure 26 The global moment creates local moment in the top plate.

The ESL-model will not capture this behavior directly (as it only represents the global behavior) and must therefore be added to the local moment from shear to calculate the total local moment.

A numerical approach was devised for the purpose of determining the additional local moment in the top face plate due to a global moment. By creating a beam model and exposing it to a pure global bending moment, the resulting local bending moment in the top face plate will correspond to the desired "secondary moment factor", M_m. The

additional local moment can then be calculated by multiplying M_m with the global bending moment from the ESL shell model.

7.2.1 Determining the local moment

To achieve a pure bending state a 4-point bending model was adopted. A reduced case of the specific set-up that was used can be seen in Figure 27.

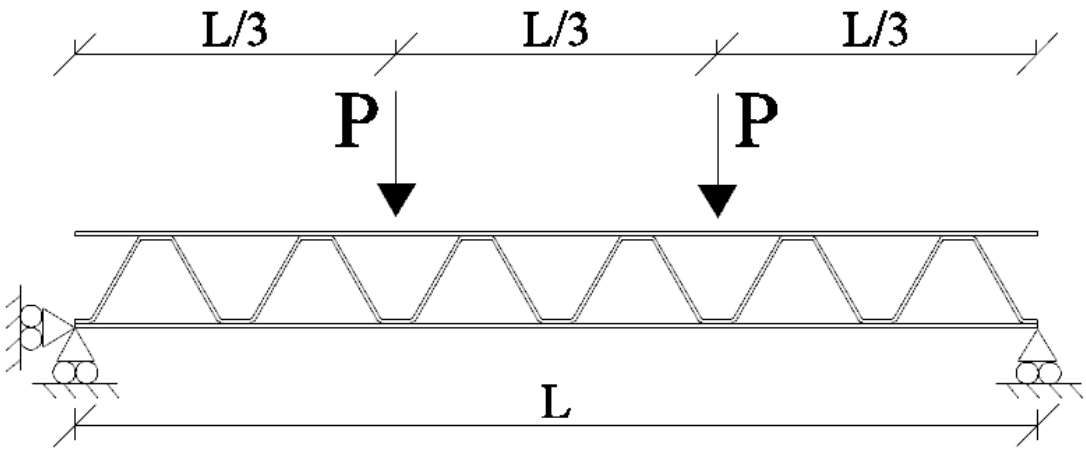

Figure 27 *Set up used for the 4-point bending model, note that the FE-model had 30 corrugation units.*

The evaluated beam is simply supported at the outer edges of the bottom face plate, with an additional horizontal boundary condition on the left edge to prevent rigid-body-motion. Two point loads were applied in the middle of two corrugation spans at equal horizontal distances from the edges of the model. The specific set up was chosen because it will always give a constant global moment between the loads, consequently, the shear force must be zero in the same region.

By evaluating results at a location far from either loads or supports, there will be no local influence from supports or the two point loads. While Figure 27 shows a model with six corrugation units, the model used in the actual analysis had a width of 30 corrugation units, in order to create sufficient distance between the applied point loads P and supports to the point in the middle of the model. For this larger model the point loads were placed a horizontal distance of ten corrugation units from each end support, also leaving a center space of ten corrugation units between the loads.

The magnitude of the applied forces is determined by simple hand calculations as the force that is required to create a global bending moment of 1 Nm in the area between the point loads. From the elemental case for a simply supported beam subjected to two point loads, the following equation is established:

$$P\ (p) = \frac{M}{10*2*p} = \frac{1*[Nm]}{10*2*p} \tag{25}$$

Where 2*p is the width of one corrugation unit, meaning P will have a unique value for each studied case geometry. Additionally, the number 10 corresponds to the number of corrugation between the support and point load.

The model was created with second order beam shear deformable elements. A set of kinematic connections were established between face plates and the corrugated core, in order to simulate the influence of the welds (analogue to how the connection was done in the 3D model).

To verify the assumption that there was zero contribution from shear force in the middle of the investigated model, the bending moment was extracted from a path along the top face plate. Results from this path are shown in Figure 28, where the x-axis corresponds to the position along the top plate [m from the left support] and the y-axis shows the resulting bending moment Nm in the top plate due to the described loading case.

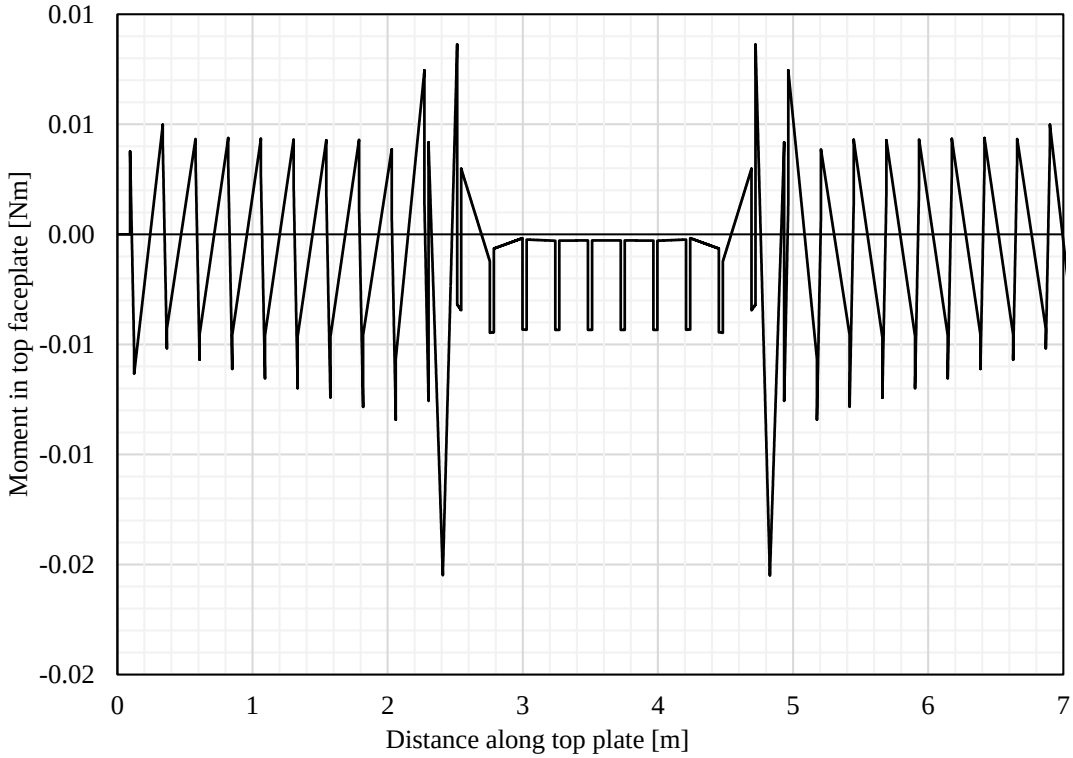

Figure 28 Moment in the top plate from the 4-point bending model

The shear forces clearly influence the moment in the area between the supports and the applied loads and the local moment peaks at the point of load application due to local influences. However, the involvement of shear forces decrease towards the middle of the model and the contribution reaches zero between the point loads, hence the step-wise constant distribution. The static moment curve in the center is deemed sufficient to show that there is no contribution from shear forces or local influences at this location.

As the results for the "moment transformation factor" can be seen directly in Figure 28 it is evident that the local moment changes in the constant global moment area. It can therefore be concluded that the transformation factor M_m will have two separate values for each geometric case – one in the upper "span" of the corrugation and one between the upper welds. Values for M_m were extracted at the static points in span and between welds and the results are summarized in Table 5 below.

Table 5 Value of the secondary moment factor

M_m:	Case 1	Case 2	Case 3	Case 4
In span	-0.00279	-0.000658	-0.000526	-0.000758
Between welds	-0.04342	-0.02055	-0.02469	-0.02469

8 3D-analysis of complete structural behavior of corrugated-core sandwich panel

In order to increase the initial understanding of the structural behavior of the sandwich panel, a complete 3D FE-model was created and analyzed in BRIDGE/Plus. This model was created according to geometry case 1 and subjected to load case 1, see Figure 29.

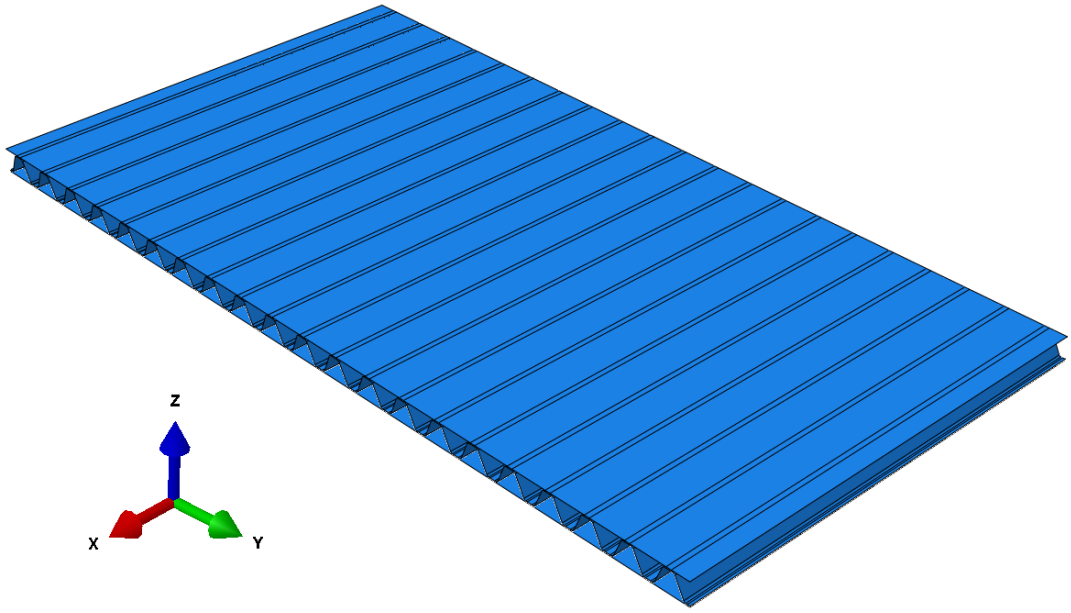

Figure 29 The 3D-model used in the initial study.

An important conclusion could be drawn from this initial study: the structure expresses two distinct separate behaviors. A certain distance away from the applied patch load the panel expresses a continuous global behavior, while in the center of the model there is a clear additional local influence from the patch load. Figure 30 shows the deformed middle section of the studied FE-model, where the indicated global behavior is highlighted in red and the presumed local influence is highlighted in yellow.

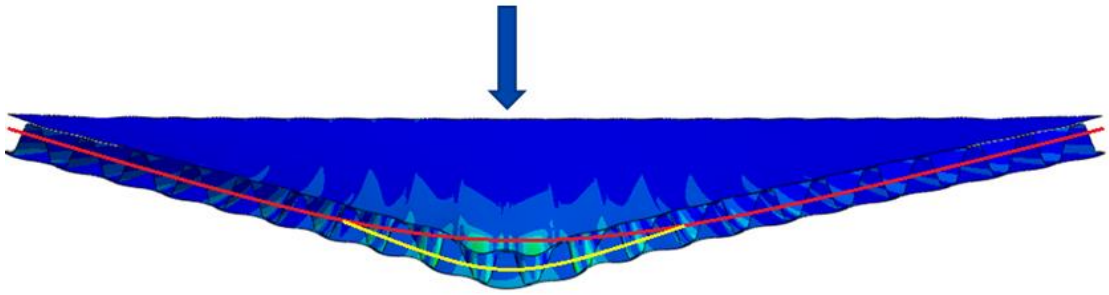

Figure 30 Deformed 3D FE-model of a corrugated core SSP subjected to out of plane patch load.

Following the results of the initial study, the project was divided into two parts: one part focusing on the global behavior of the panel and one part focusing on the combined global and local behavior.

The method chosen for the study relied on first determining a way to accurately describe the global behavior of the panel and to then move on to analyze the combined behavior. If the global behavior could be assumed to extend naturally into the middle part of the

model, then the local behavior could be singled out and evaluated during the study of the combined behavior.

Since it is not clear exactly where the local influence starts to affect the results, the global study will focus on a part of the model a "sufficient" distance away from both the patch load and edge supports. Thus, local effects originating from either the load or supports are in theory avoided, giving a response related only to global behavior.
The combined behavior will be studied directly under the applied patch load. The global and local contributions will be added by super positioning, according to the approach suggested in [30], and then compared to the results from the complete 3D shell model.

9 Study of local load effects away from load

This first part of the study focused on an area between the outer boundary conditions and the patch load at the center of the FE-models. The studied area was chosen because it should have a response that was unaffected by local influences such as boundary conditions and applied loads. Thus, the local load-effects seen in the top face plate origin from the global load effects alone.

The resulting local moment in the top face plate was studied and compared between the 3D model and the sum of the contributions from global moment shear from the ESL model combined with the local moment factors M_s and M_m. Results from the 3D model were extracted for one unit cell a distance of four unit cells both from the edge of the model and from the applied load.

To be able to compare the local moment, the global influences from the ESL-model had to be multiplied with the corresponding coefficients, M_s and M_m and then summarized. The full procedure can be seen in Figure 31.

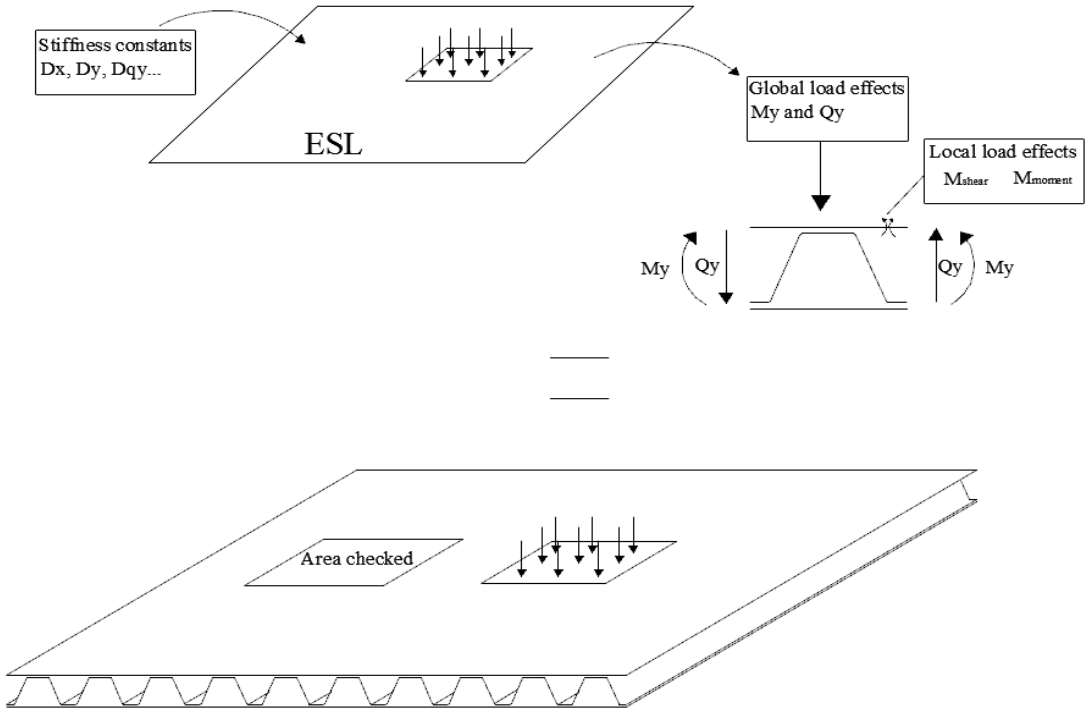

Figure 31 Flowchart of the multi scale modelling procedure.

9.1 Note on combination of contributions from 2D-models

There is a divergence between the assumption of having a constant acting shear force on the unit cell, used when determining the shear factor M_s, and the actual results showing that the shear force varies over the unit cell for which the results are plotted. For the simplified approach in this thesis the global load effect in the ESL-model at the center of the core was used to represent the entire cell. This is a simplification origin from the nature of homogenization. The case is analogous with respect to global moment.

9.2 Results of the study

Figure 32 and Figure 33 shows the results from the comparison study for the total local moment in the top face plate, for case geometry 1 exposed to Load case 1 & 2 respectively. Results for Load case 1 & 2 for all investigated case geometries can be seen in Appendix B. In every result plot the x-axis was normalized by the total width of one corrugation unit and the moment were normalized by the maximum absolute value for that specific geometry and load case. The results from geometry 2-4 matched the results from geometry 1 closely.

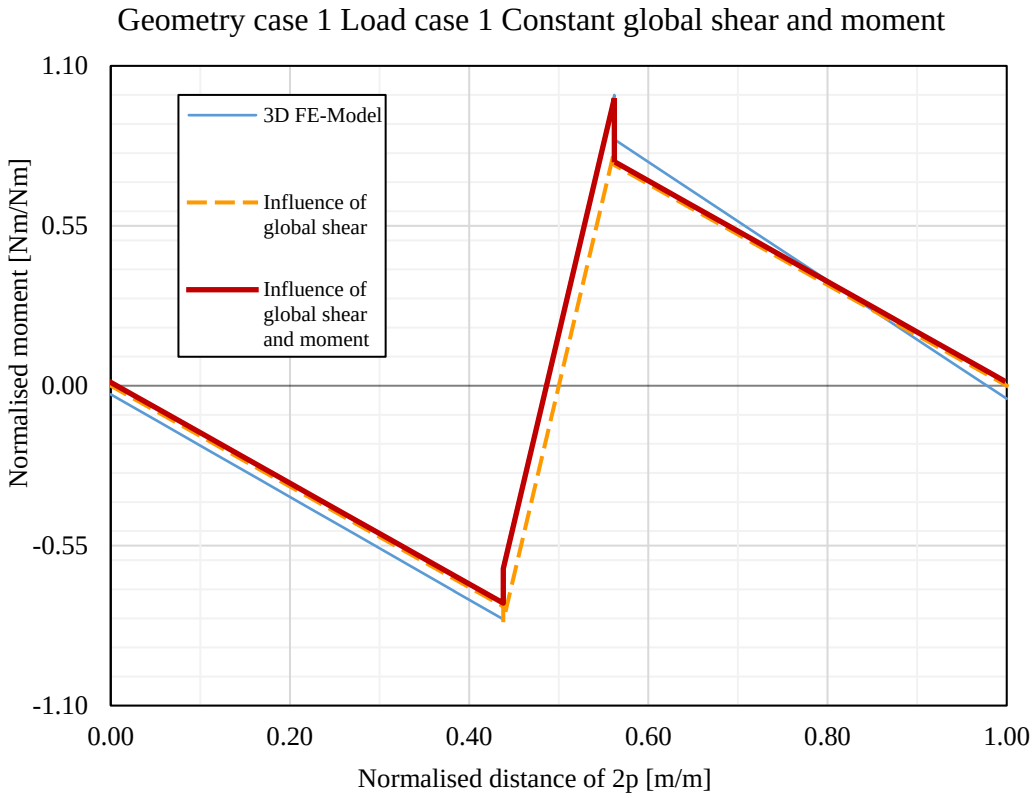

Figure 32 *Comparison of the local moment between the 3D FE-model and the contribution from ESL-model combined with M_s and M_m constants.*

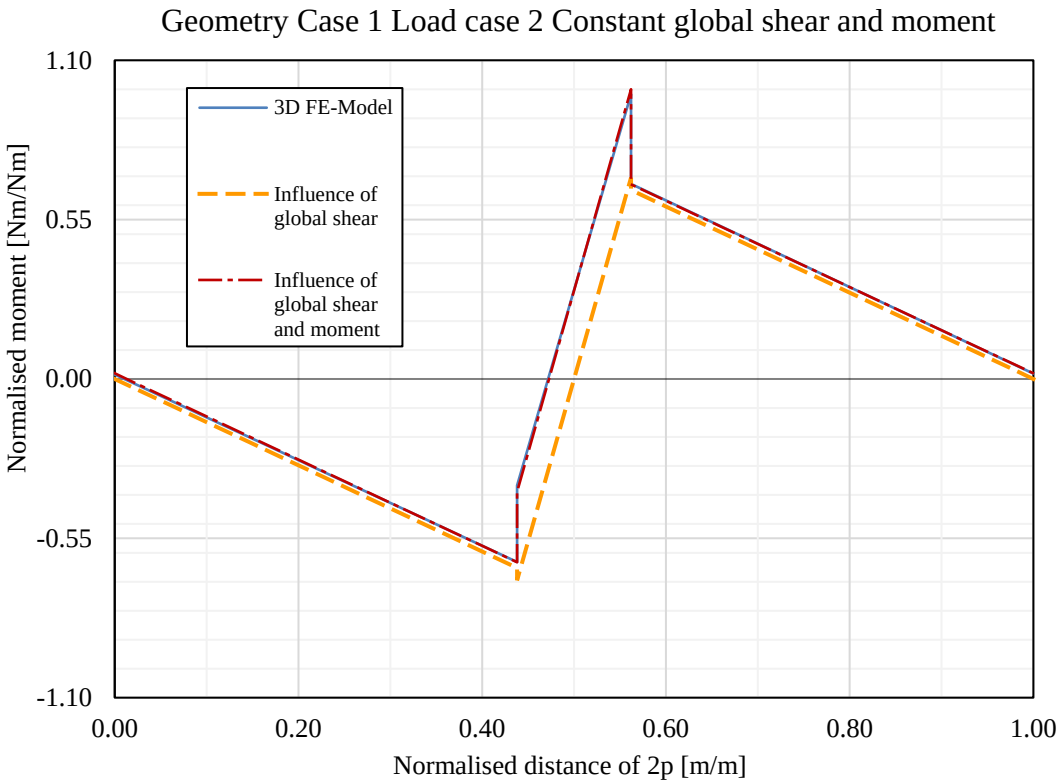

Figure 33 *Comparison of the local moment between the 3D FE-model and the contribution from ESL-model combined with M_s and M_m constants.*

Understanding of the distribution of the global forces is essential to evaluate the result plots in Figure 30 and 31. For load case 1 the global forces will vary over the length of 2p, however for load case 2 only the global bending moment will have a linear variation over the unit cell, due to the constant global shear force. In this case, when the local moment is checked a certain distance from the load, the major influence of the local moment is from the global shear force. The global bending moment in the transversal direction only has noticeably contribution at the weld points (as indicated by the sudden jump in moment).

Because of this, and that the global forces were assumed to be constant over one corrugation unit, some deviations from the 3D-model results are expected and these should be greater where the global forces have a larger gradient, i.e. load case 1. This is also in the agreement with the results the results, from Figure 32 it can be seen that the gradient of the 3D result and combined approach have a slight difference, probably because of the change in global shear force over the unit cell. For load case 2 however, the curves are almost identical, only showing slight deviations at the weld points. This proves that the shear coefficient M_s is more accurate when the global shear force is constant. Differences at the weld points might be explained by the change in moment over the unit cell. Consequently, this proves that it is possible to estimate the local moment in the top face plate from a patch load of a corrugated core SSP using only an ESL model and post processing using M_s and M_m. If the global forces are not constant over the unit cell then the accuracy decreases. However, the maximum discrepancy was calculated to 8%. The next step is to model the local response directly under the area of load application.

10 Study of local load effects directly under patch loading

As was briefly discussed in Chapter 8, contributions from both global and local effects must be considered when the response directly under the load is to be analyzed. Compared to the study in Chapter 9, this study will expand to include an additional component, due to the deformations from the direct application of the patch load. An additional 2D beam-model is here introduced to capture the local effects from the patch load, as was suggested in [30].

This chapter will; present the assumptions made in terms of applied loads and global load effects, discuss how the 2D beam-model was handled in order to capture the local effects and finally showcase and discuss the results from the study.

10.1 Choice of investigated area and extraction of results

As previously touched upon, it is not clear exactly how big of an area will be directly affected by the patch load. The patch load was applied over a 0.5 m wide area for all investigated cases, but as the geometry properties vary between different geometry cases it should be assumed that the local effects of the patch load will distribute differently as well.

In order to increase the predictability of the load distribution, the load was applied so that the center of a corrugation crest either coincided with (cases 3 and 4), or was very close to (cases 1 and 2), the center of the applied load. Figure 34 presents how the patch load was applied for geometry 1.

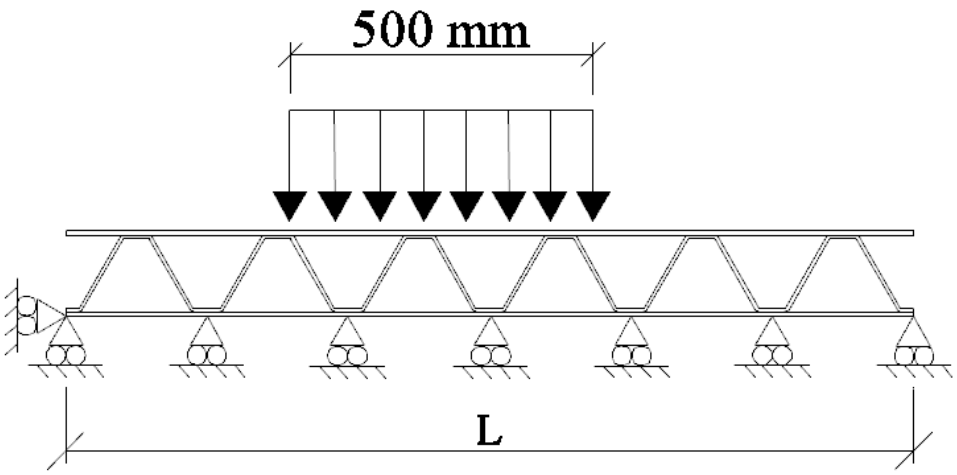

Figure 34 Sketch of the 2D FE beam-model set-up for geometry case 1, including the applied patch load.

There was also the issue of choosing a consistent method for result extraction, while still gathering data that is relevant for the study. Preferably, results would be taken from the exact same nodes for all FE-models. However with element meshing and possible areas of interest varying between different FE-models and geometries, there are some innate issues with acquiring homogenous results. This problem is mostly related to the

2D-models where the resulting load effects have to be summarized. But by utilizing some precis meshing techniques this problem was resolved.

For the sake of simplicity and consistency, all presented results are for the upper face plate and in terms of a total acting bending moment. Results for all geometry cases are presented over the width of one corrugation unit, even though one corrugation unit is slimmer than the width of load application (0.5 m) for some cases and wider for others. This relative size towards the applied load has the consequence that the load case will be more similar to a distributed load for slim geometries and more similar to a point load for wider geometries (mainly case 4).

10.2 Assumptions regarding global forces for the study under patch load

Since this study focuses on the area directly under the applied load, the shear force- and moment- distribution will look quite different compared to the study away from load. Most notably, the shear force will transition from a positive to negative sign under the area of load application, and will further be equal to zero at the center of the load.

This force distribution is not at all compatible with the previous assumption of having a constant acting shear force over the entire area of interest. Instead, the shear force is here assumed to be consistently equal to zero over the investigated unit cell. Thus, second-order moment contributions from the global shear force can be disregarded entirely for this study. This assumption would have been questionable if a larger area was to be investigated, but is deemed acceptable for results only half the width of one unit cell in each direction from the zero-shear point.

10.3 Contributions from global and local load effects for study under load

The addition of local and global load effects can for this study be summarized according to Figure 35.

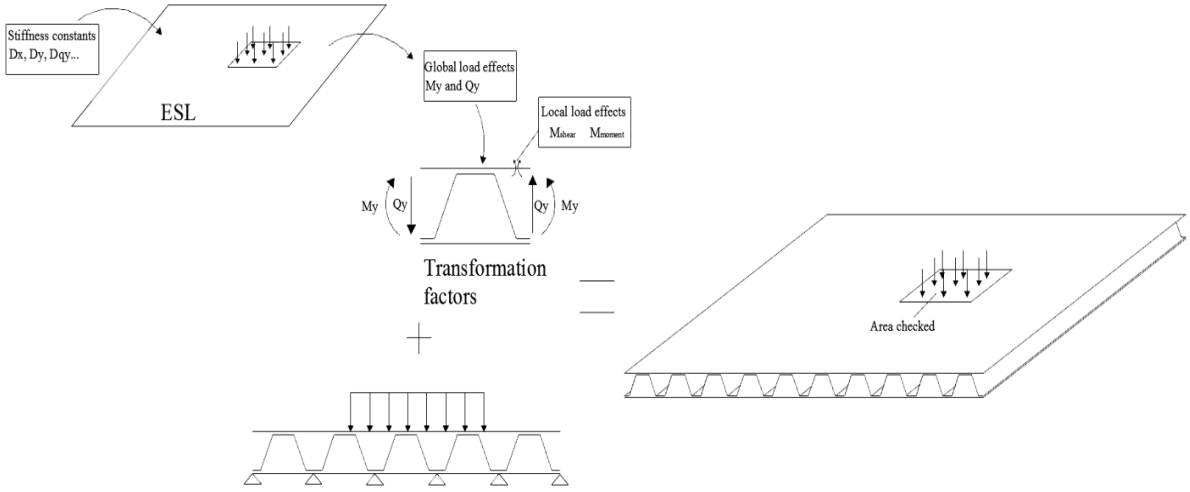

Figure 35 Summary of the different contributions for the study under load

The second-order local moment from global effects will in this study be accounted for in the same manner as they were in the previous study – global load effects are extracted from the ESL shell FE-model and converted to local moment by the transformation factors M_s and M_m. The difference here is that the global shear force is assumed to be equal to zero, meaning that global moment is the only global factor affecting the final local moment.

The additional local moment, due to the directly applied patch load, was extracted directly from a 2D FE beam-model. Since the global response is provided by the ESL homogenized plate, the local 2D beam-model must be engineered carefully in order to capture only the precise local behavior, without any global influences. The initial hypothesis was to achieve this by implementing the boundary conditions for the beam-model as suggested e.g. by Romanoff et al. [30].

10.4 Results for load case 1

Figure 36-39 shows the results of the study for all four investigated geometry cases, when subjected to Load Case 1 (plate action). The local moment was extracted from the 3D shell model in the top face plate and plotted against the combined total local moment with contributions from both ESL and 2D beam-model. The results were normalized by the maximum absolute value for the moment, for each studied case, and then plotted over a unit cell, where the horizontal distance along the extraction path was also normalized by the width of a unit cell.

The welds are critical nodes in the evaluation, as the behavior of the structure can be very different on each side of each weld. No averaging was used for the results gathered from the FE-analysis, so that two distinctive separate results are yielded in the weld node – one coming from the element on each side. The node corresponding to the weld can be clearly distinguished in the result plots as there are dramatic vertical drops in bending moment at these points.

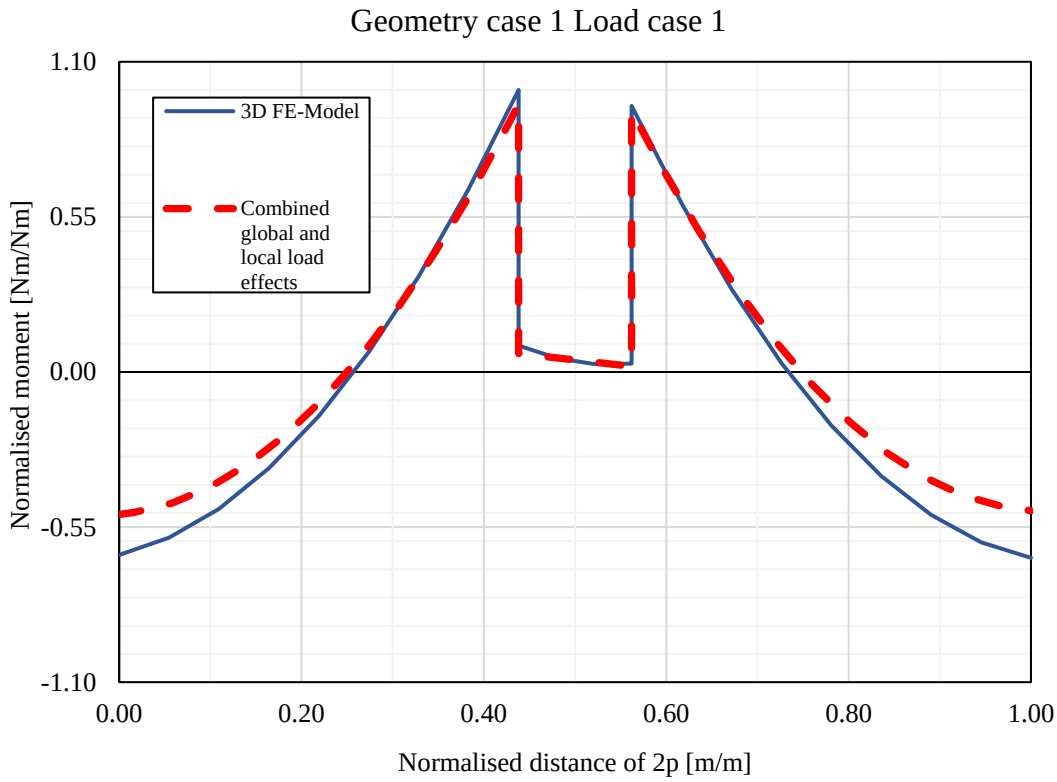

Figure 36 Local moment in the top plate for geometry case 1, load case 1.

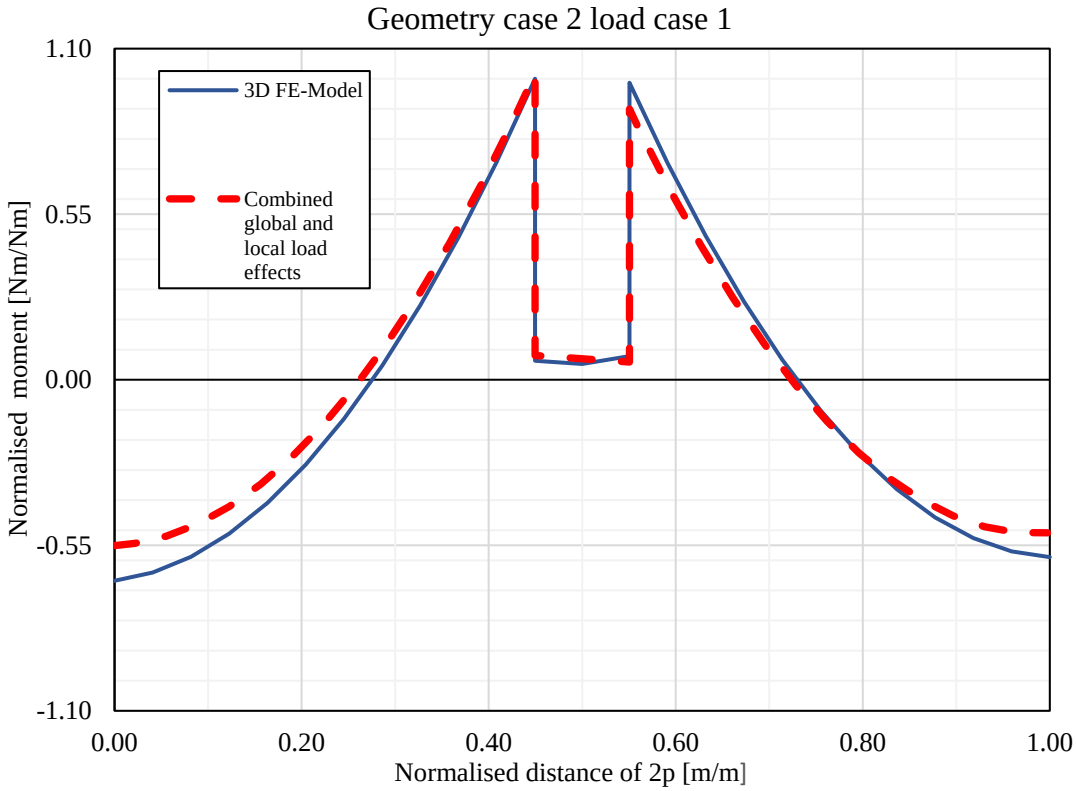

Figure 37 Local moment in the top plate for geometry case 2, load case 1.

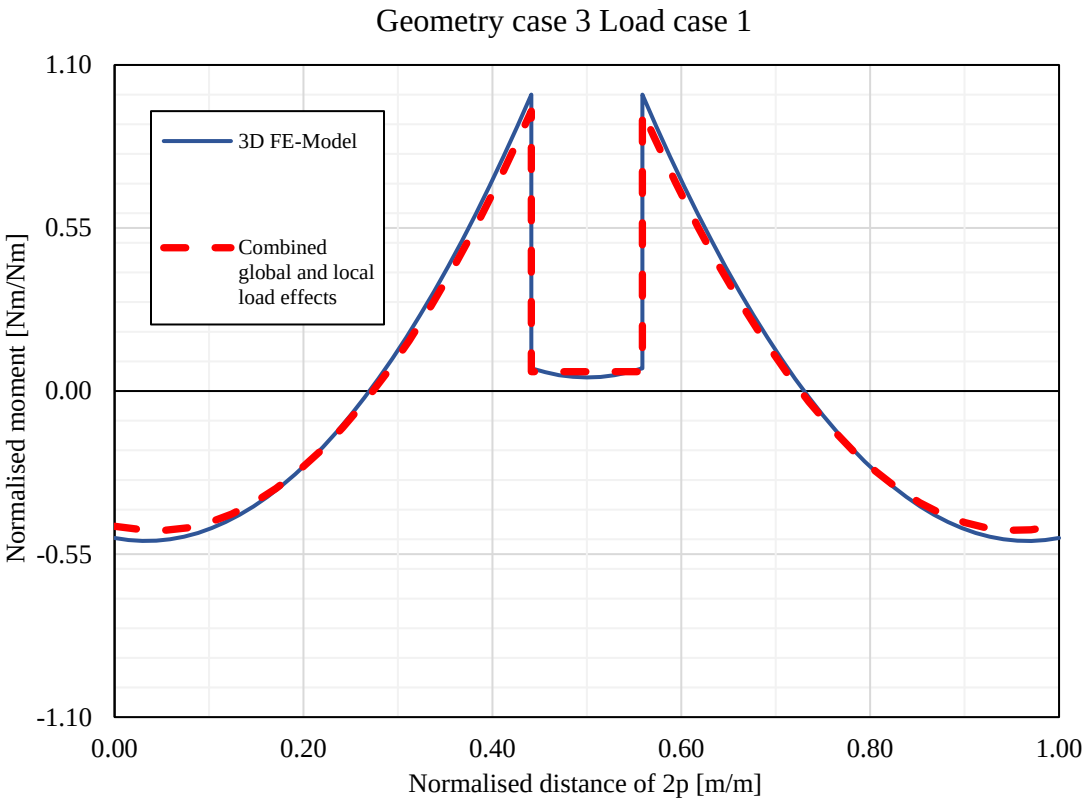

Figure 38 Local moment in the top plate for geometry case 3, load case 1.

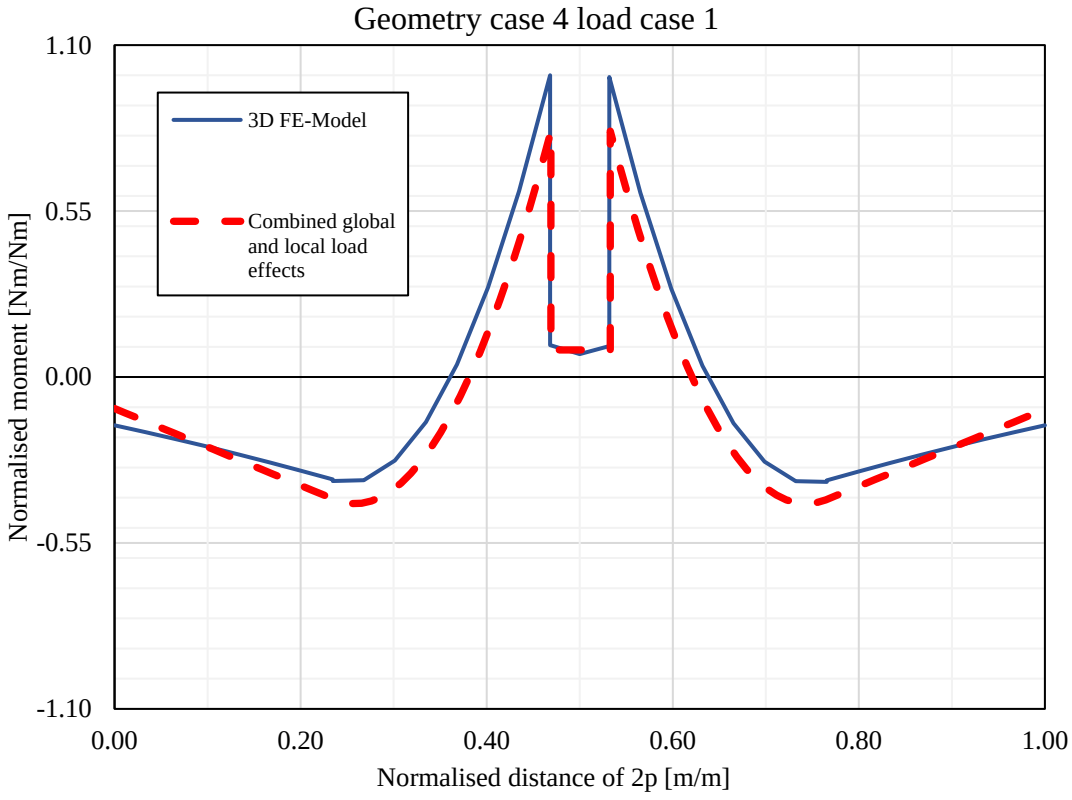

Figure 39 Local moment in the top plate for geometry case 4, load case 1.

In general, very good agreement can be seen in the center area of the plots in and around the welds, although geometry 4 displays less accurate prediction. The results at the edges of the showcased result plots ($x = 0$ and $x = 1$), do however not show the same level of accuracy. For example, geometry 2 show a result divergence here of around 17% for the compared local moment.

Similar trends can be seen in the results for all studied cases - in span as well as for the area around welds - where the moment extracted from the 3D FE-model is consistently higher than the total moment coming from the suggested combined approach.

10.5 Results for load case 2

Below, result plots are presented for all geometry cases when subjected to load case 2, see Figure 40-43.

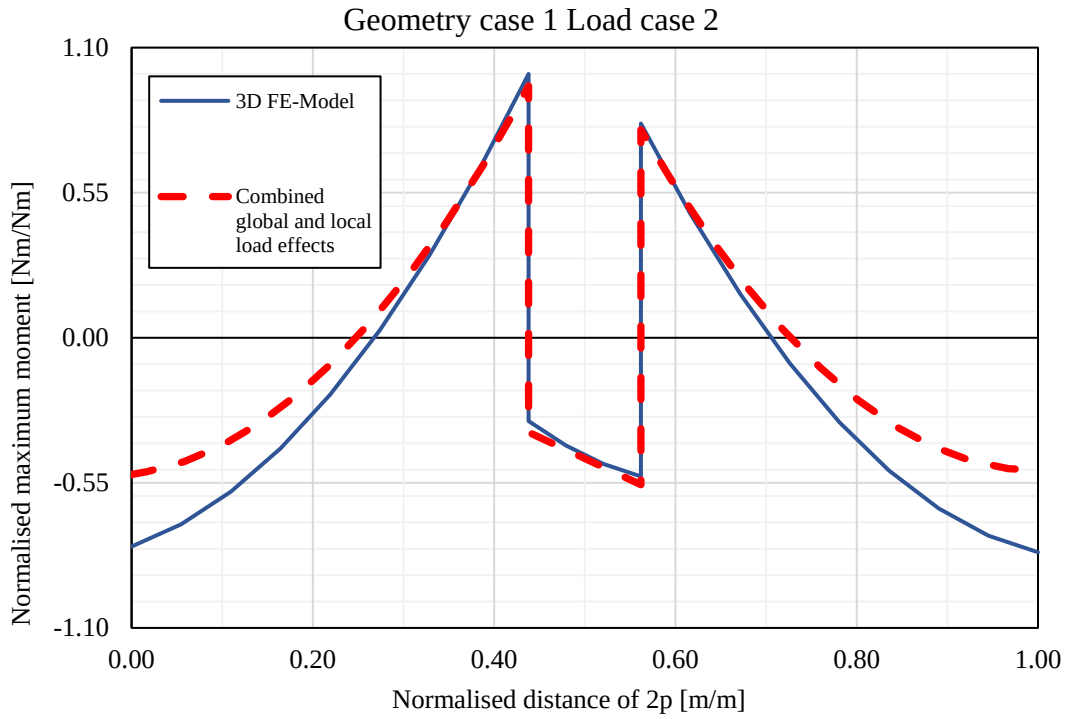

Figure 40 Local moment in the top plate for geometry case 1, load case 2.

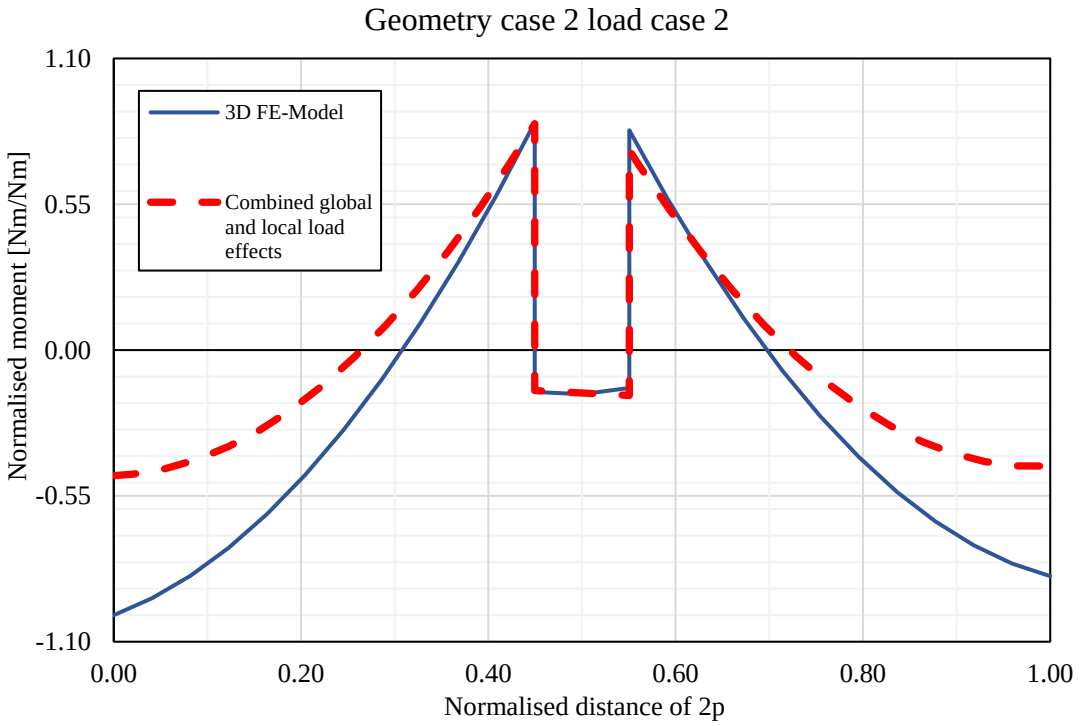

Figure 41 Local moment in the top plate for geometry case 2, load case 2.

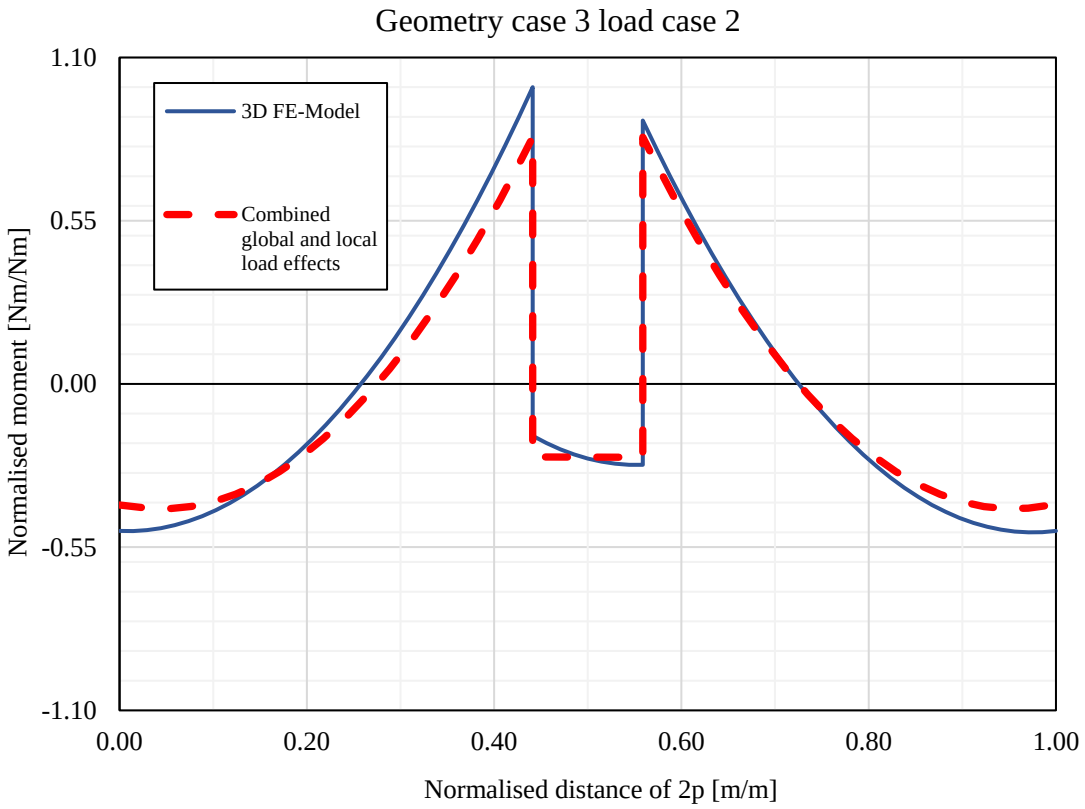

Figure 42 Local moment in the top plate for geometry case 2, load case 2.

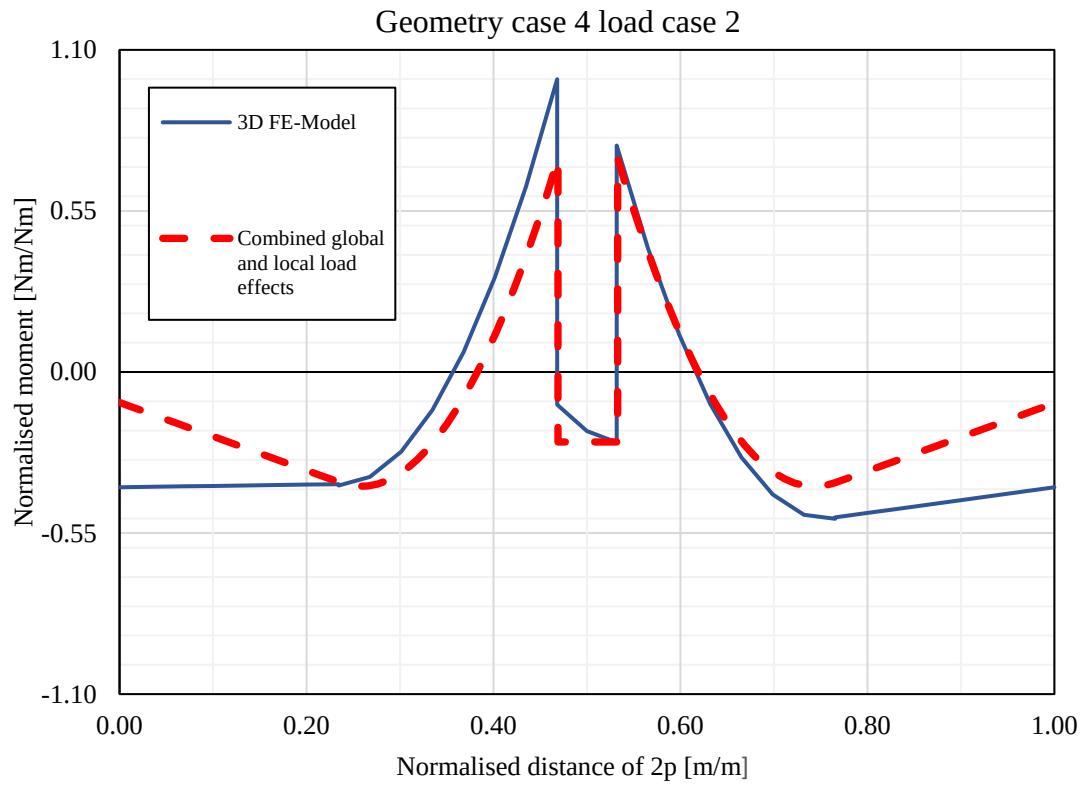

Figure 43 Local moment in the top plate for geometry case 2, load case 2.

Similar trends can be seen for both load cases. Although these results are not as clear as for Load case 1, some similarities and differences can still be observed compared to the first load case. One noticeable tendency for geometry cases 1, 2 and 3 is that the moment difference is larger in the outer regions (x = 0 and x = 1), where the moment from the 3D model has increased by larger margin than the combined 2D models. While the results for geometry case 3 matched quite well for load case 1, a clear deviation can be seen for load case 2. The results for geometry 4 are hard to interpret, but probably caused by the acting global forces or by thickness deformations due to the large height of the cross-section.

10.6 Discussion

It can be concluded that the suggested approach does not work to a satisfactory degree when analysing an area under the patch load. Some deviations are expected, due to the slight shift of the global shear force (Q_y), whose contribution cannot be evaluated with the available theory. The impact of the global moment in the transversal direction (M_y) should be accurate however, as it is basically constant over the unit cell. Although the discrepancy between the 3D results and the suggested approach is very small for some cases, the non-uniformity of the results leads to the conclusion that there is a structural behavior that neither of the 2D-models are able to capture.

It is obvious from the plots that the result agreement is better for the area in and around welds than for the areas in the outer edges of the unit cell. It is also evident for load case 2, that the increase in global forces in the transversal direction does not match the increase in local moment that is present. One possible explanation is that the local moment could be influenced by the longitudinal load distribution (along the direction of the corrugation). If this is the case, then it can be concluded that the proposed set of boundary conditions for the 2D beam model are not able to accurately simulate the longitudinal load distribution present in the 3D FE-model.

The other theory as to why the results differ might be explained by a punching-like behaviour that can be observed in the 3D model, see Figure 44. This is present for all geometries except geometry 3 where the local bending due to the directly applied load of the face plate is dominating by far, geometry 3 is also where the results had the best correlation. This kind of structural response is usually seen in flat concrete slabs in areas close to columns (as a result of the peak stress in those areas), but then related more to failure. The punching behaviour cannot be seen in the ESL due to the homogenization or the 2D local model because of the boundary conditions.

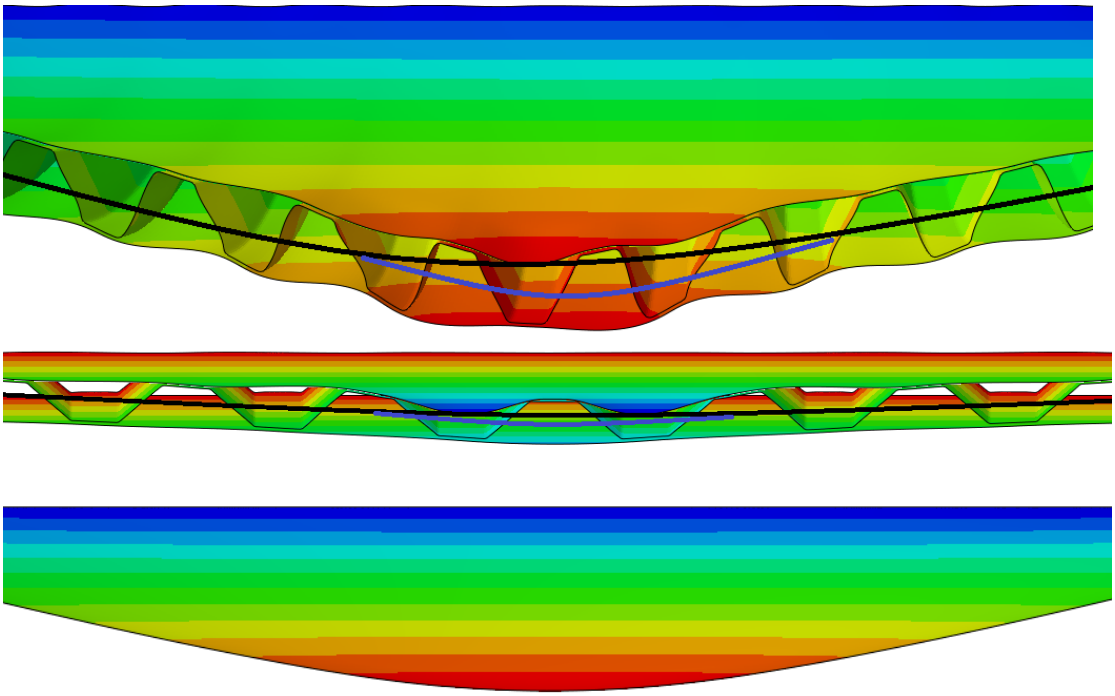

Figure 44 *The punching behavior observed in the 3D FE-model indicated by the blue line. It has a much bigger presence in Geometry 1 (top) than geometry 3 (middle). ESL model with no punching behavior (bottom).*

11 Study on how to improve the initially suggested approach

In the initial study directly under the patch load, it was concluded that the suggested combined method does not completely capture the behavior that can be seen in the 3D shell model. Two possible explanations for the result divergence are highlighted:

- Inability of the 2D beam-model to capture the longitudinal bending response of the sandwich panel. This will be a problem if the longitudinal response is a factor that affects the local moment in the top face plate, since it is not included in the results from the 2D beam-model.

- A presence of punching-like deformations in the sandwich panel, which cannot be captured in ESL shell-model.

The ESL model is not able to capture this punching-like influence, due to the nature of homogenization. Thus, inclusion of the punching effect into the suggested combined approach must be achieved either through alteration of already existing models or by extending the approach by adding the contribution from the punching effect separately.

This chapter will investigate how the 2D local FE-model, or the suggested approach itself, could be modified in order to achieve results closer to that of the 3D FE-model.

11.1 Boundary conditions removed from the local model

Previously, the vertical translation at every bottom through in the 2D beam model was prevented. The only difference compared to the previous model, is that all boundary conditions for supports situated directly under the load were removed. The idea was that this set-up would create the desired "semi-global" behavior. Assuming that the punching behavior would, in reality, be limited to an area in and around the applied patch load, this modified constellation would hopefully allow the punching deformations under the load, while still retaining the pure local behavior for the rest of the model.

By removing the BC's under the load, see Figure 45, the face plates are forced to elongate in a way that was not possible with the previous set-up. This has the important consequence that normal forces are induced in the system. The presence of normal forces has the additional implication that looking at results in terms of bending moment is no longer the best option. Therefore, results will be investigated in terms of stresses.

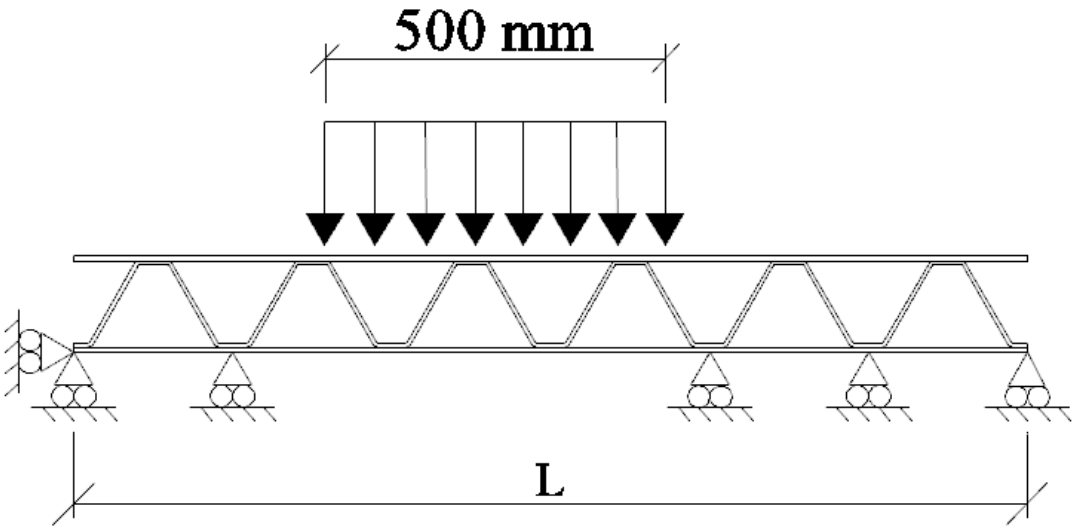

Figure 45 Sketch of the new boundary condition model.

Stresses S11 were extracted from the top fiber of the top face plate in the 2D beam model. Global bending moment from the ESL-model were converted to stress using Navier's formula; $\sigma = M/W$.

Where M is the global moment and W the section modulus of the homogenized cross-section per unit width.

Stress due to shear force was assumed to be zero, similarly to the shear force itself. The sum of stress from bending moment and S11-stress in the top fiber of the beam model were summed up and compared to the stress extracted from the 3D model.

11.1.1 Results

Results are here presented for the suggested combined approach versus the same results that were presented in the previous study for the 3D shell model. The only change is that the 2D beam-model was here modelled with the modified constellation of boundary conditions. Results are only presented for geometry case 1, although results for the other three geometries can be found in Appendix C.

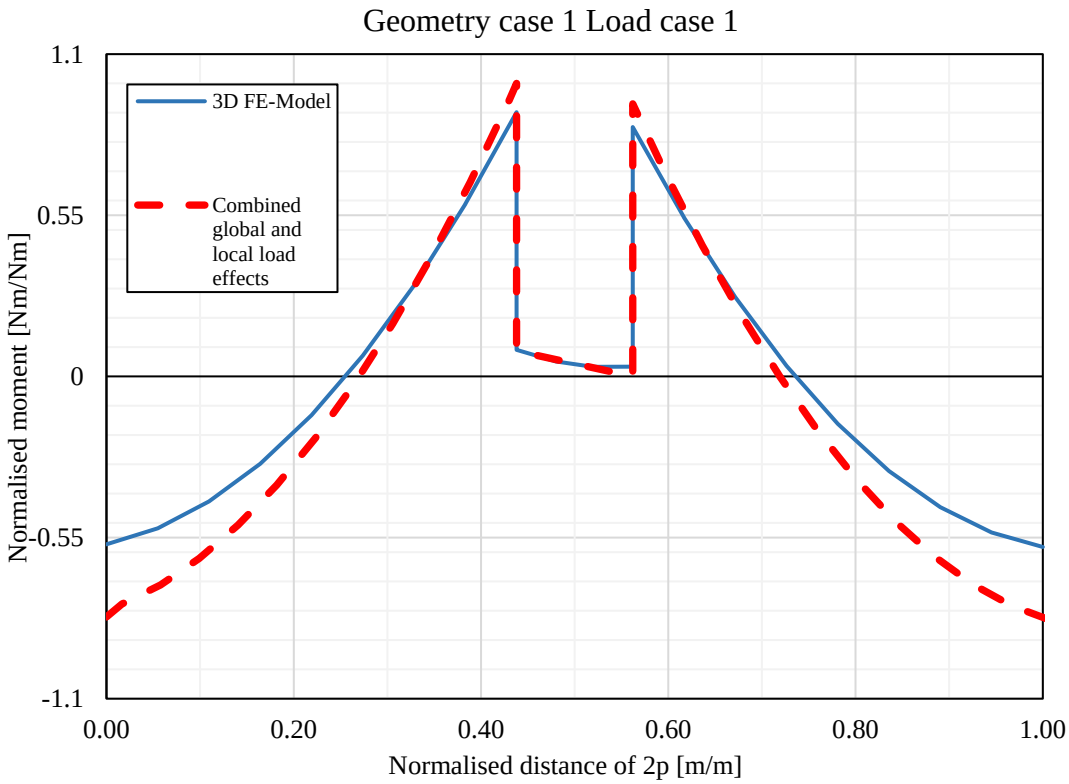

Figure 46 Results for the study with removed supports under the load.

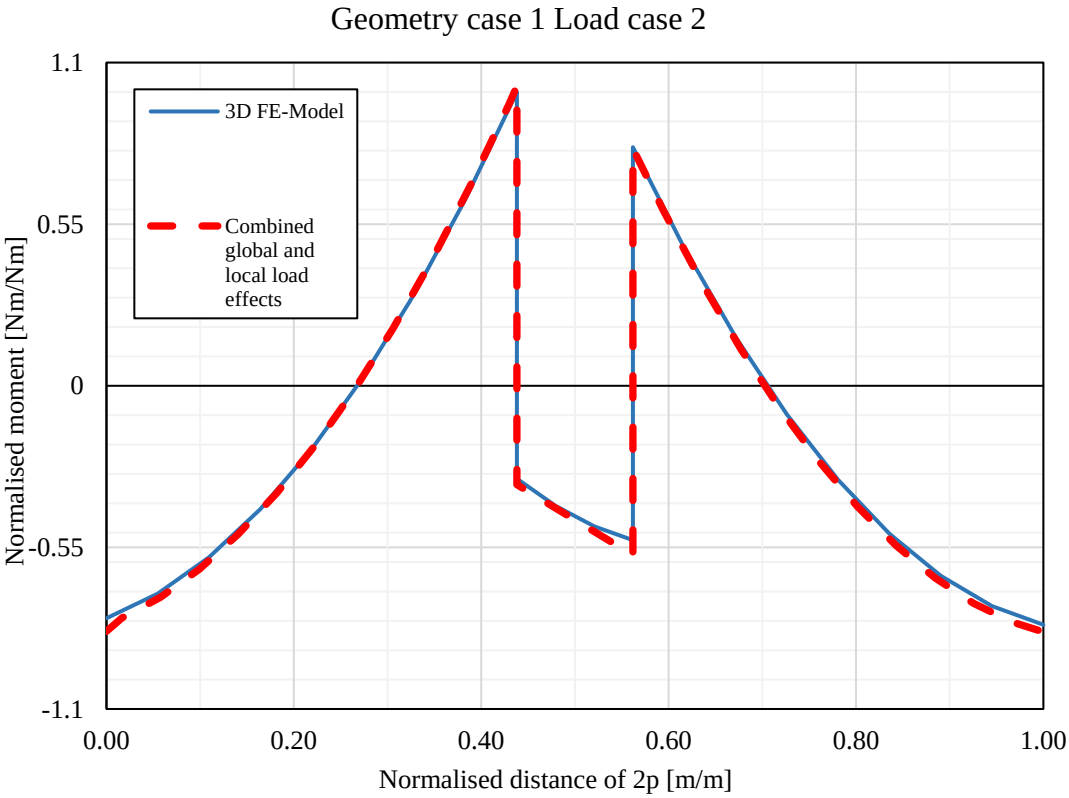

Figure 47 Results for the study with removed supports under the load.

The results for geometry case 1 show very good correlation for load case 2 and, similarly to the study in Chapter 10, good correlation around welds and not so good correlation at the unit edges for load case 1. One important difference to notice though is that the moment in the study with boundary conditions everywhere was higher in the 3D-model, while in this study the moment is larger from the investigated approach. Results in terms of stresses are presented below, for geometry case 1 subjected to load case 2.

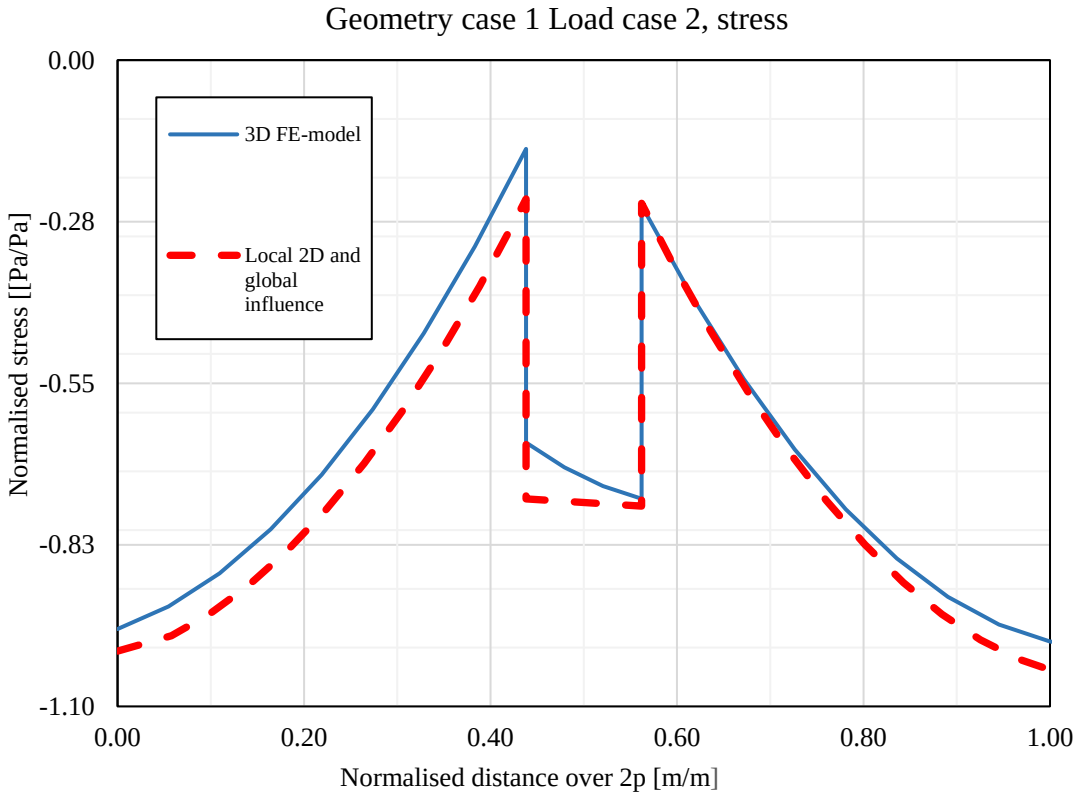

Figure 48 *Results for the study with removed supports under the load with plot of stress in the top fiber.*

11.1.2 Discussion

For this study it could be seen that the moment from the combined 2D models is actually larger than the 3D model for load case 1. This is the opposite of the other study where it was smaller. A high correlation between the 3D and the 2D models for load case 2 was noted. This is consistent for all geometry cases, except for a slight noted offset for geometry 4. However when removing the boundary conditions under the load, an eccentricity between the load and the supports is created, thus creating a global moment in the local beam model. This was taken into account by instead making a study of stress rather than moment. The stress study showed similar results as the moment, however with a slightly larger difference. Still, the problem with the plate action load case remain, and might be explained by the longitudinal load distribution.

11.2 Local 2D model with springs

It could be concluded from the study with removed supports under the load that the result were satisfactory for load case 2. Furthermore, the combined load effects from the 2D models were generally smaller for load case 1 with supports and larger without, compare Figure 36 with Figure 46. Therefore, just by looking at the results, it can be concluded that the behavior of the 2D beam model should be somewhere in between the first two studies to fit load case 1. Accordingly, an attempt were the supports directly under the load were modelled using spring elements was carried out. A setup of the modification can be seen in Figure 49.

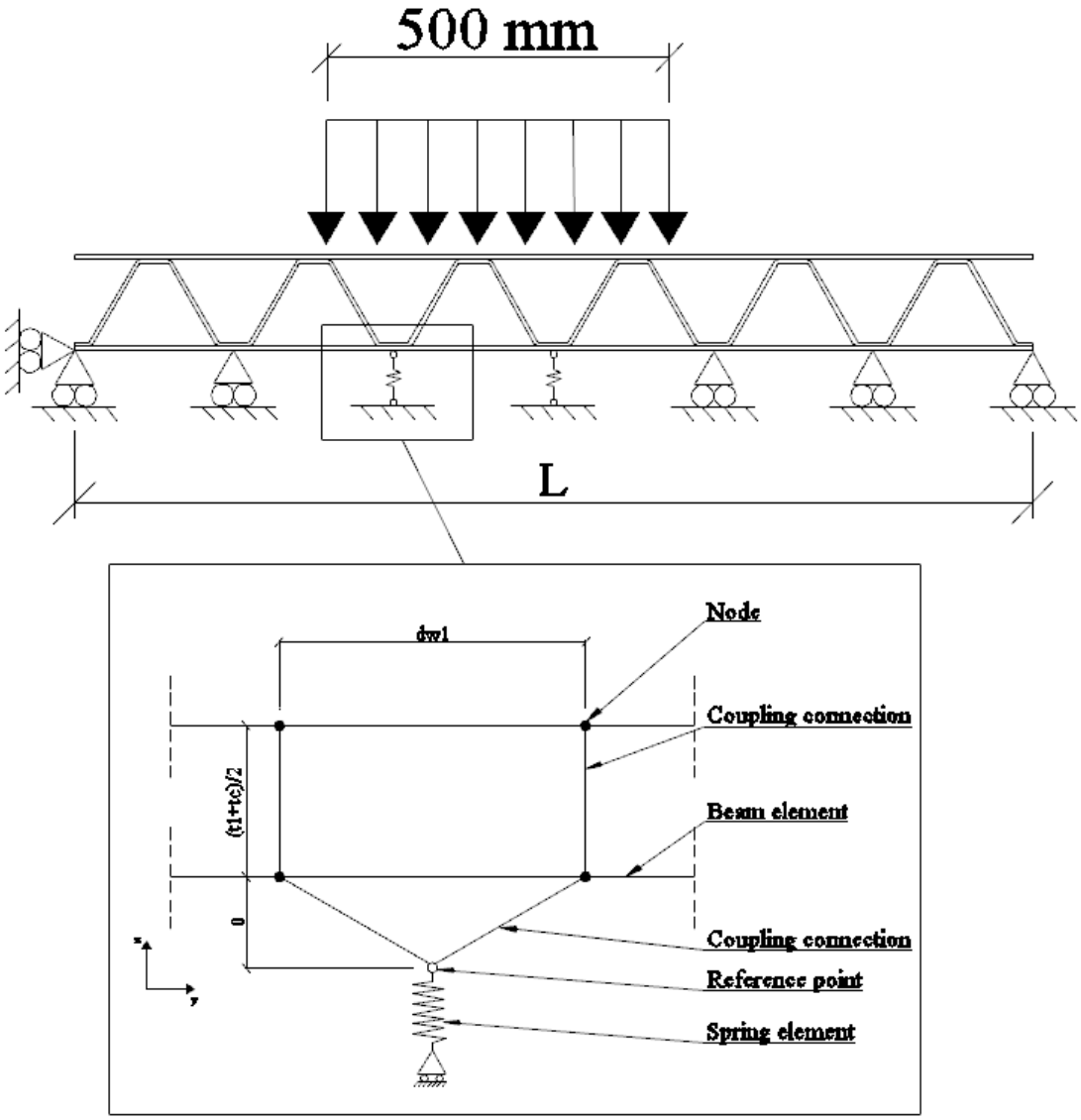

Figure 49 *Sketch of the local model and the implementation of the spring element in the FE-model.*

The magnitude of the spring-stiffness is a way to simulate the active bending stiffness of the plate in longitudinal direction (parallel to the core direction). Since the load does not simply distribute in one direction, it is hard to know exactly how big area will contribute with stiffness against deflections in the longitudinal direction. Hence, it is also hard to analytically determine the stiffness that should be inserted into the spring

elements in order to model the transversal stiffness. Therefore, the implemented stiffness had to be determined through interpolation, where results for different guessed spring stiffness's were simply compared to the results of the 3D shell model until they matched. This method was undertaken mainly to get an approximate value of a spring stiffness that could be implemented in the beam model to achieve the same results for the combined approach as for the 3D model.

11.2.1 Results

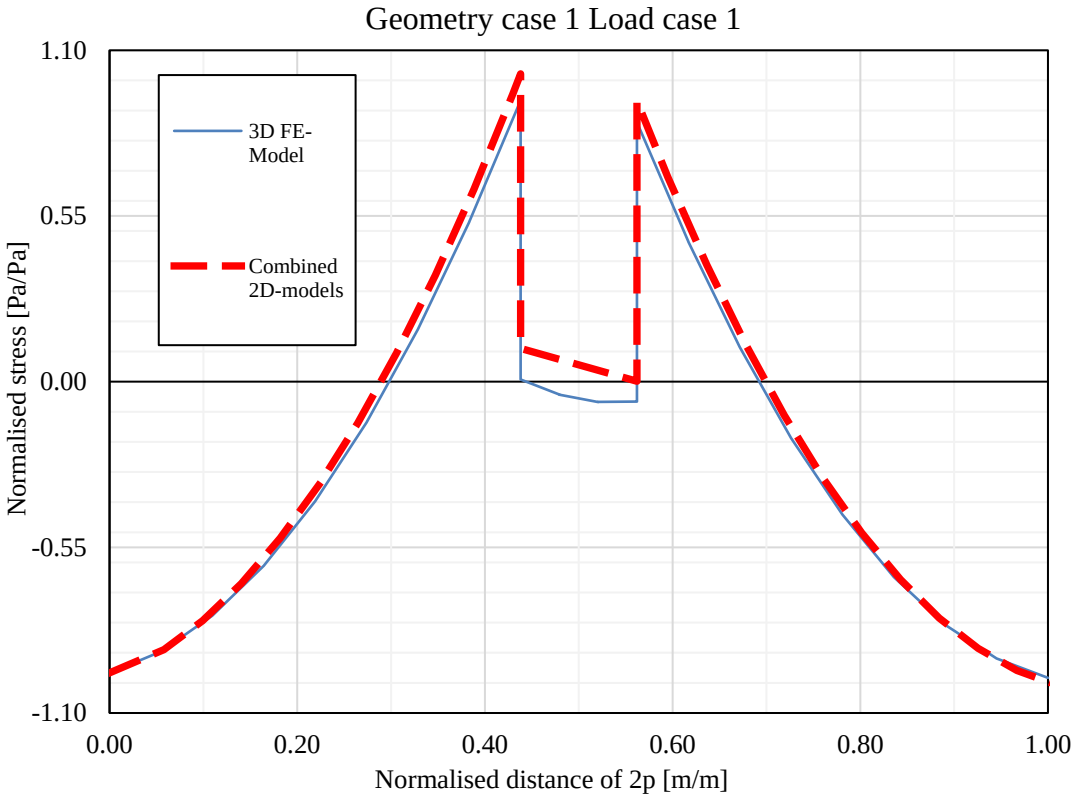

Figure 50 *Result for the study with springs as support under the load for geometry 1, the other geometries had almost identical results.*

It can be seen from all the geometry cases that the results match very closely between the 3D model and the combined approach, with only a maximum difference of about 10% at the left weld peak point. Similar results were seen for the other geometry cases and they can be found in Appendix D.

11.2.2 Discussion

Even though it seems possible to approximate the behavior of the 3D model with the described spring-method, it has a number of clear disadvantages. The most apparent issue is that the spring stiffness approach does not have an analytical way to calculate the implemented stiffness, but must instead rely on comparison to a 3D FEA. This is a fundamental flaw, since one of the main goals of the approach was to not have to rely on a 3D FE-model to analyze the corrugated core SSP. For this approach to be viable it is necessary to derive a way closed form solution.

Another issue is the uncertainties surrounding what exact number of springs to put into the 2D beam model. This might depend on the width and placement of the load and would have to be investigated for a large number of different load cases and sizes of

the plate, which in itself could be argued is too much work to validate such an unclear approach. Nevertheless, it was still shown here that it is possible to model the response of the 3D model by using only 2D models in a plate action load case.

11.3 Assessment of discrepancy by using an additional global moment

The shear-related punching-like effect was here assumed to contribute with a constant bending moment on the investigated cell. The size of this added moment was calculated by regarding the sandwich panel under a simplified load case. A simply supported beam, being subjected to an evenly distributed load corresponding to the patch load area, see Figure 51. The edge supports were placed at the position of the closest welds outside on either side of the applied load. The contributing moment could then be calculated according to elementary cases. The calculated maximum moment, found in the middle of the span of the isolated element, was inserted as a constant contribution on the final results.

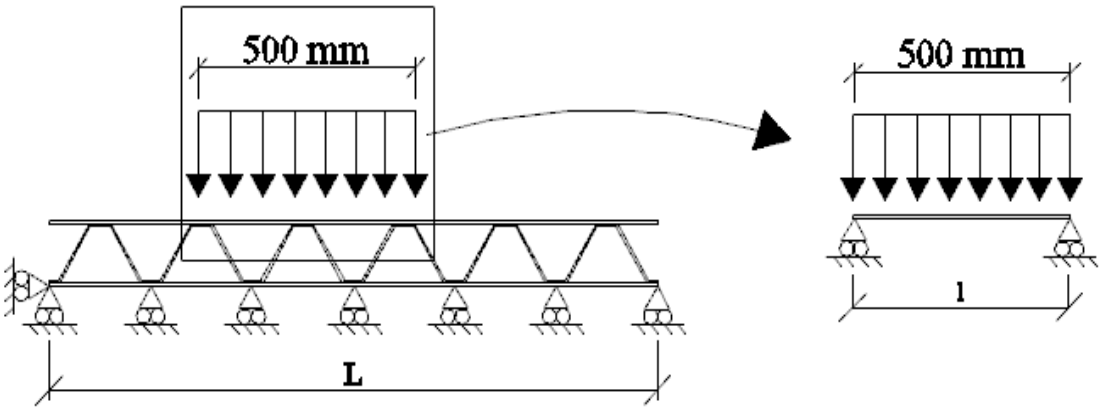

Figure 51 Sketch of the additional global transversal moment My.

The global shear force was previously assumed to be equal to zero, since the global shear force in the transversal direction will be exactly zero in the center of the applied load. This assumption will however, only be the true in the center of the unit cell. The global shear force was here given one constant value for each side of the zero-point, equal to the average value on each separate side. With these assumptions, the contribution from the shear force will be overestimated for some regions and underestimated in the other regions, hopefully resulting in a response closer to reality overall. The local moment from the global shear force was then calculated by multiplying the shear force (extracted from the ESL-model) with the shear transformation factor M_S.

11.3.1 Results

Results for this study can be seen in Figure 52-54, for geometry cases 1-3, subjected to load case 1. As the bending moment extracted from the combined approach was already larger than for the 3D FE-model for geometry case 4, the extended study presented here would obviously only yield further diverging results. Therefore this case was not included in this particular study.

The presented moment results were once again normalized against the highest calculated total moment for each studied case. The results for the combined approach include contributions from; global shear force and moment from the ESL-model, local moment from the 2D beam-model and an additional constant moment, calculated by subjecting the top beam element to a simplified load case. The results are plotted over a length of one corrugation unit, where the distance from the left side has been normalized against the total distance.

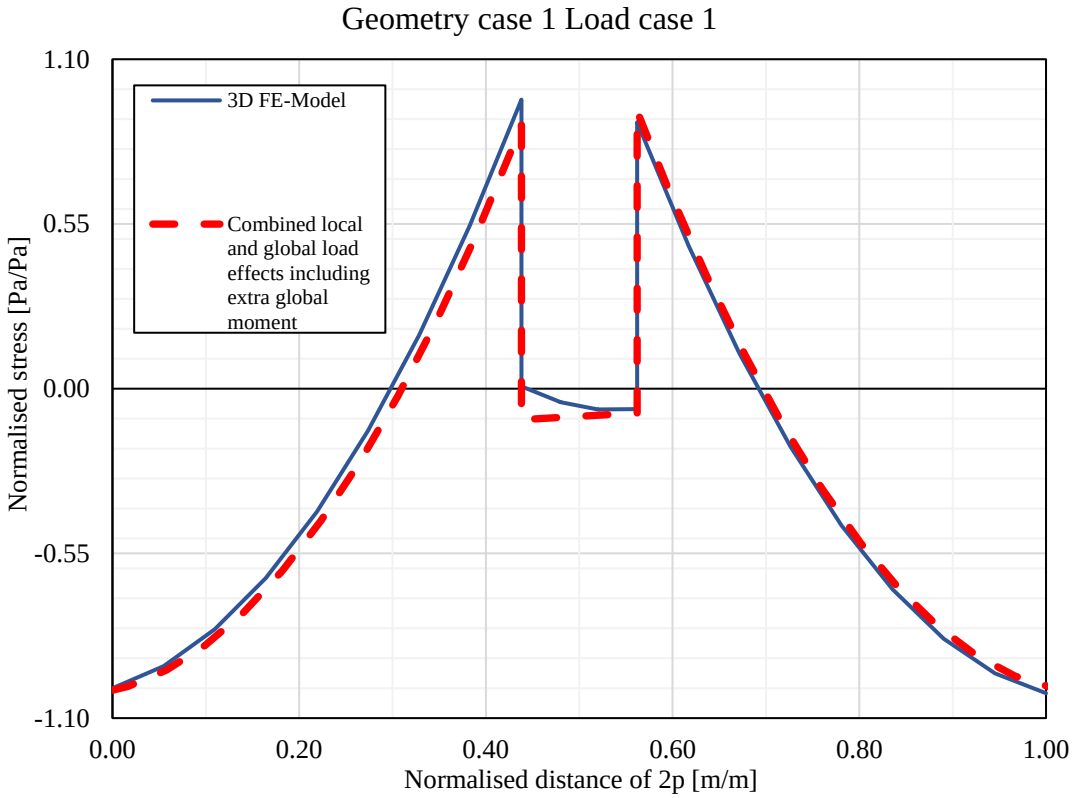

Figure 52 Result for the study with extra global moment geometry 1.

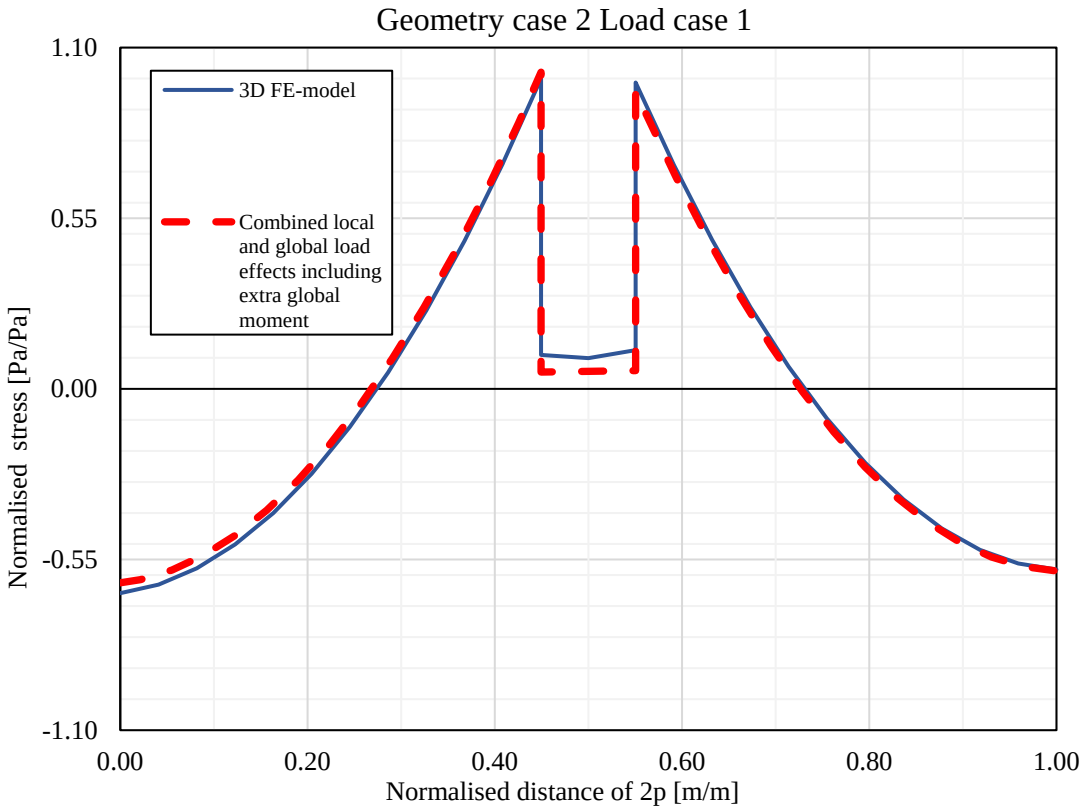

Figure 53 Results for the study with extra global moment geometry 3.

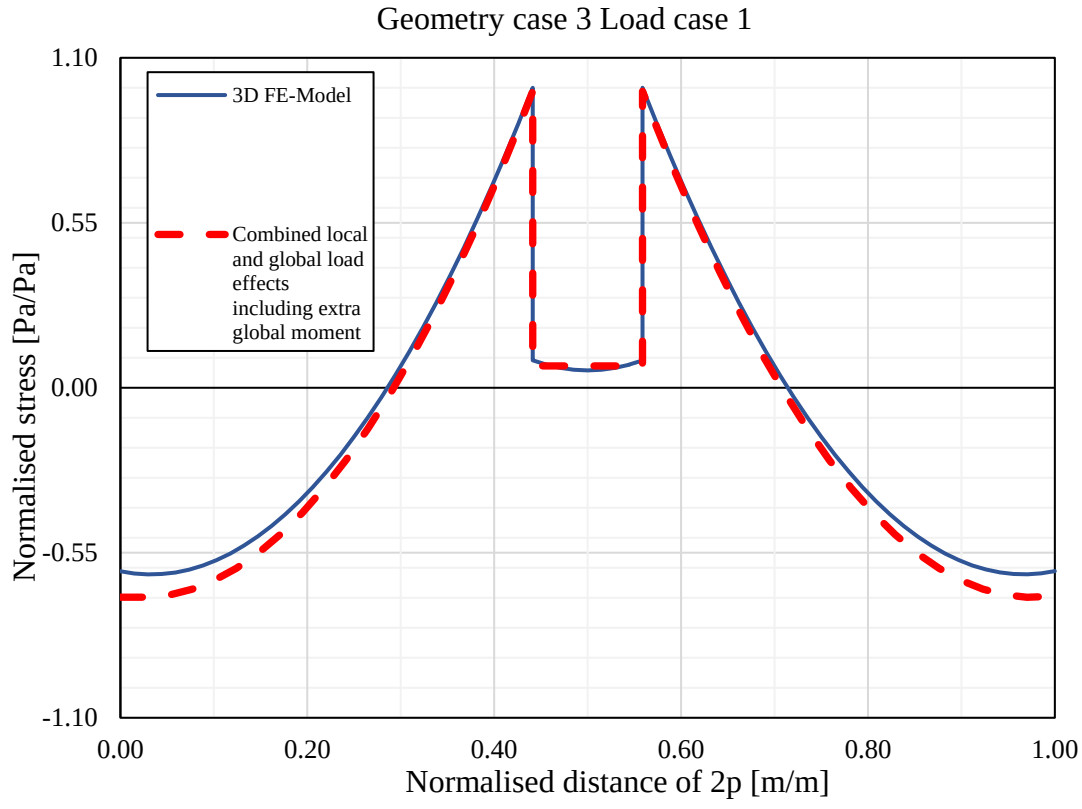

Figure 54 Result for the study with extra global moment geometry 2.

11.3.2 Discussion

The new assumptions seem to yield clear improvement for results for geometry cases 1 and 2. Results for geometry 3 are of equal accuracy compared to the previous study. For geometry case 3, the total bending moment is overestimated compared to the moment from the 3D-model. Since this geometry is naturally quite weak in the thickness direction - having a large pitch to height-ratio - it reasonable to assume that this model will exhibit some semi-global behavior even in the 2D beam local model. Therefore, the extra contribution would be redundant for this case and lead to an overestimation of the total stress.

Another factor that could possibly influence the accuracy of the presented approach, is the relation between the width of one corrugation unit and the width of load application (0.5m). For both geometry case 1 and 2, the width of load application could be divided almost perfectly over an even number of unit cells. Geometry 3 (and 4) however, did not match as accurately, meaning there was some parts on the beam element between the edge supports and the area of load application. Thus, this method is not accurate for all cross sections whereas case 1 and 2 could be estimated well with Equation 26:

$$M_{extra} = ql^2/8 \tag{26}$$

The fact that altering the global sectional forces in the region of the patch load yield accurate stress predictions in the constituent members indicate that the displayed divergence originates from the adopted plate theory in the ESL-model. Possible causes of this divergence can be the assumption of the shear strain distribution on the cross section or an effect of in plate compression of the cross-section in the 3D-model, among others.

12 Discussion

This chapter will present a broad discussion of aspects of the presented work that have not already been addressed throughout the report. For discussions targeted at results from specific studies, see the discussion-section for that particular study.

This thesis suggests a way of FE-modelling that could simplify the design of corrugated core SSPs. The method is based to a large extent on the principles proposed by Romanoff et al. in [30]. While Romanoff et al. [30] presented the suggested approach for a web-core sandwich panel, this thesis tried to apply the same evaluation approach for a panel with a corrugated core geometry. As there are several differences between web-core and corrugated-core panels, the initial theory had to be expanded and additional contributions, exclusive for corrugated-core panels, had to be considered.

The general uncertainty and lack of previous theory on the subject creates a big question regarding what was the explicit cause to the divergence of the results in the presented study. The error might for example have come from: the local 2D beam-model, assumptions made in the adopted plate theory or even something else that has not been discussed in this thesis. As the major differences can be seen in the outer region of the unit cell, where the impact of the local moment induced shear is zero, it is likely that the error originates from something else.

One of the key assumptions in this project, related to the structural behavior of the panel, was the choice of boundary conditions for the 2D beam-model. While the first set-up of boundary conditions seemed reasonable, it was seen that it did not capture the punching-like behavior. In order to find a good constellation of BCs, several set-ups were afterwards investigated. Even though the final set of boundary conditions gave good results, the working process to reach this set-up, as well as for every new iteration of the set-up, was deemed to be too complicated to be worthwhile using on a regular basis. While these approaches are not recommended to be used on a large scale, they still show that it is possible to approximate the response of the 3D model by using only 2D models, which is encouraging for future studies on the subject.

Another important assumption was made as a consequence of implementing the transformation factors M_s and M_m, as they were both derived for a state of constant global shear force and moment. This was shown to impact the results (compare Figure 32 with Figure 33). For the study away from load, the gradient of the shear force is small over the unit cell, whereby the impact is modest. For the second study however, the shear force changes rapidly under the area of load application and it also changes sign in the middle of the applied load. Consequently, utilizing transformation factors based on assumptions of constant shear forces is an inherent approximation in the homogenization approach and will always affect the accuracy to some extent.

13 Conclusions and further studies

This project studied multiscale modelling of corrugated core SSPs subjected to patch loading. A suggestion whereby the full 3D response could be captured with only 2D model(s), was made as this would simplify e.g. the early design phase. Four different geometric cases of the SSP together with one load case for plate action and one for beam action were analyzed.

Three major conclusions were drawn from the project. The first one, which was found early in the project was:

- The global moment in the transversal direction creates a local moment in the top face plate of the corrugated core SSP (described in Section 7.2).

More specifically, it was not possible initially to match the real case of the 3D-model with only the shear induced local moment. After investigating the matter further it was found that the global moment might cause a local moment similar to the global transversal shear in the top face plate. This was then verified by the means of a 4-point bending analysis. The contribution was seen to be largest in the weld region and smaller in the outer regions of the unit cell. It was also noted that the impact changed between the geometric cases. It was, however, not investigated exactly what parameters had the most influence on the size of the moment induced local moment. It was also noted that the 4-point bending analysis was very time consuming. If possible, this should be investigated in further studies in order to find an analytical expression for the contribution.

Further, when the moment- and shear-induced local moment factors are known, it was shown that:

- It is possible to estimate the local moment in the top face plate away from the load with just an ESL-model and the corresponding shear- and moment-induced local moment factors (see Chapter 9).

While the estimation for the plate action load case showed a slight deviation, it was also shown that the beam action load case leads to perfectly matched results. As discussed in the previous chapter, this difference between the load cases is most probably because of the constant shear force in load case 2, which is beneficial. Nevertheless, it was concluded that a very good estimation could be made. Consequently, the difference was not enough to disregard the proposed methodology and the same kind of approach was therefore used in the study directly under the load as well.

It is suggested that further research should investigate how the varying shear force over a unit cell impacts the local moment in the top face, as this has previously only been done for the case with constant global shear. If this relation could be determined, similar results to the beam action case can probably be achieved. Similar research could be done on the global moment in the transversal direction, however, efforts should preferably be put into finding an analytical expression first.

Finally, the last study tried to develop a method where the local moment and stress under load could be estimated more accurately. This was done by expanding the

initially suggested approach, both by changing boundary conditions for the local model and also by an approach that added global sectional forces. While a general solution could not be found, results still indicate that:

- It is possible to estimate the local stress/moment in the top face plate directly under a patch load using an ESL-model and a local 2D beam model (see Chapter 11 and 12). However, more research is required to further investigate this field.

A few points as to why a general solution could not be found is discussed in Chapter 11 and also in the discussion directly related to each result. Future studies should be carried out to further investigate what the cause of the difference is. Possible causes of error pointed out in this work was the 2D beam model and the adopted plate theory.

14 References

[1] C. Huang and A. R. Mangus, “An International Perspective:Widening Existing Bridges with Orthotropic Steel Deck Panels,” *Structural Engineering International,* vol. 4, pp. 381-389, 2008.

[2] S. R. Bright and J. W. Smith, “A new design for steel bridge decks using laser fabrication,” *The Structural Engineer,* pp. 49-57, 2007.

[3] J. Maljaars, F. van Dooren and H. Kolstein, “Fatigue assessment for deck plates in orthotropic bridge decks,” *Steel Construction - Design and Research,* vol. 5, pp. 93-100, 2012.

[4] I. Koc and E. Beneus, “Innovative road bridges with steel sandwich decks,” CHALMERS UNIVERSITY OF TECHNOLOGY, Göteborg, 2014.

[5] V. Caccese and S. Yorulmaz, “Laser Welded Steel Sandwich Panel Bridge Deck Development: Finite Element Analysis and Stake Weld Strength Tests,” University of Maine Department of Transportation, Orono, 2009.

[6] P. Nilsson, “Steel-sandwich elements in bridge applications,” CHALMERS UNIVERSITY OF TECHNOLOGY, Göteborg, 2015.

[7] L. Persson, “A parametric study of shear-induced fatigue in corrugated steel sandwich elements,” CHALMERS UNIVERSITY OF TECHNOLOGY, Göteborg, 2016.

[8] SANDCORE, “Best Pratise Guide for Sandwich Structures in Marine Applications.,” Prepared by the SAND.CORe CO-ordination Action on Advanced Sandwich Structures in the Transport Industries Under European Commision Contract No.FP6-506330.

[9] A. Romeo, D. P. Boso and U. Galvanetto, “APPLICATION OF SANDWICH STRUCTURES TO AUTOMOTIVE RIMS,” in *18th International Conference on Composite Materials*, Jeju Island.

[10] U. Alwan and D. Järve, “New Concept for Industrial Bridge Construction,” CHALMERS UNIVERSITY OF TECHNOLOGY, Göteborg, 2012.

[11] J. Romanoff, Bending response of laser-welded web-core sandwich plates - Doctoral Dissertion, Espoo: Helsinki University of Technology, 2007.

[12] C. Libove and S. B. Batdorf, “A general small-deflection theory for flat sandwich plates,” National advisory committee for aeronautics, 1948.

[13] P. Kujala and A. Klanac, “Steel SDandwich Panels in Marine Applications,” *BRODO GRADNJA,* vol. 56, no. 4, pp. 305-314, 2005.

[14] M. Wouters, “Hybrid Laser-MIG welding: An investigation of geometrical considerations, Licentiate Thesis,” Luleå University of Technology, Luleå, 2005.

[15] D. Dackman and W. Ek, “Steel sandwich decks in medium span bridges,” CHALMERS UNIVERSITY OF TECHNOLOGY, Gothenburg, 2015.

[16] C. Libove and R. E. Hubka, “Elastic constants for corrugated-core sandwich plates,” NACA, Wachington, 1951.

[17] P. Nilsson, M. Al-Emrani and S. R. Atashipou, “Transverse shear stiffness of corrugated core steel sandwich panels with dual weld lines,” *Thin-walled structures,* vol. 117, pp. 98-112, 2017.

[18] MSC Software, “MSC Software - Simulating Reality, Delivering Certainity,” 11 July 2013. [Online]. Available: http://simulatemore.mscsoftware.com/choosing-the-right-finite-element-msc-nastran/. [Accessed 29 June 2017].

[19] MSC Software, Linear Static Analysis User's Guide, Santa Ana: MSC.Software Corporation, 2012.

[20] A. Stühmeyer, “The thick shell element for metalforming and other applications,” in *5th European LS-DYNA Conference*, Birmingham, 2005.

[21] SIMULIA, “Abaqus 6.12 Analysis User's Manual Volume IV: Elements,” Dassault Systèmes, Providence, 2012.

[22] J. Dean, “Introduction to the Finite Element Method (FEM) - Lecture 2, First and Second Order One Dimensional Shape Functions,” [Online]. Available: http://www.ccg.msm.cam.ac.uk/images/FEMOR_Lecture_2.pdf. [Accessed 30 06 2017].

[23] SIMULIA, “Abaqus 6.12 Getting Started with Abaqus: Interactive Edition,” Dassault Systêmes, Providence, 2012.

[24] E. Carrera, “Historical review of Zig-Zag theories for multilayered plates and shells,” *Applied Mechanics Reviews,* vol. 56, no. 3, pp. 287-308, 2003.

[25] ANSYS, “ANSYS Online Manuals release 5.5,” ANSYS, [Online]. Available: http://ans2.vm.stuba.sk/html/elem_55/chapter4/ES4-181.htm. [Accessed 29 June 2017].

[26] K. H. Tan, P. Montague and C. Norris, “Steel sandwich panels:finite element, closer solution, and experimental comparisons, on a 6m x 2.1m panel,” *The Structural Engineer,* vol. 67, no. 9, pp. 159-166, 2 May 1989.

[27] S. Kazemahvazi and D. Zenkert, “Corrugated all-composite sandwich structures. Part 1: Analytical model,” *Composites Science And Technology,* vol. 69, no. 7-8, pp. 913-919, 2008.

[28] L. Valdevit, Z. Wei, C. Mercer, F. W. Zok and A. G. Evans, “Structural performance of near-optimal sandwich panels with corrugated cores,” *International Journal of Solids and Structures,* vol. 43, pp. 4888-4905, 2006.

[29] M. Leekitwattana, S. W. Boyd and R. A. Shenoi, “Evaluation of the transverse shear stiffness of a bi-directional corrugated-strip-core sandwich beam,” *Journal of Constructional Steel Research,* vol. 67, pp. 248-254, 2011.

[30] J. Romanoff, P. Varsta and R. Heikki, “Laser-welded web-core sandwich plates under patch loading,” *Marine Structures,* vol. 20, pp. 25-48, 2007.

[31] T. Lok and Q. Cheng, “Elastic Deflection of Thin-Walled Sandwich Panel,” *Sandwich structures and Materials,* vol. 1, 1999.

[32] T. Adolfsson, “Element to element joints of corrugated core steel sandwich bridge decks,” Chalmers, Gothenburg, 2016.

[33] S. R. Bright and J. W. Smith, “Fatigue performance of laser-welded steel bridge decks,” *The Structural Engineer,* pp. 31-39, 2004.

[34] H. G. Allen, Analysis and Design of Structural Sandwich Panels, Southampton: Pergamon Press, 1969.

[35] W.-S. Chang, E. Ventsel, T. Krauthammer and J. John, “Bending behaviour of corrugated-core sandwich plates,” *Composite structures,* vol. 70, pp. 81-89, 2004.

[36] J. Samuelsson, “FE-Design 2003 - Improved Usage of High Strength Steel by an Effective FE-based Design Methodology for Fatigue Loaded Complex Welded Structures,” Volvo, Stockholm, 2004.

[37] J. Hoffart and E. Hasen, “Welding design & fabrication,” ESAB Welding & Cutting Products, 1 Oct 2008. [Online]. Available: http://weldingdesign.com/archive/design-implications-sandwich-panels. [Accessed 31 Jan 2017].

[38] Z.-G. Xiao, K. Yamada, S. Ya and X.-L. Zhao, “Stress analyses and fatigue evaluation of rib-to-deck joints in steel orthotropic decks,” *INternational Journal of Fatigue,* vol. 30, pp. 1387-1397, 2008.

APPENDIX A

The convergence studies of the 3D FE-model geometry case 2-4 are presented in this section.

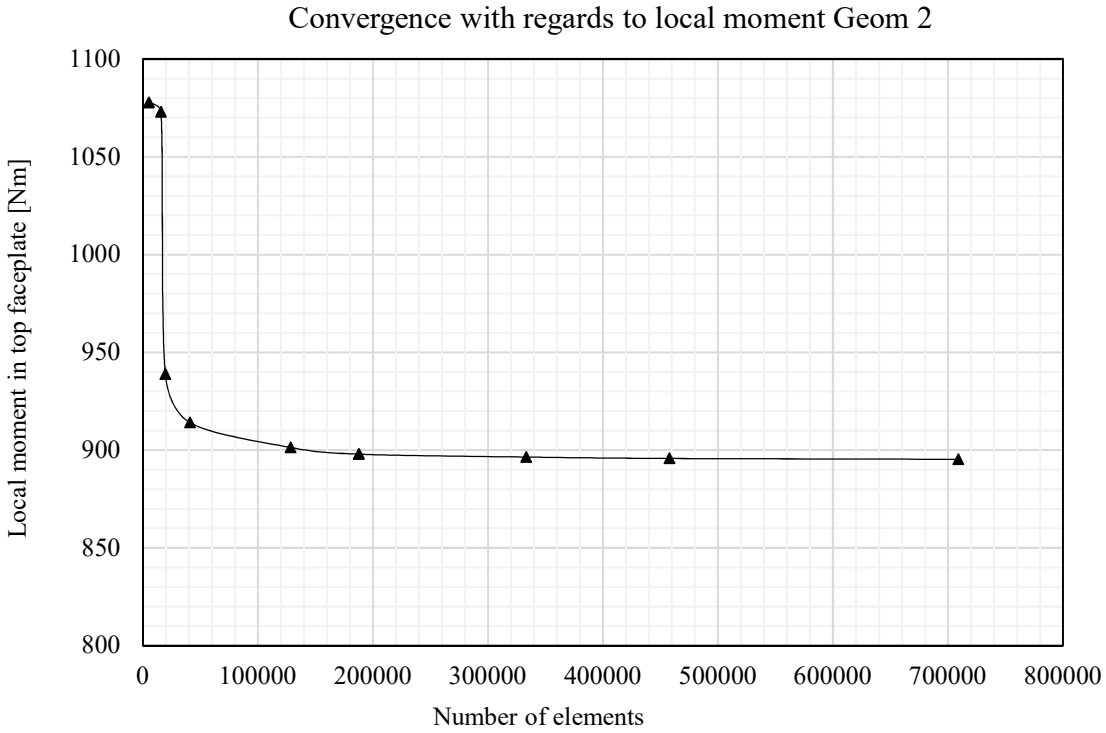

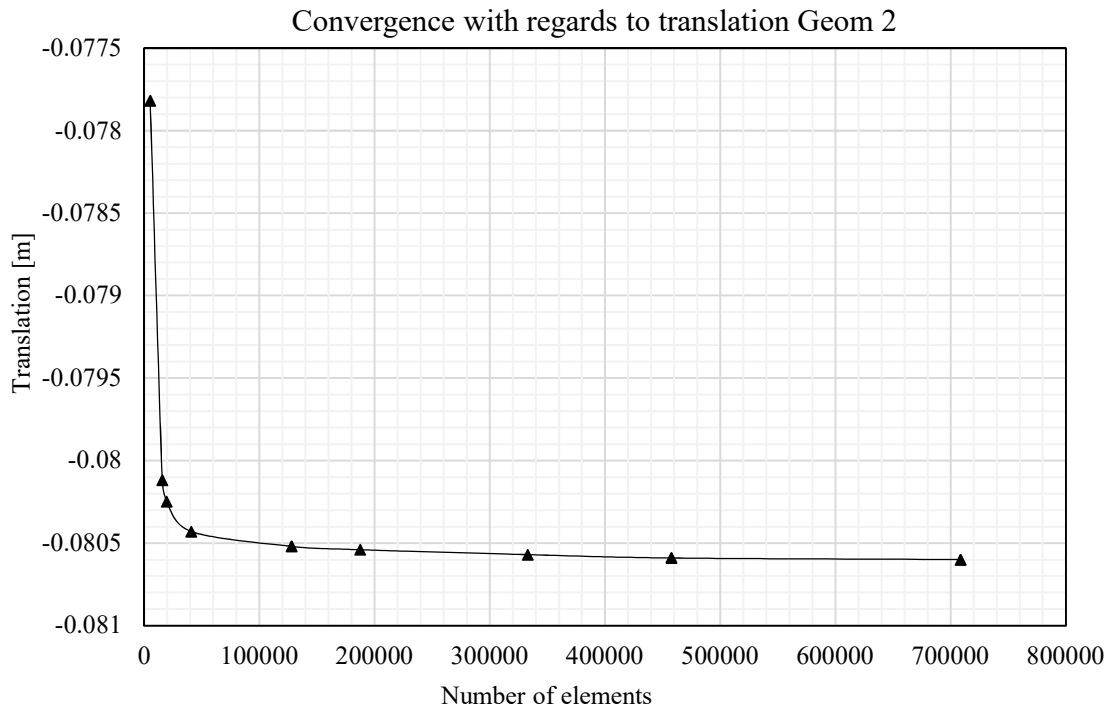

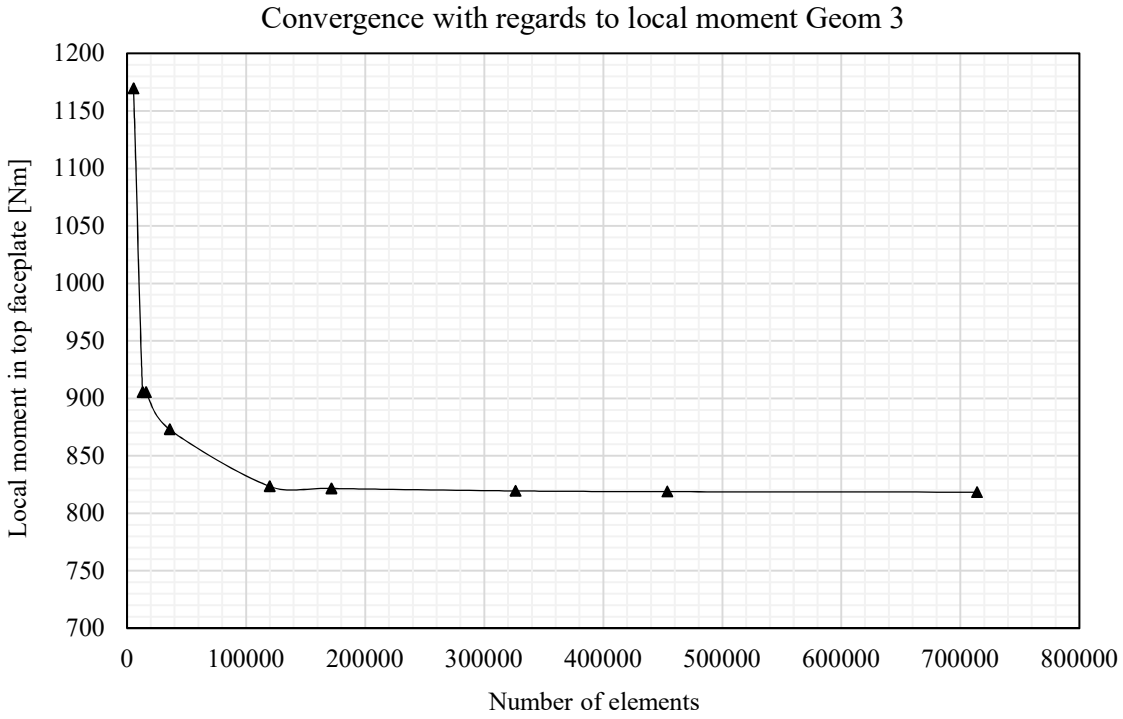
Convergence with regards to local moment Geom 3
Local moment in top faceplate [Nm]
1200
1150
1100
1050
1000
950
900
850
800
750
700
0
100000
200000
300000
400000
500000
600000
700000
800000
Number of elements

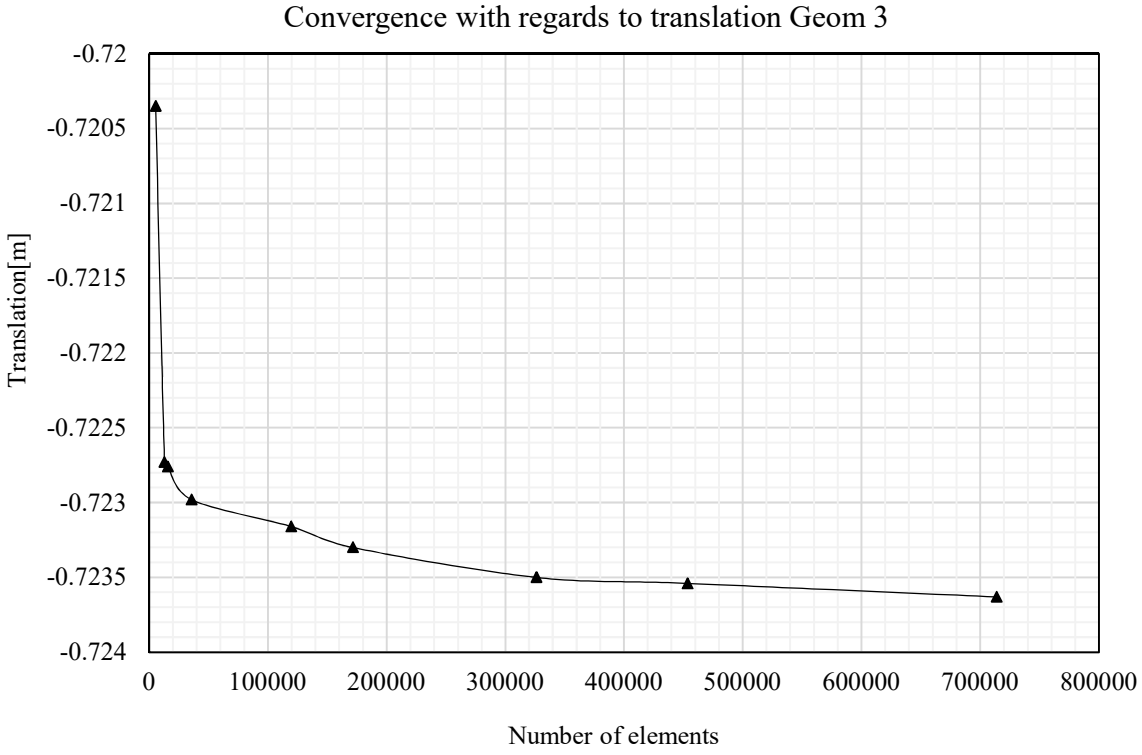
Convergence with regards to translation Geom 3
Translation[m]
-0.72
-0.7205
-0.721
-0.7215
-0.722
-0.7225
-0.723
-0.7235
-0.724
0
100000
200000
300000
400000
500000
600000
700000
800000
Number of elements

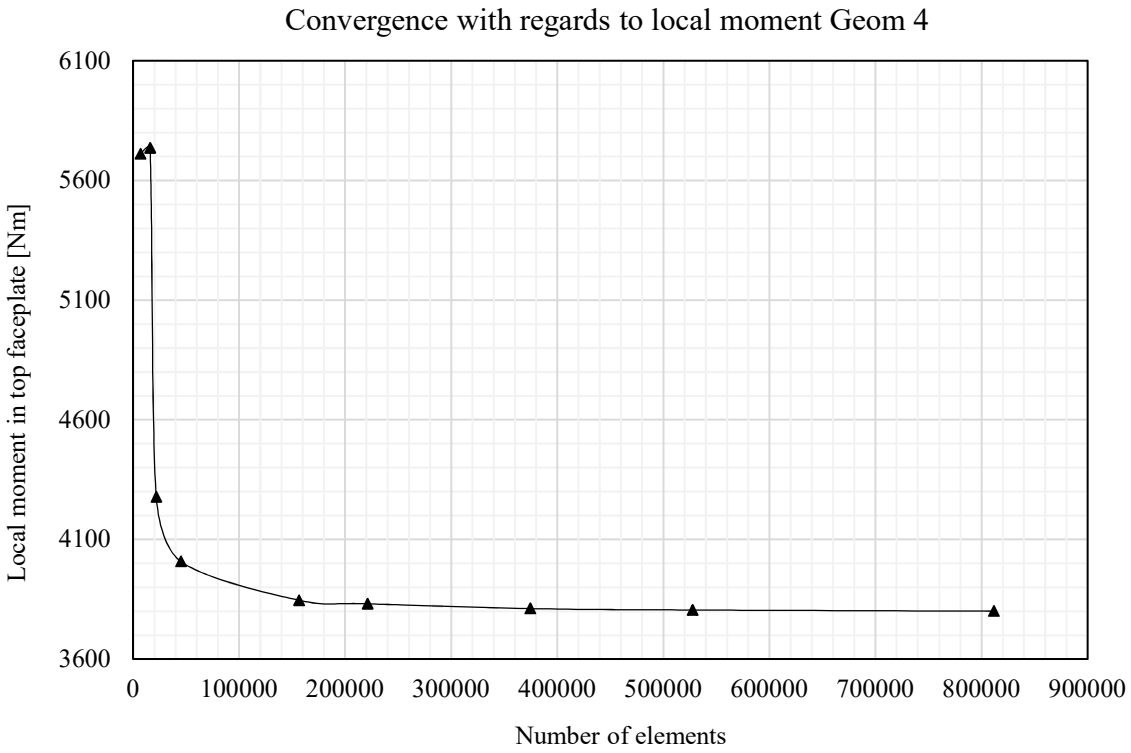
Convergence with regards to local moment Geom 4
Local moment in top faceplate [Nm]
6100
5600
5100
4600
4100
3600
0
100000
200000
300000
400000
500000
600000
700000
800000
900000
Number of elements

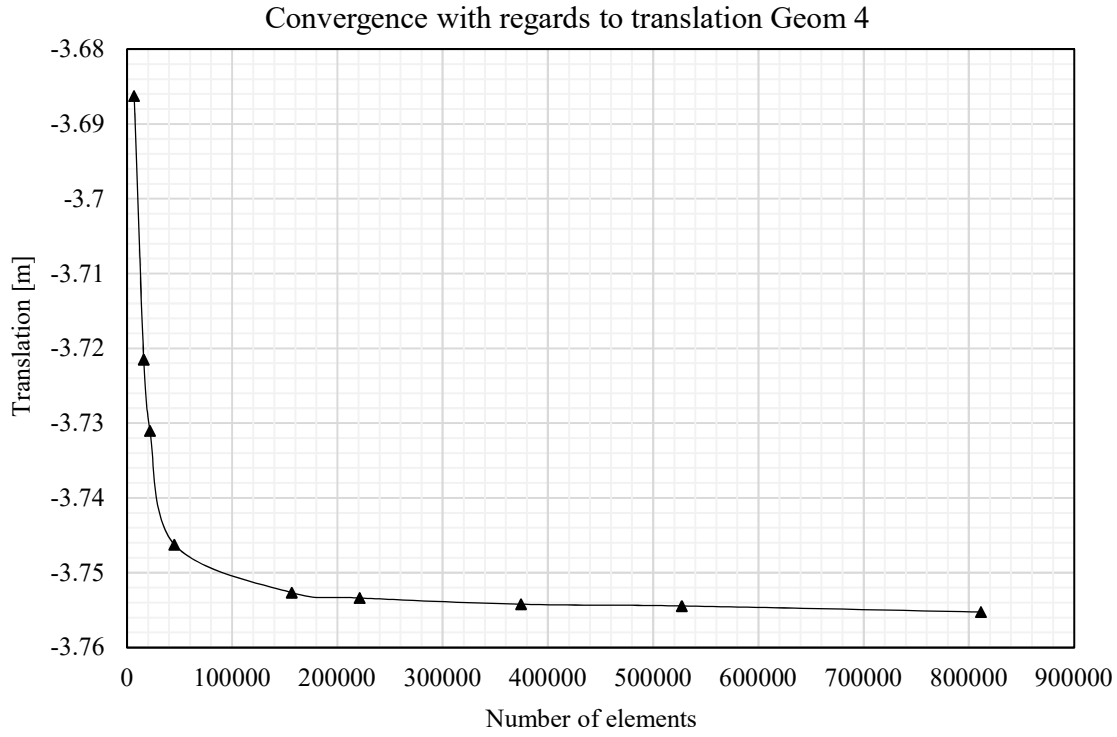
Convergence with regards to translation Geom 4
Translation [m]
-3.68
-3.69
-3.7
-3.71
-3.72
-3.73
-3.74
-3.75
-3.76
0
100000
200000
300000
400000
500000
600000
700000
800000
900000
Number of elements

APPENDIX B

The remaining geometric cases plot's of the study under load are presented in this part of the appendix.

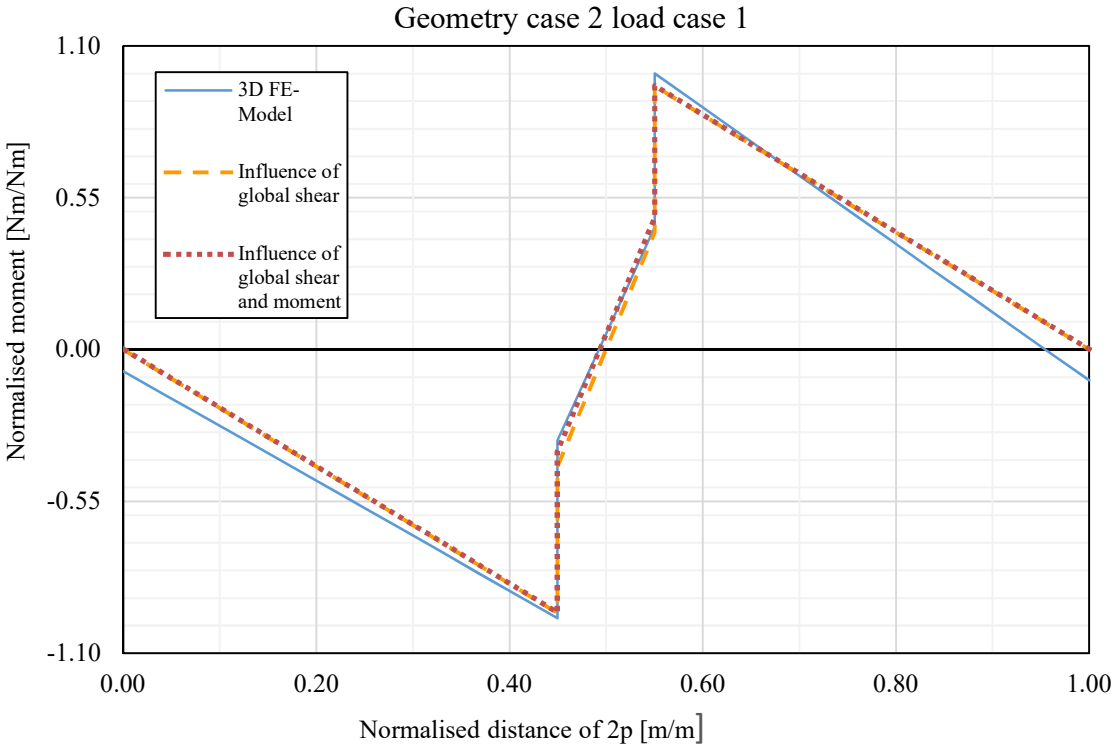

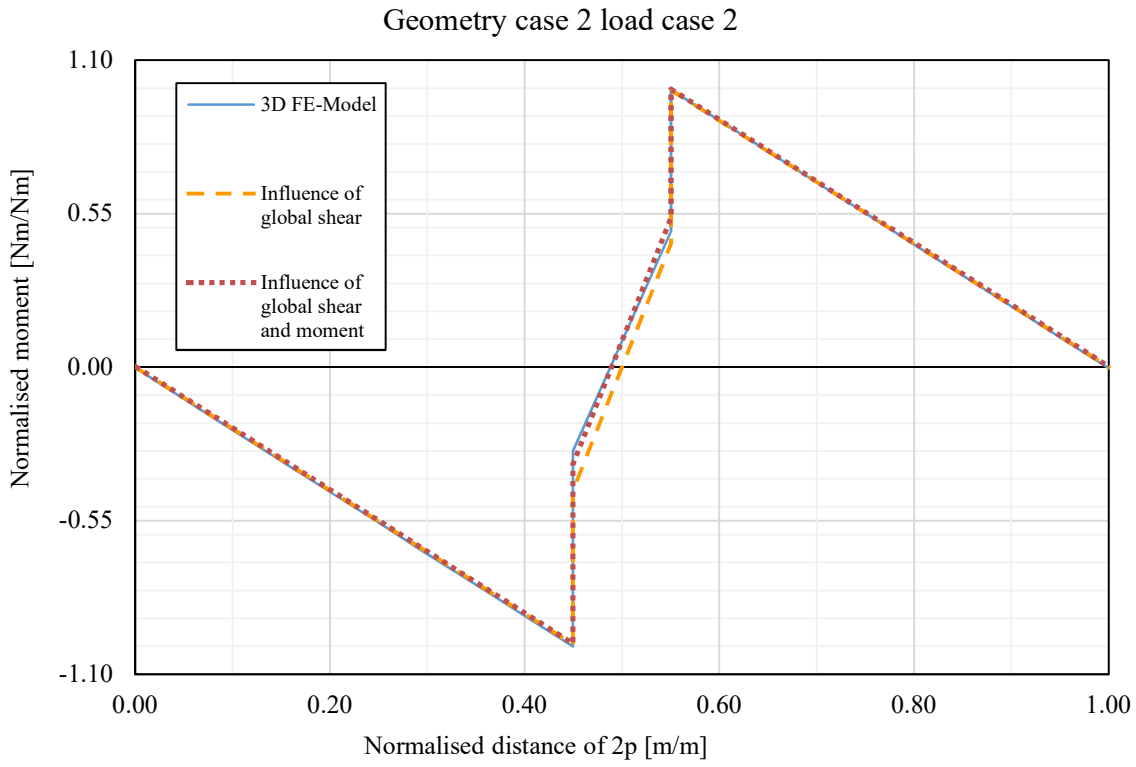
Geometry case 2 load case 2
1.10
0.55
0.00
-0.55
-1.10
0.00
0.20
0.40
0.60
0.80
1.00
Normalised moment [Nm/Nm]
Normalised distance of 2p [m/m]
3D FE-Model
Influence of global shear
Influence of global shear and moment

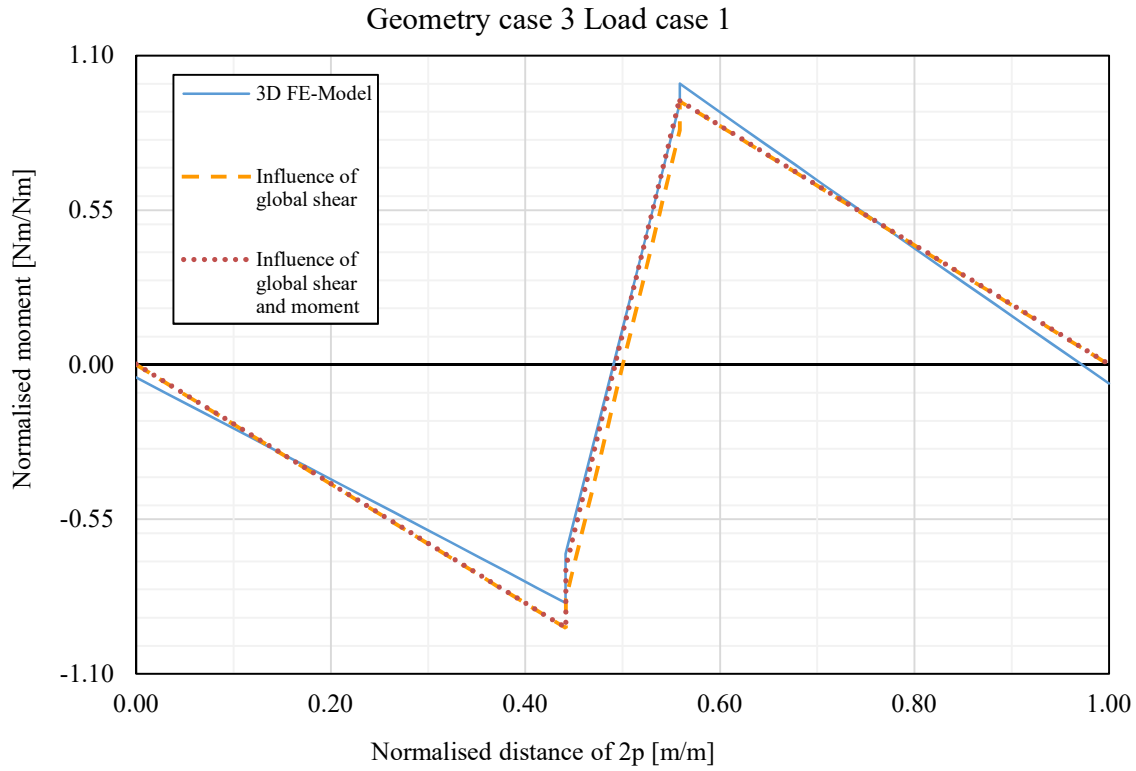
Geometry case 3 Load case 1
1.10
0.55
0.00
-0.55
-1.10
0.00
0.20
0.40
0.60
0.80
1.00
Normalised moment [Nm/Nm]
Normalised distance of 2p [m/m]
3D FE-Model
Influence of global shear
Influence of global shear and moment

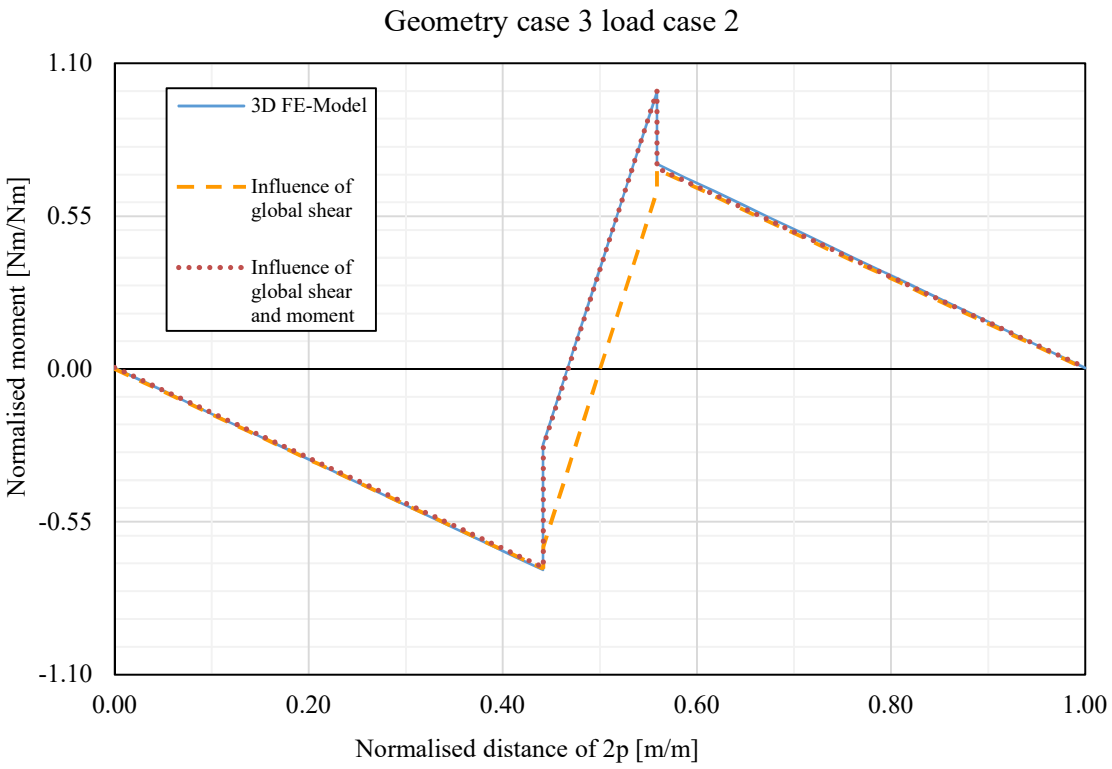
Geometry case 3 load case 2
1.10
0.55
0.00
-0.55
-1.10
Normalised moment [Nm/Nm]
3D FE-Model
Influence of global shear
Influence of global shear and moment
0.00
0.20
0.40
0.60
0.80
1.00
Normalised distance of 2p [m/m]

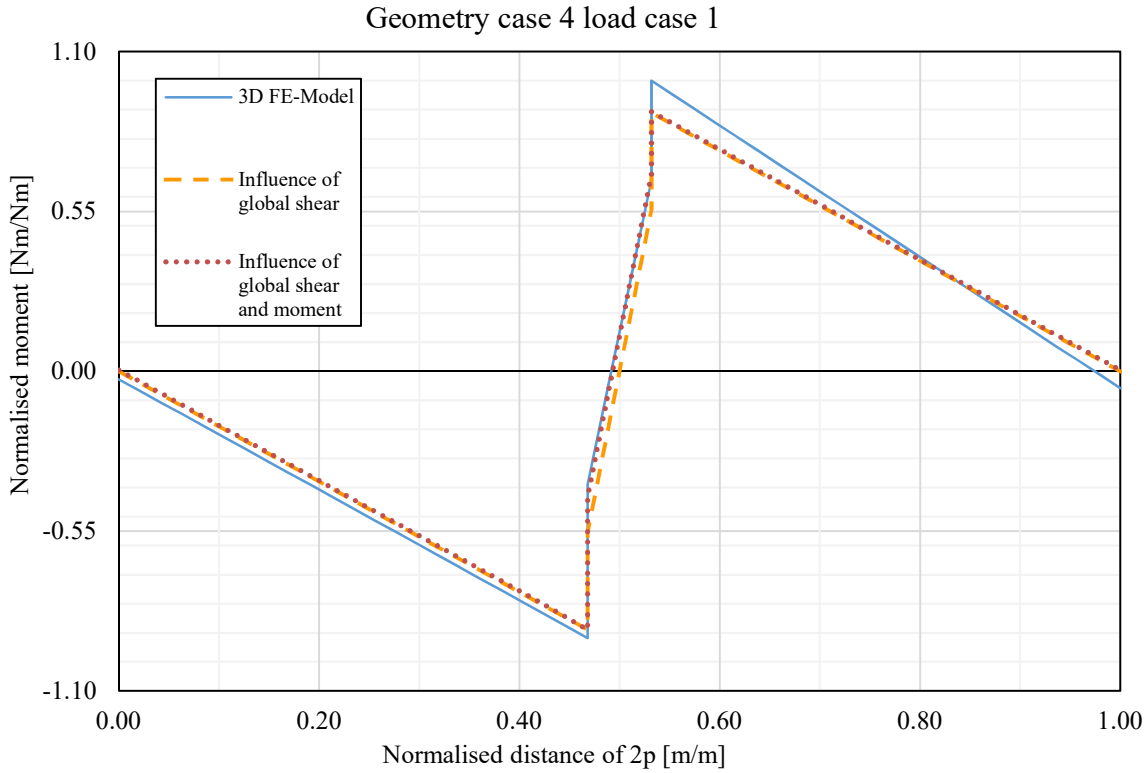
Geometry case 4 load case 1
1.10
0.55
0.00
-0.55
-1.10
Normalised moment [Nm/Nm]
3D FE-Model
Influence of global shear
Influence of global shear and moment
0.00
0.20
0.40
0.60
0.80
1.00
Normalised distance of 2p [m/m]

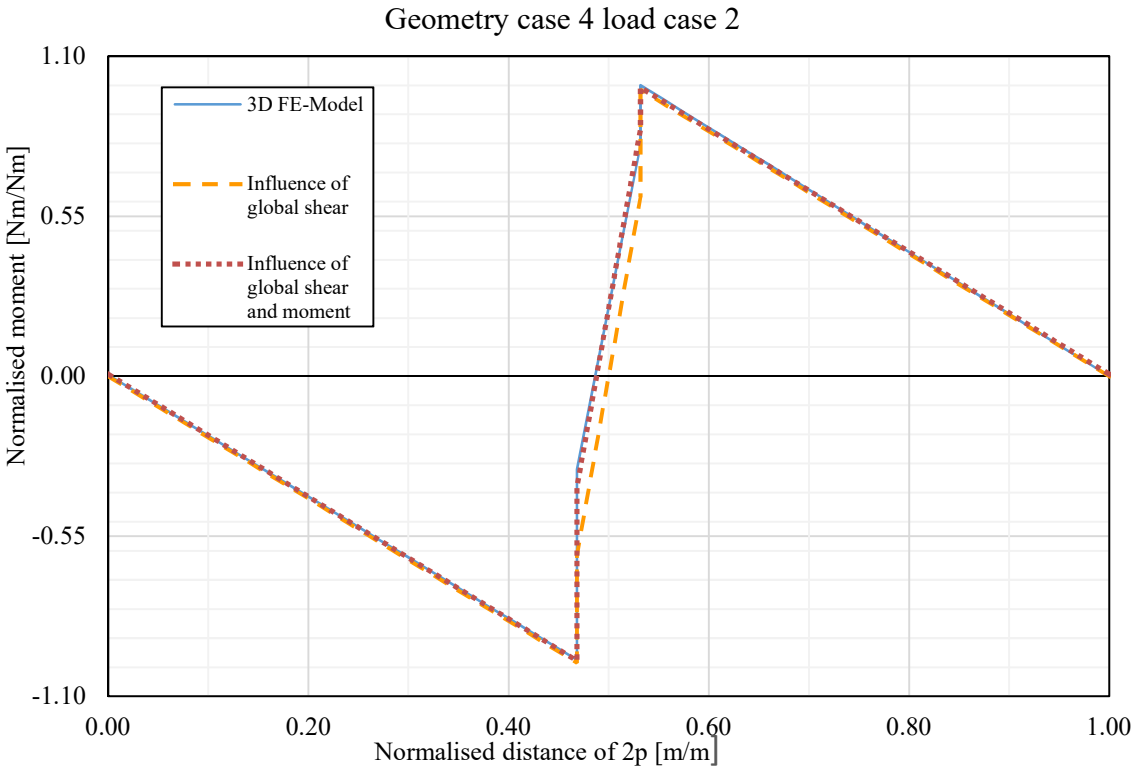
Geometry case 4 load case 2
1.10
0.55
0.00
-0.55
-1.10
Normalised moment [Nm/Nm]
3D FE-Model
Influence of global shear
Influence of global shear and moment
0.00
0.20
0.40
0.60
0.80
1.00
Normalised distance of 2p [m/m]

APPENDIX C

The remaining geometric cases plot's of the study with removed supports under the load are presented in this part of the appendix.

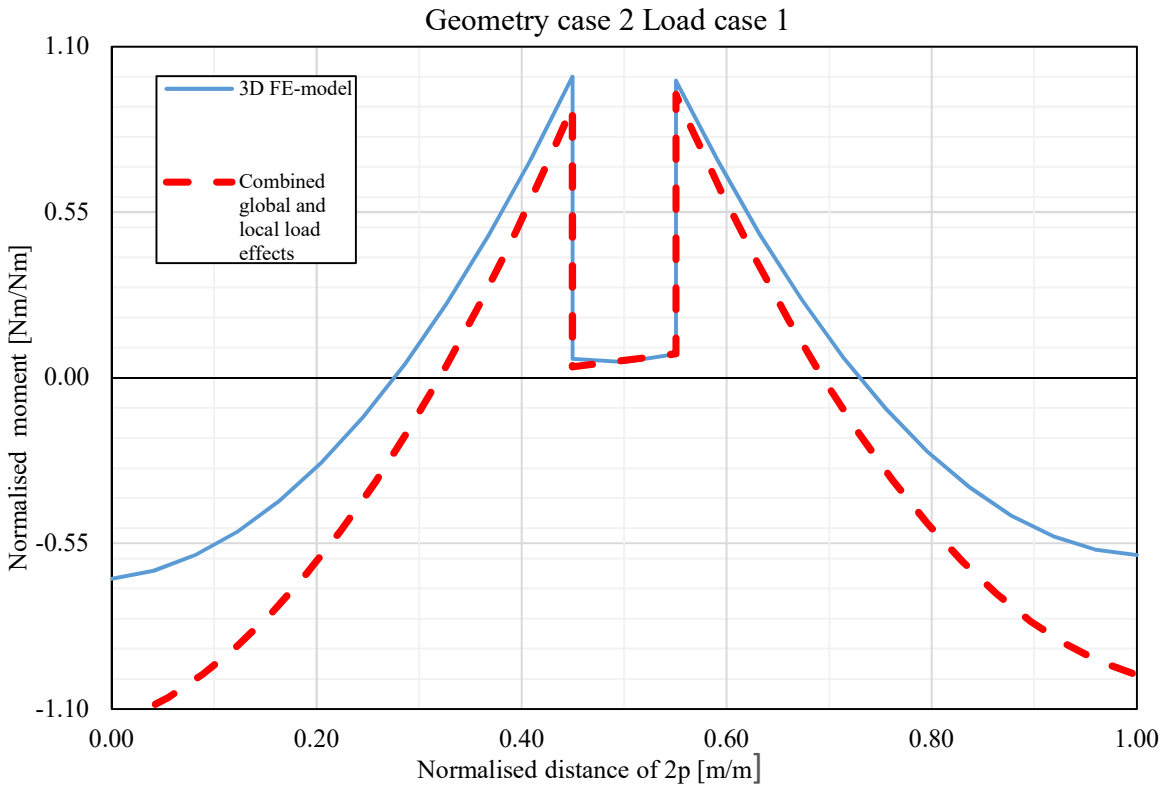

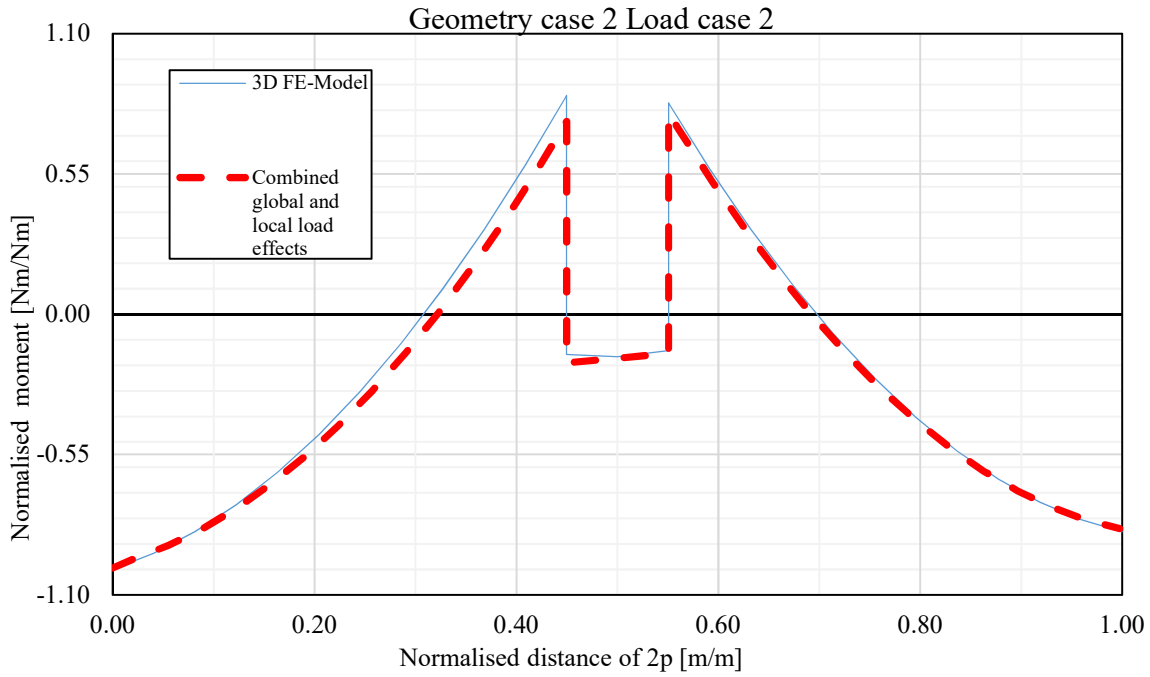

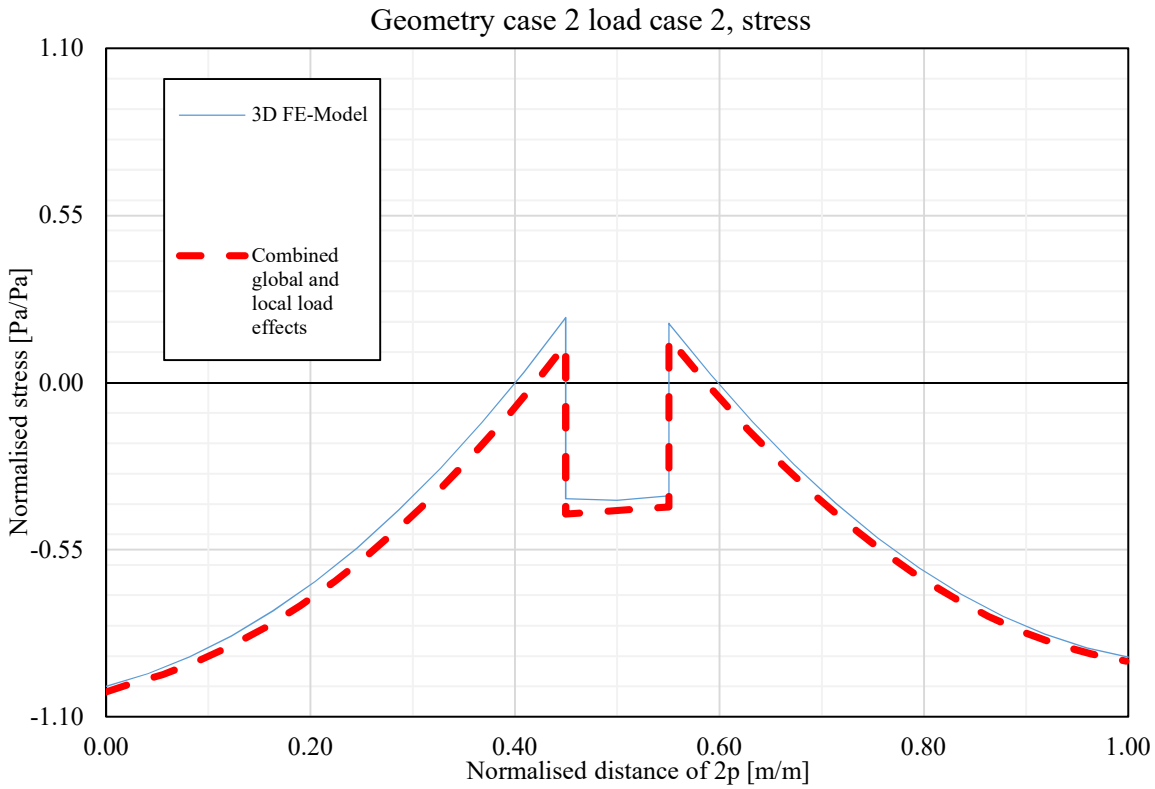
Geometry case 2 load case 2, stress
1.10
0.55
0.00
-0.55
-1.10
Normalised stress [Pa/Pa]
3D FE-Model
Combined global and local load effects
0.00
0.20
0.40
0.60
0.80
1.00
Normalised distance of 2p [m/m]

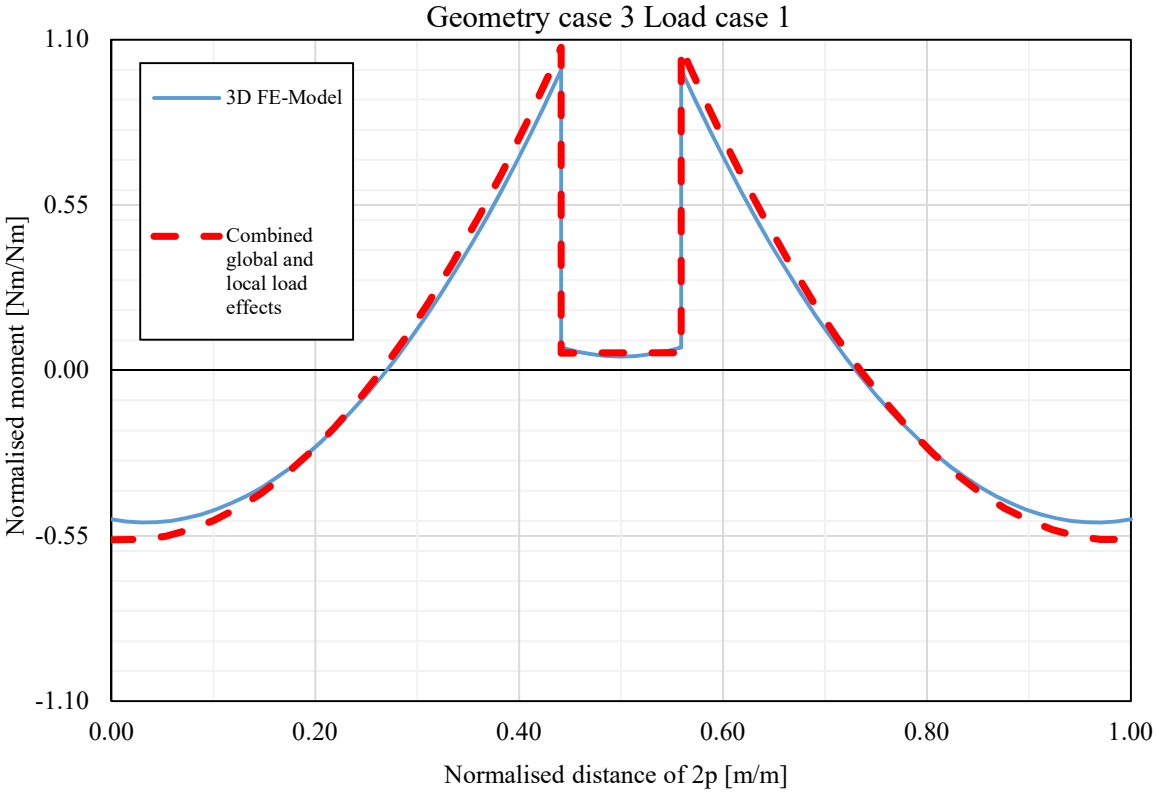
Geometry case 3 Load case 1
1.10
0.55
0.00
-0.55
-1.10
Normalised moment [Nm/Nm]
3D FE-Model
Combined global and local load effects
0.00
0.20
0.40
0.60
0.80
1.00
Normalised distance of 2p [m/m]

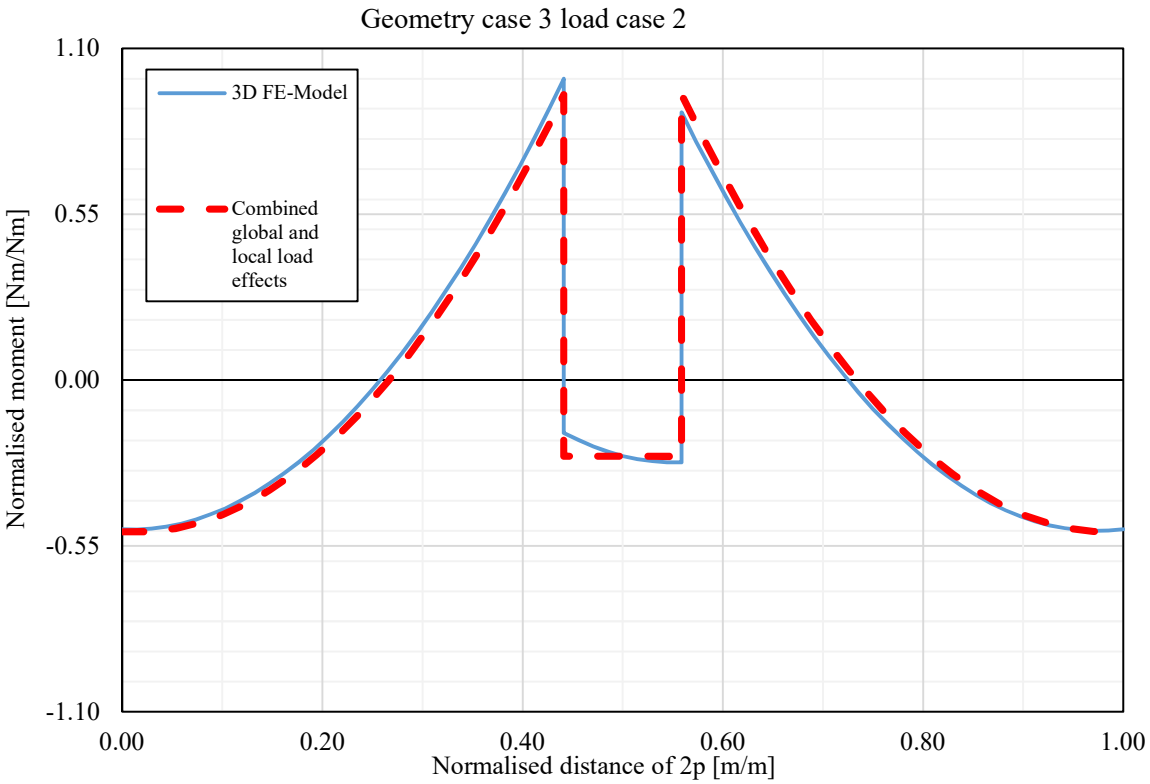
Geometry case 3 load case 2
1.10
0.55
0.00
-0.55
-1.10
Normalised moment [Nm/Nm]
3D FE-Model
Combined global and local load effects
0.00
0.20
0.40
0.60
0.80
1.00
Normalised distance of 2p [m/m]

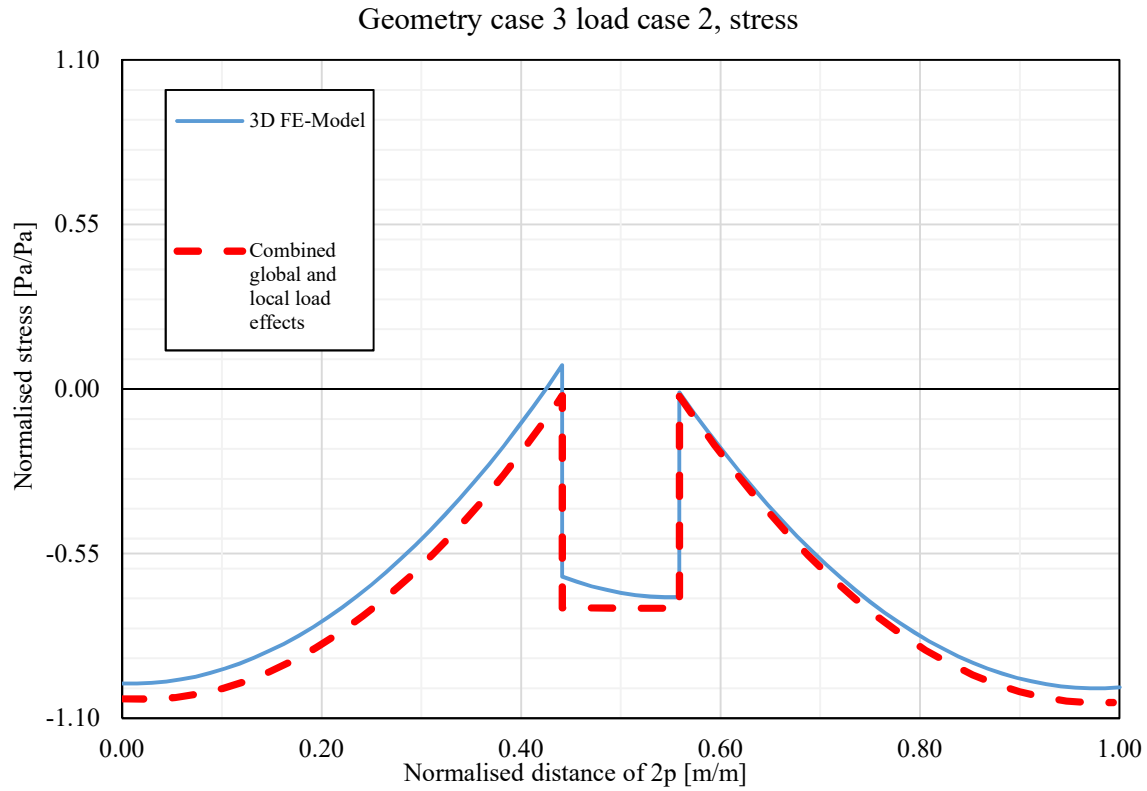
Geometry case 3 load case 2, stress
1.10
0.55
0.00
-0.55
-1.10
Normalised stress [Pa/Pa]
3D FE-Model
Combined global and local load effects
0.00
0.20
0.40
0.60
0.80
1.00
Normalised distance of 2p [m/m]

Geometry 4

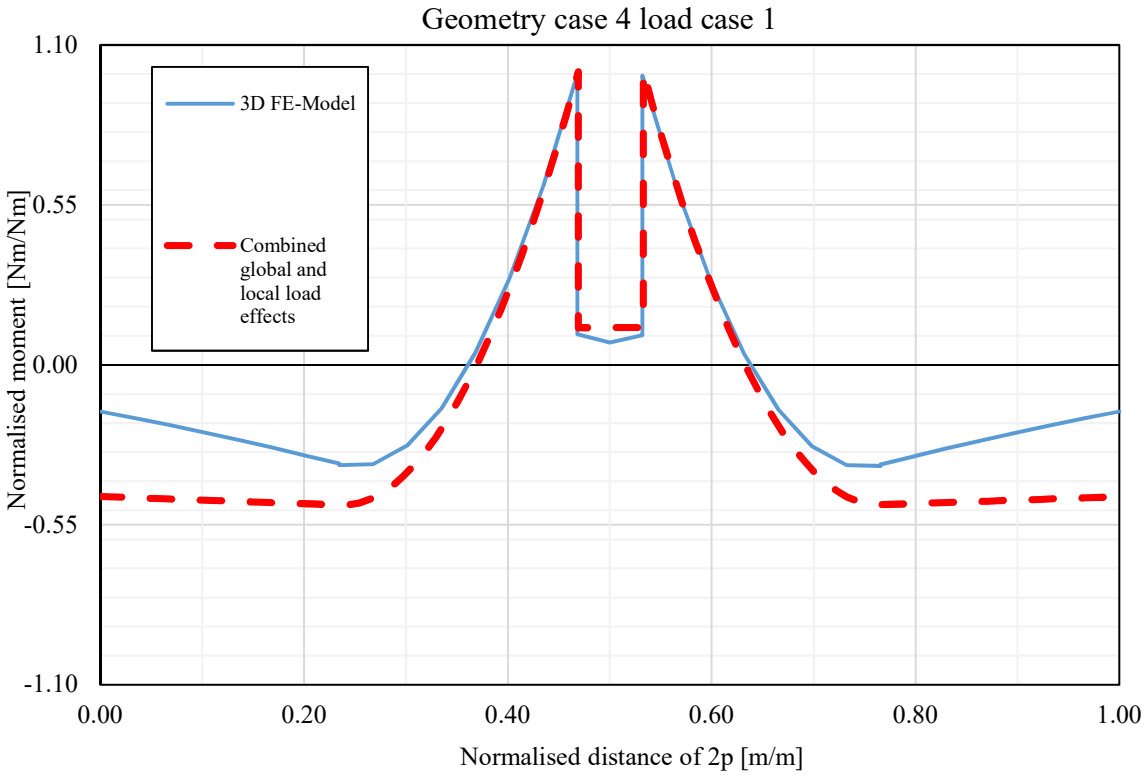
Geometry case 4 load case 1
1.10
0.55
0.00
-0.55
-1.10
Normalised moment [Nm/Nm]
3D FE-Model
Combined global and local load effects
0.00
0.20
0.40
0.60
0.80
1.00
Normalised distance of 2p [m/m]

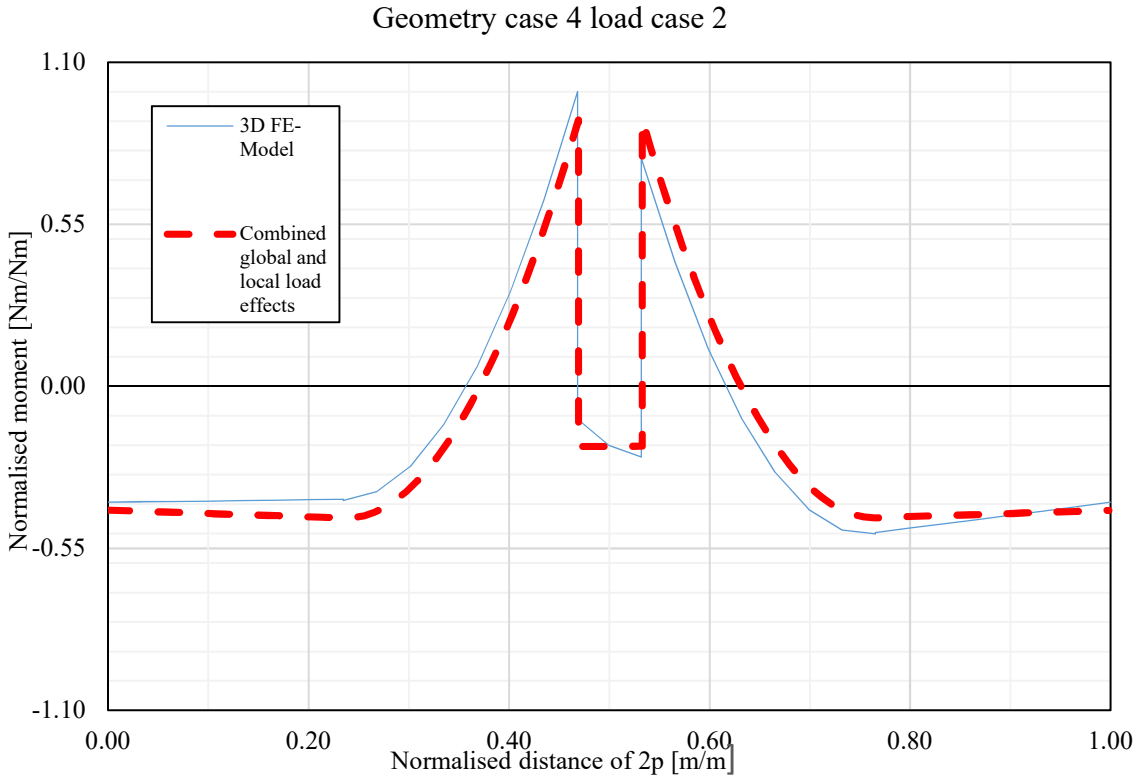
Geometry case 4 load case 2
1.10
0.55
0.00
-0.55
-1.10
Normalised moment [Nm/Nm]
3D FE-Model
Combined global and local load effects
0.00
0.20
0.40
0.60
0.80
1.00
Normalised distance of 2p [m/m]

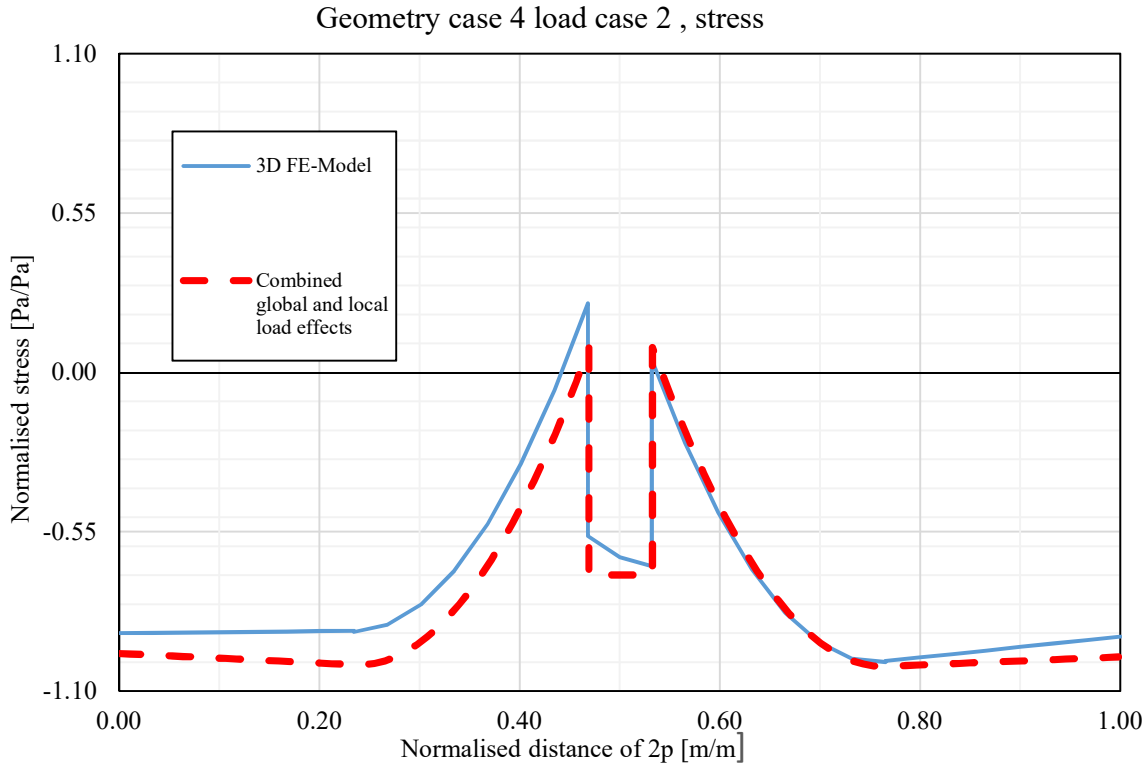
Geometry case 4 load case 2 , stress
1.10
0.55
0.00
-0.55
-1.10
Normalised stress [Pa/Pa]
3D FE-Model
Combined global and local load effects
0.00
0.20
0.40
0.60
0.80
1.00
Normalised distance of 2p [m/m]

APPENDIX D

The remaining geometric cases plot's of the study with springs as supports under the load are presented in this part of the appendix.

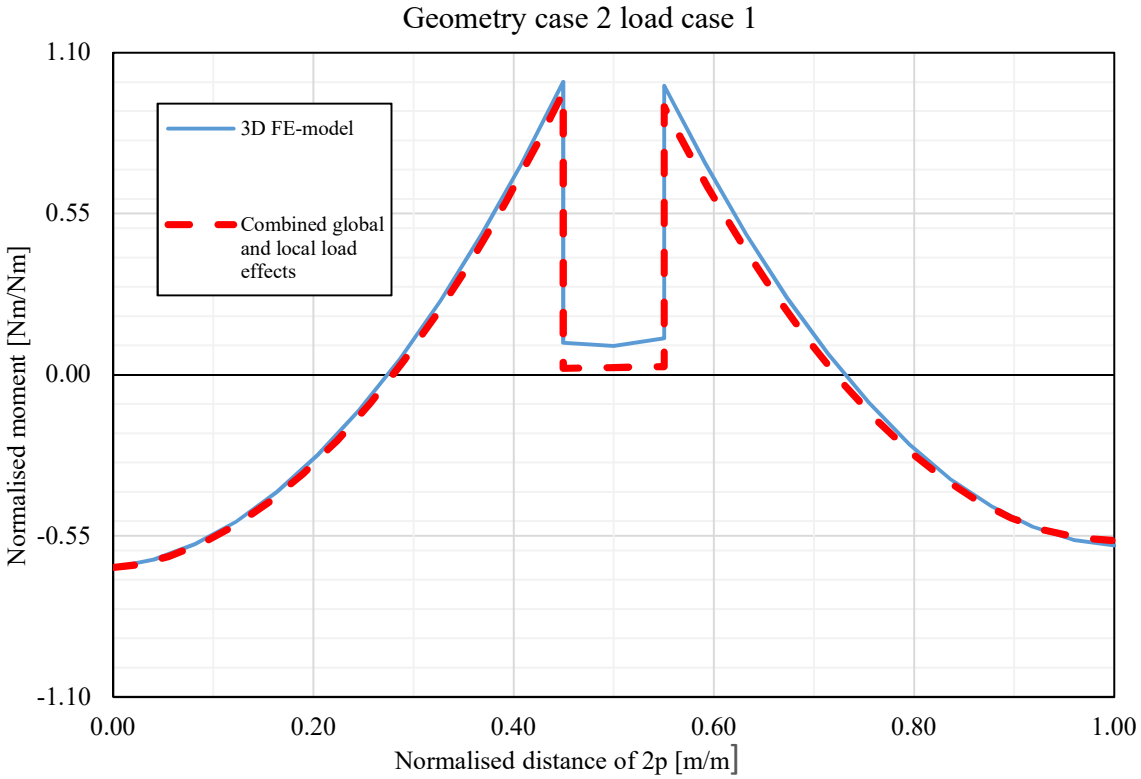

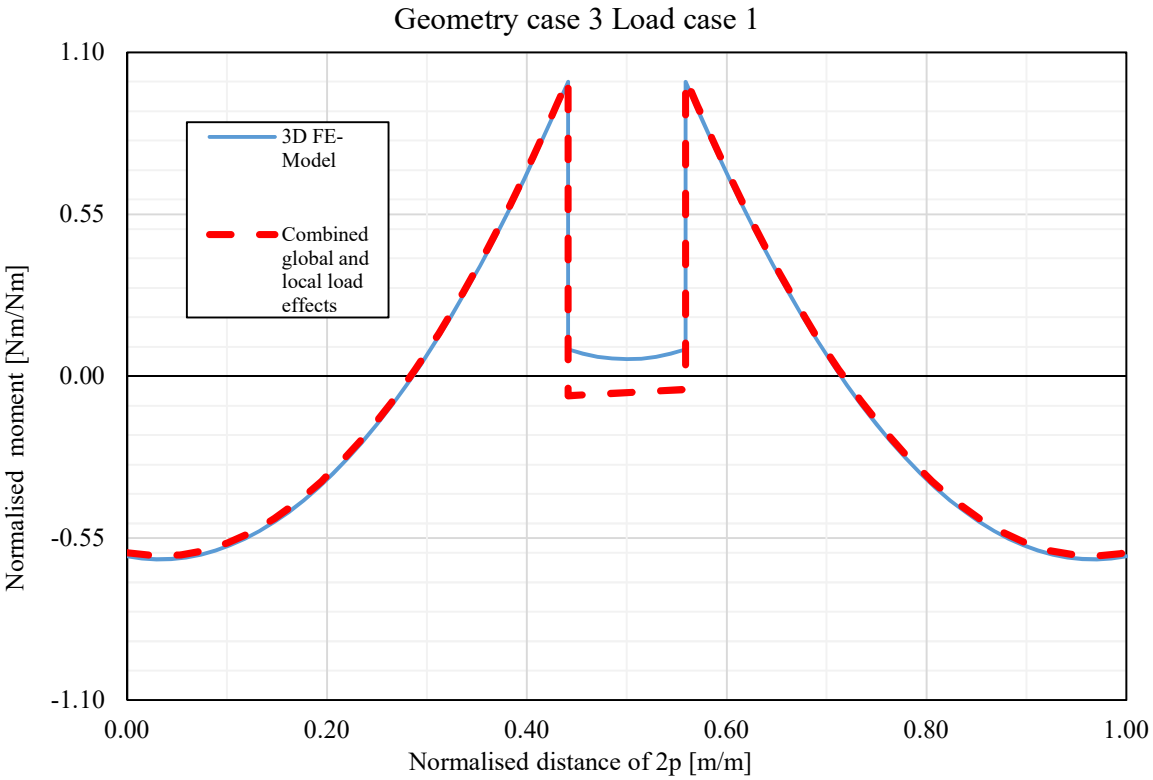
Geometry case 3 Load case 1
1.10
0.55
0.00
-0.55
-1.10
Normalised moment [Nm/Nm]
3D FE-Model
Combined global and local load effects
0.00
0.20
0.40
0.60
0.80
1.00
Normalised distance of 2p [m/m]